THREE LEVEL INNOVATION OF THE POWERED ABOVE ELBOW PROSTHETIC ARM USING PNEUMATIC ARTIFICIAL MUSCLES

by

DANIEL AUSTIN CHRIST

A THESIS

Submitted in partial fulfillment of the requirements
for the degree of Master of Science
in the Department of Mechanical Engineering
in the Graduate School of
The University of Alabama

TUSCALOOSA, ALABAMA

2011

ABSTRACT

This thesis presents a novel above elbow prosthetic arm design, innovating on three different levels: the actuation method, system integration, and the mechanism design. The Chemo-Muscle actuation system expands pneumatic artificial muscles to mobile applications. The integrated design makes use of the internal dead space of the muscle, incorporating external components and reducing fuel consumption. A novel design is presented using smaller muscles to control multiple degrees of freedom, providing 50% more strength than other prosthetic arms and an excellent range of motion for each degree of freedom. A simple control method is proven and the future development is discussed.

DEDICATION

To my wife, Amy

Thank you for your generous kindness, love and support.

Now and always.

LIST OF ACRONYMS AND ABBREVIATIONS

AE	Above Elbow
APL	John Hopkins Applied Physics Laboratory
CAD	Computer Aided Design
CNC	Computer Numerically Controlled Machining
DARPA	Defense Advanced Research Project Agency
DOF	Degree(s) of freedom
EMG	Electromyographic Signal
OIF/OEF	Operation Iraqi Freedom/Operation Enduring Freedom
PAM	Pneumatic Artificial Muscle
RIC	Research Institute of Chicago
TMR	Targeted Muscle Reinnervation

ACKNOWLEDGMENTS

I would like to thank the National Science Foundation GK-12 program for their financial support as well as for the opportunity to be part of such a unique educational fellowship experience. I would like to thank Dr. Xiangrong Shen for providing me with the opportunity to work on this project and for his assistance and encouragement along the way. I would like to thank Dr. Beth Todd for introducing me to many great programs The University of Alabama offers and helping me to get involved and give back. I would also like to thank Dr. Rajnish Sharma for his assistance and enthusiasm as a member of my thesis committee. Finally, I would like to thank my fellow students, Garrett Waycaster, Marco Wu, Alston Pike and Miguel Sequera for their support, encouragement and camaraderie.

CONTENTS

LIST OF TABLES

LIST OF FIGURES

Chapter 1:

Chapter 2:

Chapter 3:

Chapter 4

Chapter 5

Chapter 6

CHAPTER 1:

INTRODUCTION

1.1 MOTIVATION & OBJECTIVE

1.1.1 MOTIVATION

In 2007, the National Limb Loss Information Center reported that approximately 1.7 million Americans were living with limb loss [1]. By the year 2050 this number is projected to increase to 3.6 million [2]. The majority of limb loss, nearly 80%, involves lower-limb loss and therefore the majority of limb-loss research and prosthetics development are focused on the lower limbs. Upper-limb loss, however, is considerably less developed in terms of prosthetic technology and offers a completely different set of unique challenges and issues [3]. There are several reasons why upper-limb loss research trails that of lower-limb loss: 1) upper-limb loss is less frequent; 2) the measurement of upper-limb activity is more difficult than with lower-limbs due to more intricate and complicated movements and more degrees of freedom, 3) upper-limb prostheses are more challenging to design for the same reasons; and 4) trauma is the primary cause of upper-limb loss, as opposed to dysvascular conditions for the lower limbs. The population is, therefore, is generally more heterogeneous and therefore more difficult to study [3].

In 2005, over 40,000 persons in the United States were living with major upper-limb loss. 62% of these were amputations due to trauma-related injuries [2]. The proportion of trauma-related upper-limb loss increases during times of warfare. Limb loss involved the upper limb in 14 to 15 percent of 5,283 Vietnam service members, 18.5 percent of 89 British World War II veterans, 14 percent of 14 Persian Gulf service members, and 12.5 percent of 200 Iraq-Iran conflict service members during the late 1980s [3]. As of January 2009, 161 (22%) of 737 service members in the Operation Iraqi Freedom/Operation Enduring Freedom (OIF/OEF) conflict had limb loss involving the upper limb. [3]

The proportion of service members with multiple-limb loss has also increased during all 20th century conflicts, as well as during OIF/OEF. The mortality of those wounded on the battlefield has apparently decreased, thus allowing more persons with multiple-limb loss to survive their injuries [3] Service members who sustained multiple-limb loss during previous conflicts typically required lengthy initial hospitalizations, had difficulty with prosthetic fit to achieve high levels of function, and had decreased age-associated function compared with those with single-limb loss [3].

A recent Department of Defense Rehabilitation Directive aims to restore wounded service members from OIF/OEF to the highest possible functional level so the loss of a limb does not prevent a return to Active Duty [3]. The end goal is to be able to return the service members to pre-injury functionality.

The plot in **Figure 1-1** shows the activity level of upper limb amputees from two categories. A more positive score indicates combination of more strenuous activities of daily living usually done using prosthesis. A more negative score indicates less strenuous activities usually not done or done with assistance. Note: No hand limb loss in Vietnam group [3]. Those in the Vietnam category have had a significantly longer time getting used to their prosthetics than those in the OIF/OEF category [3]. Both categories, however, have a significant decline in activity score when the upper-limb loss level includes the loss of the elbow.

The amputees are favoring using their sound hand or not completing as many tasks due to the increased task complexity at this amputation level [3]. This is simply because current prosthetics are not capable of providing the needed functionality at this level. An above elbow (AE) prosthetic must be able to reproduce the many degrees of freedom (DOF) found in a

biological arm as well as an appropriate amount of strength in order to even attempt to restore pre-injury functionality.

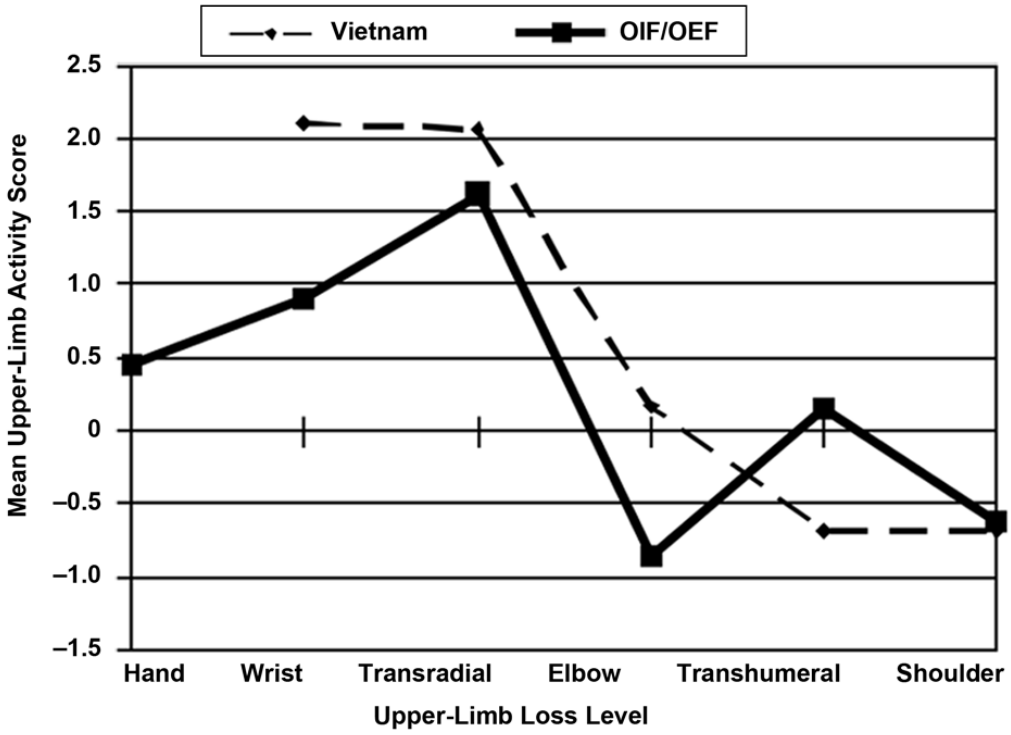

Figure 1-1: Mean upper-limb activity measure score by Vietnam and OIF/OEF groups.

1.1.2 OBJECTIVE

The objective of this research is to develop and test a new AE prosthetic device. This process seeks to improve upon the designs of current AE prosthetics by innovating on three different levels: the actuation method, system integration, and the mechanism design.

This device shall provide increased functionality and strength by using a new type of actuation system, The Chemo-Muscle Actuation system. This system allows for the use of pneumatic artificial muscles in mobile applications such as prosthetics. The efficiency of the Pneumatic Artificial Muscle will also be addressed by inserting an incompressible volume into the muscle chamber. This space can also be utilized to hold other required components such as valves and pressure sensors turning the actuator into an integrated/inclusive system of

components that would reduce the overall required size of the system. The prosthetic design will better emulate a biological system by using a set of smaller muscles in different ways to control multiple DOF. This will also conserve space and allow the entire AE prosthetic, elbow and wrist joints, to be controlled from the forearm region of the prosthetic while still having high functionality and strength. In addition to functionality, other biological similarities such as overall size and weight will be considered.

1.2 PROSTHETICS: BACKGROUND AND LITERATURE REVIEW

1.2.1 TRADITIONAL UPPER LIMB PROSTHETICS

Unlike the continuous advancement of the lower limb prosthetic, the upper limb prosthetic remained essentially the same from the U.S. Civil War until the last five years [4]. This traditional prosthetic is a mechanical, body powered device that offers limited functionality. They have a maximum of three degrees of freedom: Elbow flexion and extension, hook articulation, and, in advanced models, wrist rotation. These motions are controlled by a series of steel cables and harnesses, shown in **Figure 1-2**. These harnesses limit the range of motion and functional envelope of the individual [5]. When a patient uses the prosthesis outside the functional envelope, it becomes difficult to articulate the hook without having to use gross body motion. In the case of unilateral amputees, these big-scale movements make it harder for amputees to use their sound arm. As a result, they often rely on their sound arms functionality and do not use the prosthesis.

Figure 1-2: Traditional Body Powered Prosthetic Arm [5]

Although traditional upper limb prostheses are the most commonly available, most inexpensive, and are typically the lightest and most durable commercially available prostheses, only about 50% of the patients who own them use them regularly [5-6]. After the initial shock of amputation wears off, usually within a year or two, patients in rehabilitation clinics and at VA hospitals stop wearing their prostheses. This is even true at extreme levels of amputation. Wearing the burdensome prosthetic is simply not justified by the small amount of assistance it provides [4].

It has been found that the cable and harness method provides some tactile feedback, but the motion comes with a large 'mechanical disadvantage' [6]. It takes much more energy to move the prosthetic than it would to move a sound arm. This increase in energy puts more strain wear on the body of the amputee. Long-term use of a body-powered prosthesis can accelerate debilitating shoulder issues and anterior muscle imbalances [5].

In 1998, Cupo and Sheredos [5] discussed one of the most advanced body powered prosthetics available at that time, the AdVAntage Arm. Its design was one of the last mechanical, body powered designs to be considered for commercial production and is still likely the most functional type of body powered prostheses available today. As shown in **Figure 1-3**, the AdVAntage Arm is a nylon cable driven arm, however the elbow joint contains a locking mechanism that allows the user to alternate controlling the elbow and the hook. This allows them to function independently rather than both motions being based on the same shoulder movement. A patient could reach out the arm, locking it in place, pick something up with the hooks, and then while holding on to the object they could unlock the elbow and move it freely. To Drop the object, they would again have to lock the elbow and switch to controlling the hook. This design seems to address multiple needs for amputees; however some issues still needed to be addressed. The prosthesis had a steep learning curve, making it difficult to adjust too quickly. Its ratchet mechanism made too much noise. It did not look much like a biological arm. The locking mechanism was inconsistent and it was difficult to determine which state it was in. Finally, it was not accepting of task specific terminal devices, such as hands, hooks or other tools.

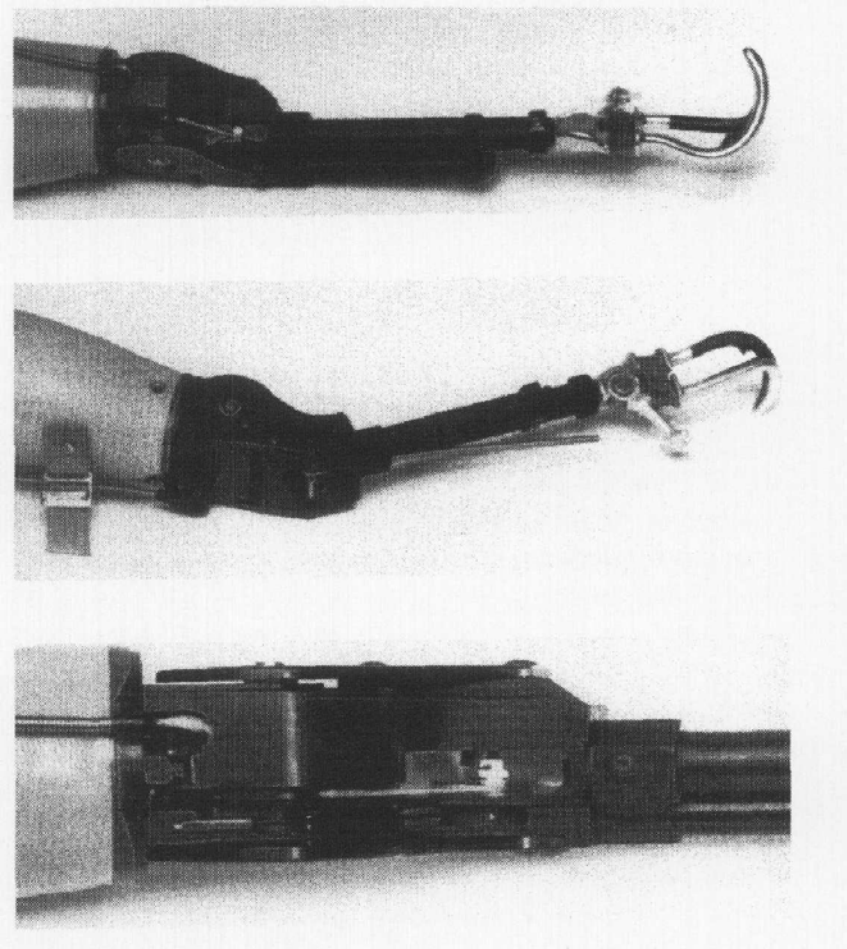

Figure 1-3: AdVAntage Arm [5]

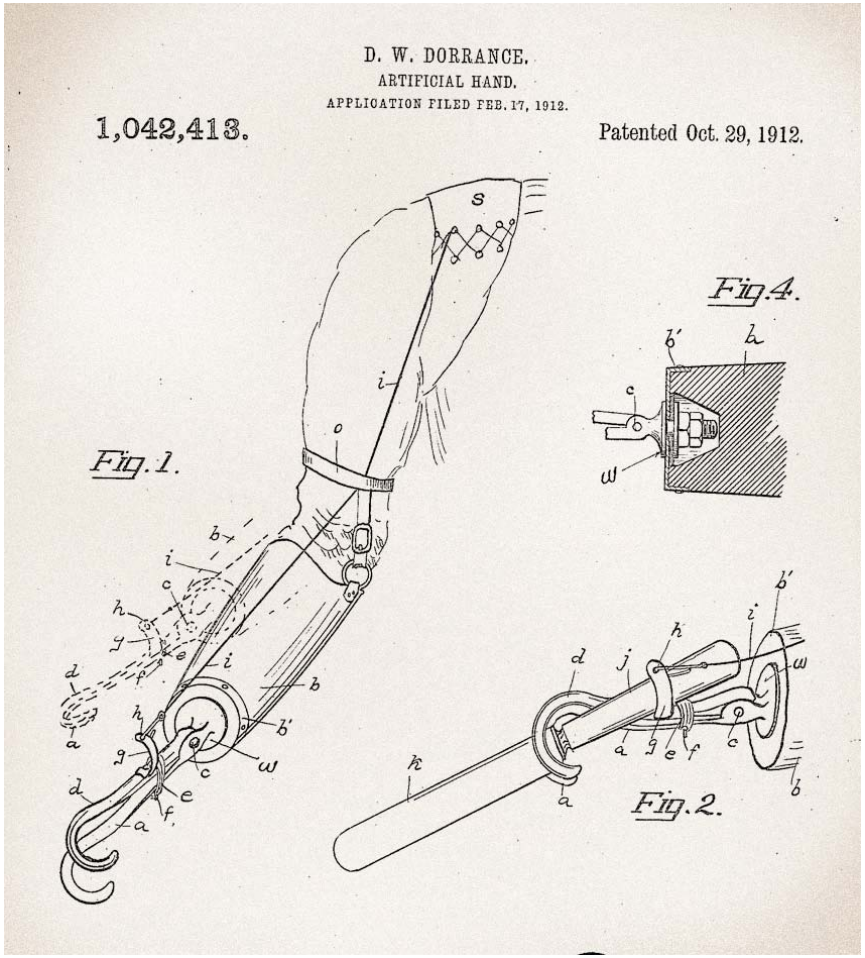

Figure 1-4: Dorrance's original patent of the artificial hand [7]

Despite this more advanced variation on the cable driven arm, the majority of body powered prosthetic arm users prefer the simpler design patented by D.W. Dorrance in 1912, shown in **Figure 1-4** [7]. Modern versions use more advanced materials such as silicones and plastics in the socket, carbon fiber instead of wood or fiberglass in the frame, titanium instead of steel in the hook, Spectra (a strong, lightweight synthetic fiber similar to nylon) instead of steel cable for control. Despite these stronger, lighter materials, the prostheses are nearly indistinguishable from those made for soldiers after WWII [7].

1.2.2 EARLY ELECTRONIC PROSTHETICS

The development of electronic prosthetics stemmed from the need for better control and more degrees of freedom than traditional prosthetics could provide. Some arms were built with only a couple DOF, but attempted to use a newly developed type of prosthetic control; myoelectric control. Toledo et al [8] provide a review of AE prosthetics in 2009. They cite the two leading early electric prosthetic arms as being the "Boston Arm," developed in the late 1960's, and the "Utah Arm," developed in the early 1980's. Both are myoelectric arms; this means that they are controlled by reading the electrical signals generated by the flexing of human muscles. The electrodes and circuitry used in the Utah Arm are shown in **Figure 1-5**. For comparison, modern electrodes are shown in **Figure 1-6** [8]

The first part of the "Boston Arm" developed was the elbow, first called the "Boston Elbow." This developmental prosthetic was essentially a 1 DOF myoelectric elbow joint [8]. It was mainly a proof of concept for the idea that a prosthetic could be controlled by electromyographic (EMG) signals. Mann and Reimers [10] discuss the EMG control of the "Boston Arm" elbow joint. In their study they were attempting to develop a non-visual feedback method for the electric servo powered joint. This would help address the lack of tactile feedback

the amputee was used to with a traditional prosthetic arm. They found that by adding an auditory feedback signal they were able to achieve virtually identical kinesthetic performances from the traditional prosthetic and the "Boston Arm". Images of the "Boston Elbow" and the "Boston Arm" are shown in **Figure 1-7**.

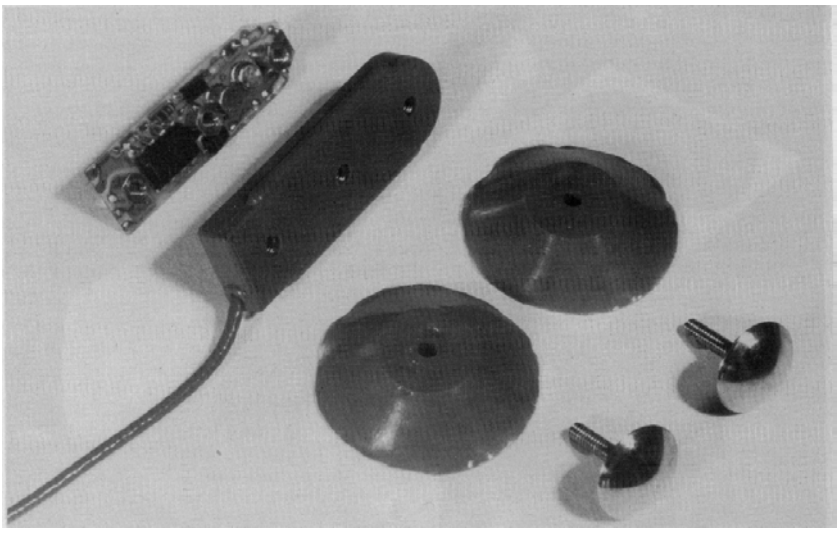

Figure 1-5: Myoelectric preamplifier circuitry and skin contact electrodes utilized in the Utah Arm [11]

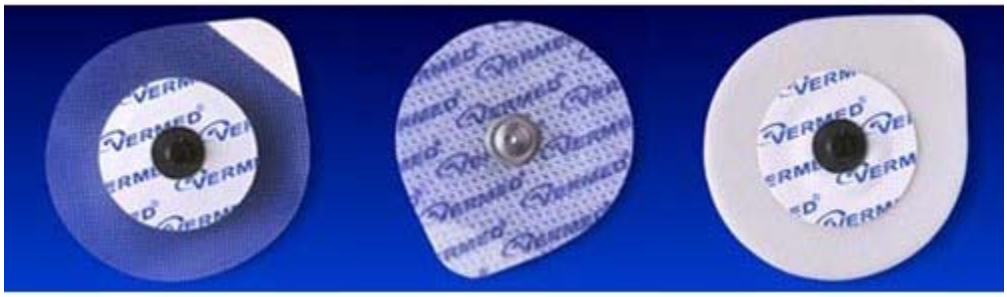

Figure 1-6: Modern Electrodes made by Vermed [9]

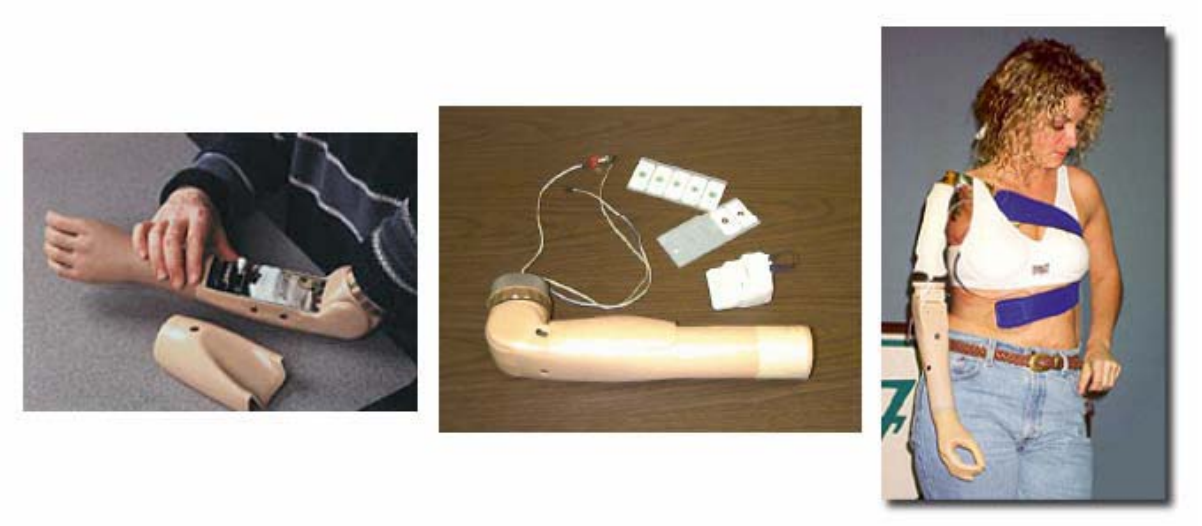

Figure 1-7: The Boston Elbow and the Boston Arm [8]

In 1982, Jacobsen et al [11] wrote a paper on the development of the Utah Arm. Unlike the initial version of the "Boston Elbow," the Utah Arm, shown in **Figure 1-8**, provides multiple degrees of freedom. At the AE level it provides elbow flexion and wrist rotation plus the additional DOF provided by the hand or other terminal device. Totaling six DOF, the remaining motions are provided by the upper portion of the arm, some passively. The method of control is also different. By using proportional control the Utah Arm is able to move slowly or quickly to any position. This provides a more natural response with less effort for the patient than the traditional on/off movement [8]. For this reason, Toledo et al call the Utah Arm the premier myoelectric arm for above elbow amputees since 1981 [8].

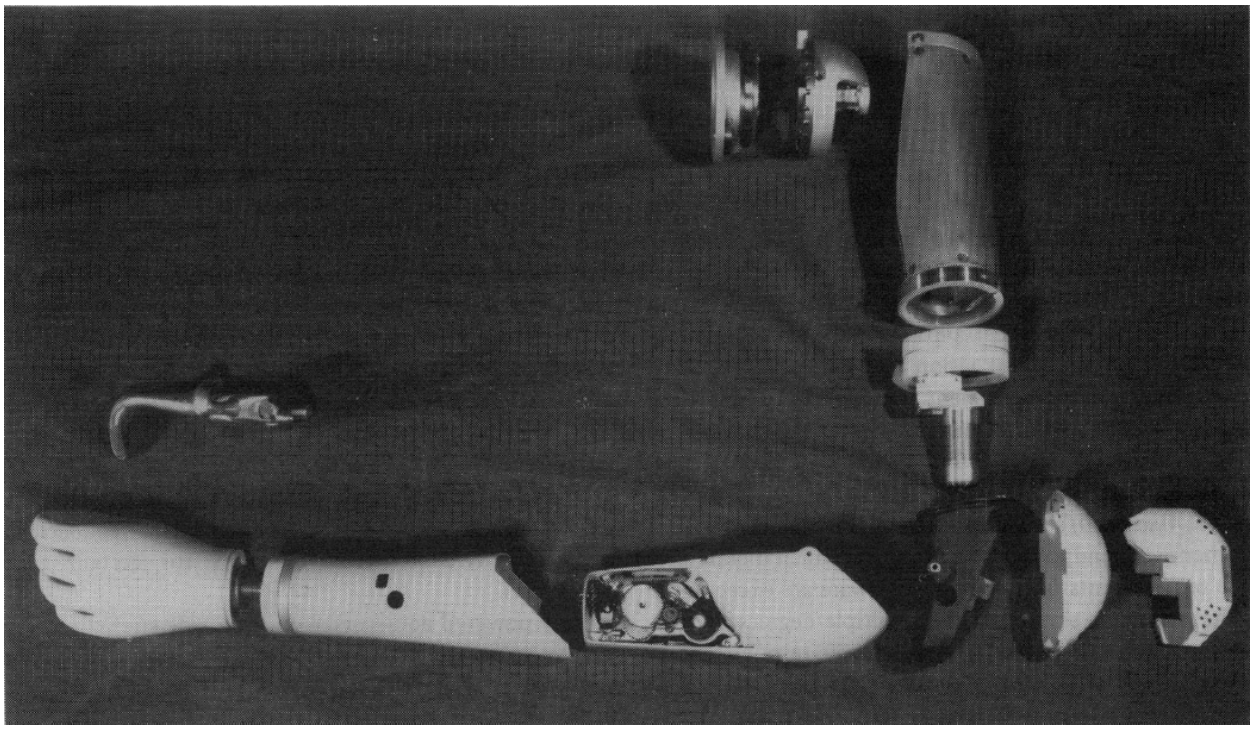

Figure 1-8: Disassembled components of the six degree-of-freedom Utah arm [30]

1.2.3 REVOLUTIONIZING PROSTHETICS

Jacobsen et al [11] also make a very important statement in their paper about the Utah Arm. They describe not only how their product works, but have extensive commentary on how it could work practically for developers, manufacturers and Investors. They describe the funding availability for upper limb prosthetics research as being in a paradoxical position. Funding is not available without additional demonstrated success. However, success cannot be achieved without additional funding. Furthermore, the cost of these systems cannot be reduced without widespread use, and widespread use cannot be achieved without better systems. They say that, therefore, in the absence of "risk funding" and, as a result of development complexities, the evolution of new prosthetic limbs will undoubtedly proceed at a disappointing pace [11].

Over 20 years later, the Defense Advanced Research Project Agency (DARPA) agreed. From 1981 to 2005 there was little advancement in upper limb prosthetics. Electric and

myoelectric arms were commercially available, however it was found that amputees were choosing traditional prosthetics or adapting to life without using any type of prosthetic [4]. The most advanced modern AE arms provided three DOF that could be controlled one at a time, not unlike the Utah arm. DARPA decided that upper limb prosthetics did not need evolution, it needed a revolution. In 2005 DARPA began the Revolutionizing Prosthetics program providing nearly $100 million by 2009.

The program was split into two parts: The 2007 project was headed by Dean Kamen's New Hampshire based Deka Research and Development Corp. They were given a two-year deadline to make an advanced prosthetic arm with the world's best existing technologies. The 2009 program is spearheaded by Johns Hopkins University's Applied Physics Laboratory (APL), in Laurel, Md. APLs goal is to develop the most human integrated prosthetic possible. This includes a new level of "thought control" and a sense of feel not currently available in prosthetics. The initial goal of the Revolutionizing Prosthetics program to develop a mechanical arm with all the 22 DOF of a biological arm, although DARPA admits that they may decide to build an arm with 15 to 18 degrees of motion and less strength that could potentially cost less per system than the initial prototypes might [12].

In the 2007 portion of DARPAs project, Deka was charged with making the most advanced prosthetic arm possible. Adee [4] discussed the project in a 2008 report. To Kamen, the most advanced arm possible meant an arm that provided more functionality and less discomfort to the user. With this in mind Deka engineers developed the "Luke arm," shown in **Figure 1-9**. This prototype provided 18 degrees of freedom and the ability to utilize both fine motor control and power. Subjects were able to pluck chocolate-covered coffee beans off of the table one by one, pick up a power drill, unlock a door, and shake a hand. Most amazingly, all 18

degrees of freedom cam be controlled independently and simultaneously. This is a large step towards more functionality and making the arm feel more like a biological arm to the user.

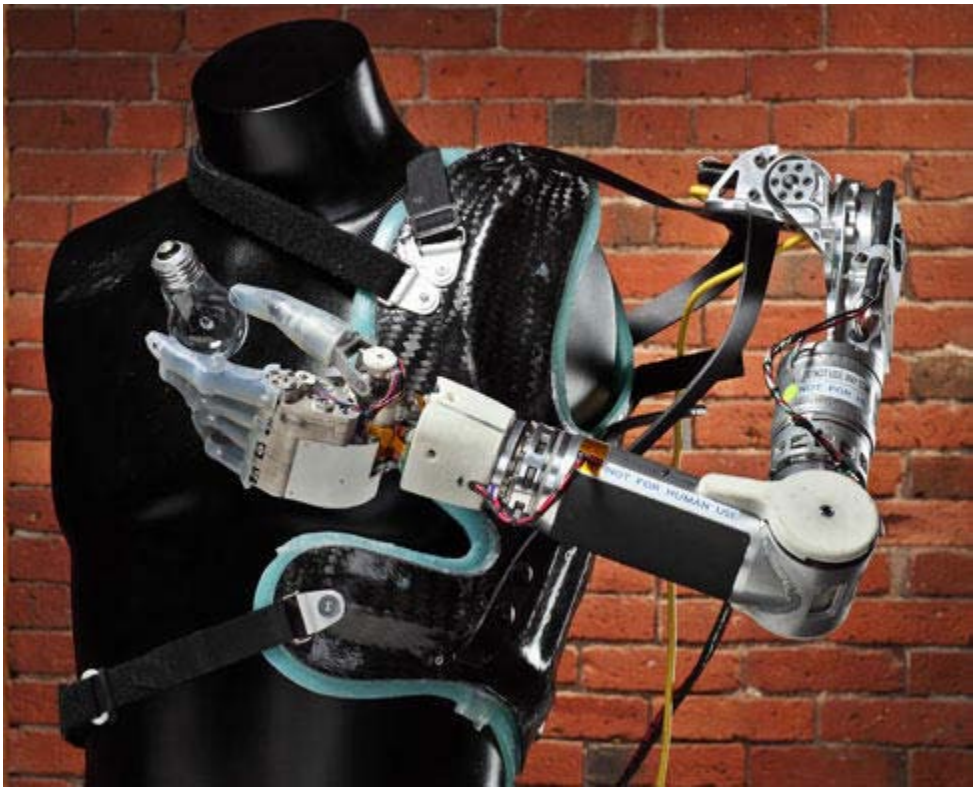

Figure 1-9: Deka's "Luke" Arm prosthetic prototype [15]

The “Luke” arm was also designed for flexibility. The entire design is modular to enable any level of amputee to use the needed portion of the arm. It is also designed to take any form of signal input. Deka also created a foot joystick system that allows simple non-invasive control options to the user. They also included a simple method of grip feedback given by a tactor. A tactor is a small vibrating motor about the size of a bite-size candy bar that is secured against the user’s skin. A sensor on the Luke hand, connected to a microprocessor, sends a signal to the tactor, and that signal changes with grip strength. When a user grips something lightly, the tactor vibrates slightly. As the user’s grip tightens, the frequency of the vibration increases.

The 2009 portion of DARPAs program is spearheaded by Johns Hopkins University's Applied Physics Laboratory (APL), in Laurel, Md. APL's goal is to create prosthetics that would essentially be "thought controlled." The team wanted more than control for amputees; they also wanted to restore the ability to feel heat, cold, pressure, and surface texture. "The idea is to develop a prosthetic arm whose hand can grasp and throw a baseball, play the piano, or pick up a flower and place it in a vase as naturally as a biological arm," says Stuart Harshbarger, a biomedical engineer at APL [10].

Figure 1-10: APL's prosthetic arm prototype [16]

In order to achieve this higher level of thought control, APL partnered with the Research Institute of Chicago (RIC), the "#1 Rehabilitation Hospital in America [11]. RIC developed surgical techniques to reroute existing nerves in amputees so that they better interface with the electronics in the prosthetic arm. The procedure, called targeted muscle reinnervation (TMR) surgery, redirects the residual nerve bundles that once connected the spinal cord to the 70 000 nerve fibers in the arm. After an amputation, these nerves remain in place, and they continue to

work—they just aren't connected to anything functional. The pectoral muscles also remain intact, but they too are no longer driving an arm. So RIC surgically threaded the residual nerves from their original locations into the chest, where they innervated, or grew into, an area of pectoral muscle slightly smaller than a compact disc. The prosthetic socket with EMG contacts, can read these nerve signals. The amputee is then able to control the prosthetic by sending signals to the same nerves they did before the amputation. The researchers found that the redirected nerves restored not only muscle function but also sensation. The patients sensed a touch on their chests as if someone were touching their missing hands—even if it was just a tap. By placing the tactor on the chest next to the electrodes, they created a complete feedback loop. They have also developed ways to transmit heat and cold from the hand as well [11].

Otto Bock Healthcare Products, in Vienna, is the transition partner for DARPA, meaning that it will manufacture the devices after DARPA has stopped funding the project [13]. Otto Bock had also been developing a prosthetic arm. The DynamicArm is an adjustable elbow module that can lift up to 6 lbs and statically hold over 50 lbs [14]. The integrated AFB (Automatic Forearm Balance) stores the energy released when the arm is lowered and helps lift it during flexion, allowing the arm to swing quietly and naturally while walking. The DynamicArm also incorporates Bluetooth technology for programming and training without cords or cables. While developing their biological interface system, APL used a DynamicArm and made a custom socket and terminal device to use with it. Otto Bock has since come out with a DynamicArm system for Targeted Muscle Reinnervation (TMR). Otto Bock is also the world's leading provider of terminal devices [6].

1.2.4 OTHER RELATED RESEARCH

Goldfarb and his team at Vanderbilt University in Nashville, TN have published many papers on their monopropellant powered prosthetic arm design [17-20]. In these papers, they use traditional pneumatic cylinders with a chemically produced hot gas as the actuating fluid. The benefit of using this chemically produced hot gas is that the entire system can be mobile and non-tethered. This allows the pneumatic actuators to be a viable actuation device for a prosthetic design.

Fite et al describe the "Liquid Fueled Actuation" in a 2006 paper [17] and with more detailed in a 2008 paper [18]. They describe the use of a monopropellant cartridge as being similar to the use of a battery pack. Rather than current at a given voltage, the propellant cartridge outputs gas flow rate at a given pressure. The high pressure output is used to power the gas cylinders needed for actuation. Each cylinder is sized appropriately for the required energy of each joint. They also describe the design of a 21 DOF AE arm prosthetic. Of the nine independent actuators, one provides direct drive actuation for the elbow, three provide direct-drive actuation for the wrist, and the remaining five actuate an under actuated 17 degree of freedom cable driven hand. This prototype is shown in **Figure 1-11**.

Figure 1-11: Vanderbilt's prosthetic arm prototype [18]

In these two papers, Fite et al also describe the design of a miniature 4-way servo valve. This valve is designed to be compact, fast and be able to withstand the high temperatures of the exothermic catalytic reaction. An intricate valve bank and gas distribution system is also described. Overall the arm provides good control tracking using off board, cold nitrogen gas and demonstrates the functionality of the miniature servovalves and the arm prototype. It is able to provide 50% of the force of a biological human arm thanks to the high power density of the cylinder actuators. This is significantly more strength than any electric motor based prosthetic device [17].

In a 2008 paper, Withrow et al [19] from Vanderbilt University discuss a forearm actuation unit. This unit is similar to the fore arm portion of the arm discussed in the earlier papers [17, 18] except that this unit is redesigned to fit into the envelope of an average female arm. This envelope shape is described in **Figure 1-12**. The new design contains 14 actuators, three for the wrist motion and 11 for individual finger movements. The forearm actuation unit has a mass of 930g (2.05 lb), which includes the weight of all components (excluding electronics and the liquid propellant cartridge), and was projected to deliver approximately 50% of the

strength of a biological forearm. This design also implements the previously discussed miniature servovalves.

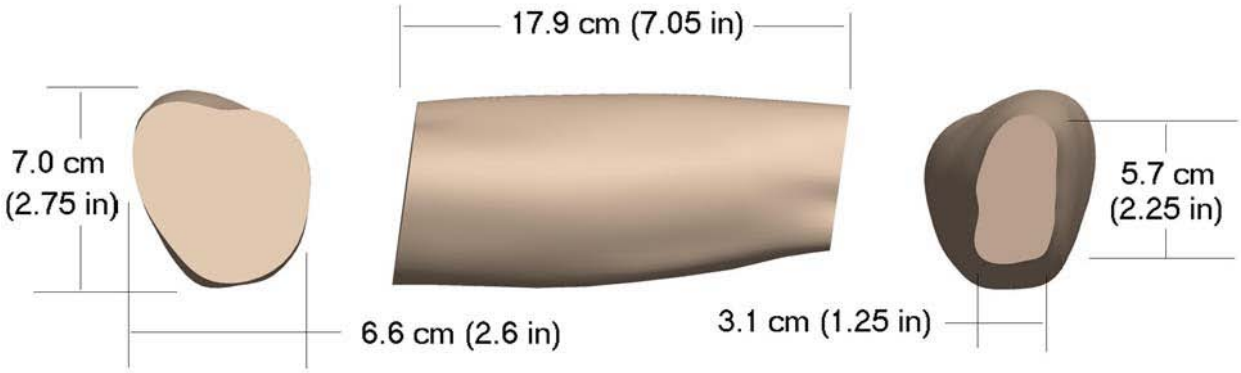

Figure 1-12: Geometric Envelope of a 50% female forearm [19]

The 11 hand actuators from the forearm design [19] could be used to control an articulated hand such as the one presented by Dalley et al [20] in a 2009 publication. However this hand is designed to be run with only five actuators. They show that this is the minimum number of actuators required to make the eight canonical hand positions that represent a large number of possible biological hand positions.

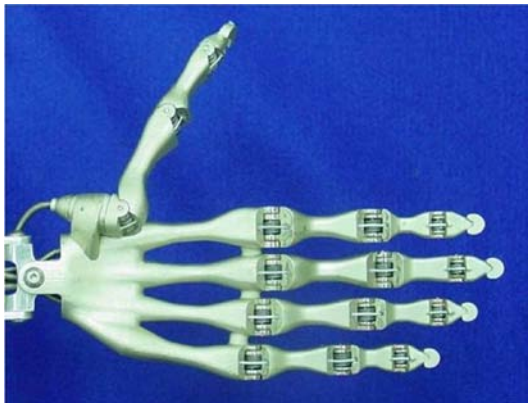

Figure 1-13: Vanderbilt's prosthetic hand prototype [20]

The hand is designed with multi-appendage cable differentials that help equalize the torque on the linked joints and eliminate the need for position sensing and alternating position/grip control in the hand. The hand was also designed with a high strength to weight ratio by utilizing CAD

software to eliminate excess material. The resulting shape is a hollow, monocoque structure that is strong, lightweight, and reminiscent of a biological skeletal hand. This prototype is shown in **Figure 1-13**. They state that their future work includes incorporation of the actuation units into the hand itself so that no additional space is required proximal (closer to the center of the body) to the wrist.

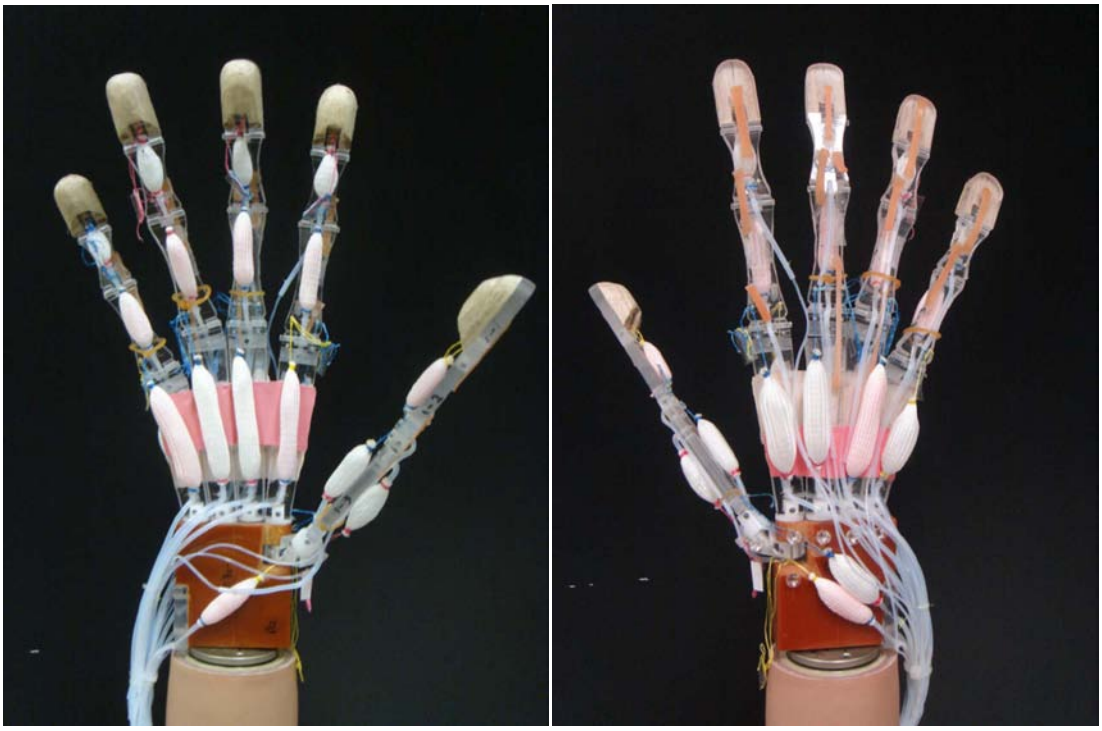

Figure 1-14: PAM powered prosthetic hand, front (left) and back (right) [21]

One such hand is discussed in a 2009 publication by Takeda et al [21]. They present the development of a prosthetic hand with a tendon driven wrist. The wrist mechanism is large and although functional, is not very practical. The hand however is capable of controlling each joint of each finger independently with the actuators on the hand directly proximal to the joint. The actuators used are custom made miniature McKibben pneumatic artificial muscles (PAMs) which will be explained in more detail in the next chapter. These custom actuators are small enough to fit on the fingers of the prosthesis, and yet are able to produce enough force to grasp a

plastic bottle. With increased grip strength, this design could be an extremely functional, lightweight and simple prosthetic hand.

1.3 PNEUMATIC ARTIFICIAL MUSCLES

1.3.1 BIOLOGICAL MUSCLES

Before attempting to understand the function of artificial muscles, it makes sense to study the biological muscles they seek to mimic. The biological muscles that voluntarily control the body's motion are called skeletal muscles because they actuate the joints of the skeleton. They work similarly to the other types of muscles in the body in that they are actuated by chemical reactions in the muscle tissue. In the case of skeletal muscles, this reaction causes motion in what is called sliding filament theory. The filaments are actually two different types of myofilaments, thick and thin myofilaments. Thin myofilaments measure about 5 nm in diameter while thick ones measure around 16nm [22]. Thin myofilaments are made up mainly of the protein actin and connect to base structures called Z lines. Thick myofilaments are similarly made of the protein my myosin. Thick and thin myofilaments overlap each other in bundles called sacromeres. This is all shown in **Figure 1-15**.

During muscle contraction, nerve impulses cause chemical reactions that release energy and open the myosin-binding sites on actin. This causes the myosin cross bridges to move towards the H-zone, the empty middle section of a myosin covered thick myofilament. This motion forces the thick and thin myofilaments to move past each other and the sacromeres to shorten. This is also shown in **Figure 1-15**.

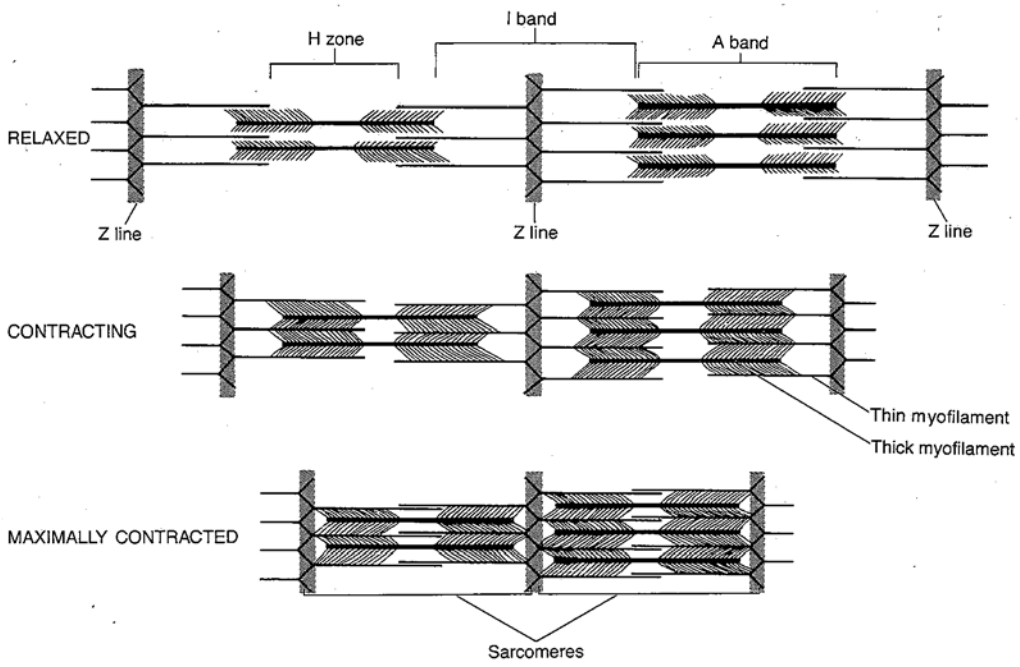

Figure 1-15: Sliding Filament Theory of muscle contraction [22]

The individual shortening of each of these sacromeres, lined up end to end, causes a gross shortening of the muscle organ as a whole. This shortening induces a force on the attached bones and is used to actuate the intermittent joint. Muscles also work in groups with at least two muscles responsible for the actuation of a joint, but typically more than two. Some of these muscles are used to flex or contract the joint while others are used to extend the joint. This antagonistic set up allows for powered motion in both directions of the joint as well as for intermediate position control and stiffness. In the case of the elbow joint, there are actually seven main muscles that control the forearm movement. These muscles and their functions are listed in **Table 1-1** and are shown in **Figure 1-16**. Some of these muscles have functions that affect joints other than the elbow. These actions are not included in **Table 1-1**. Flexion and extension are the major bending motion of the elbow with flexion decreasing the inner angle of the elbow and extension increasing the joint angle. Pronation and supination are the rotational

motion of the forearm with pronation turning the palm posterior or inferior and supination turning the palm anterior or superior.

Table 1-1: Muscles that move the forearm and their functions

Muscle	Action on Forearm
Biceps Brachii	Flexes and supinates
Brachialis	Flexes
Brachioradialis	Flexes, semi-supinates and semi-pronates
Triceps Brachii	Extends
Anconeus	Extends
Pronator Teres	Pronates and Flexes
Pronator Quadratus	Pronates

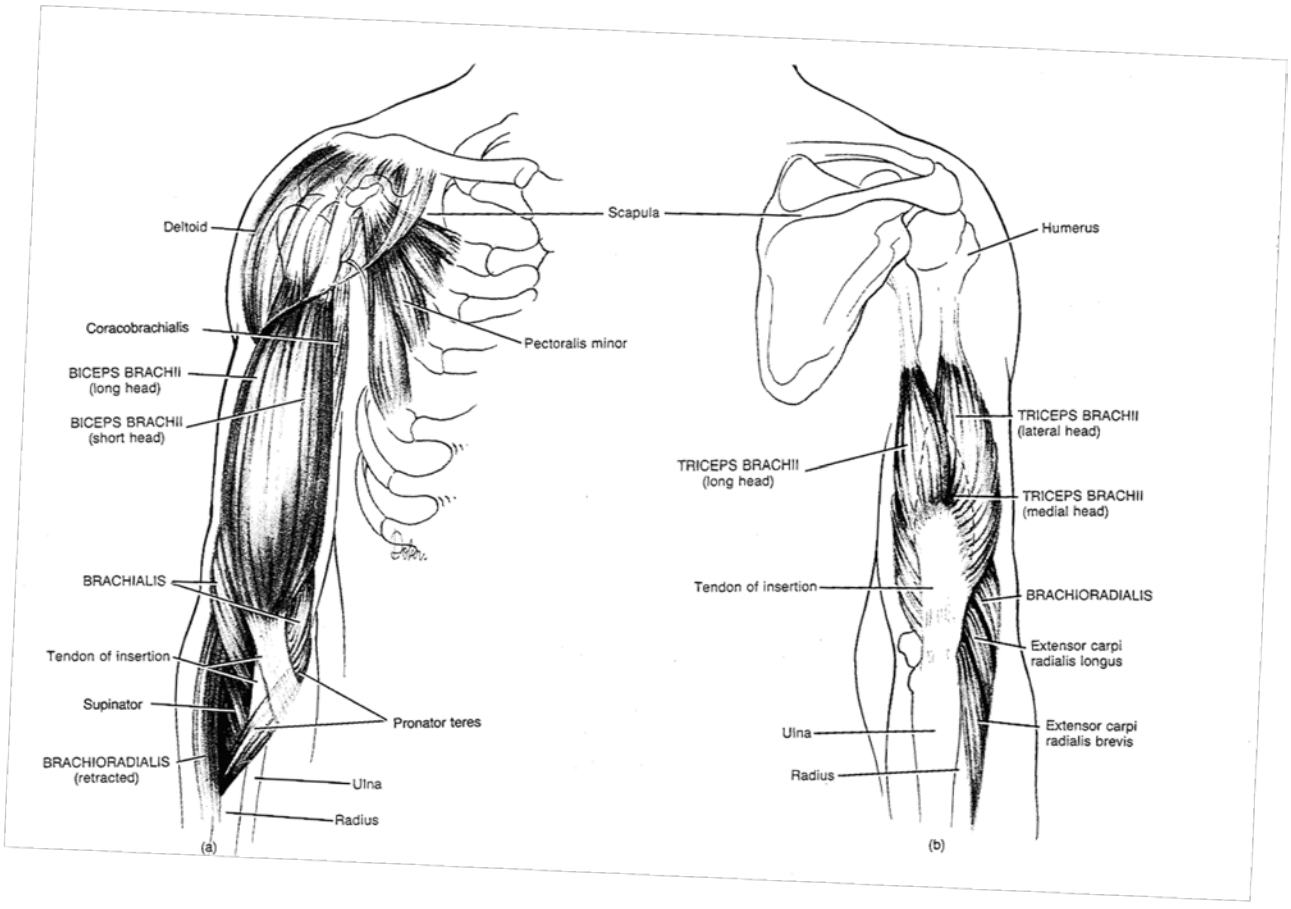

Figure 1-16: Human arm skeletal muscle structure (a) Outer and (b) Inner layers [22]

1.3.2 PNEUMATIC ARTIFICIAL MUSCLE CHARACTERISTICS

Pneumatic artificial muscles (PAM) are muscle-like actuators that contract under pressure, exerting a pulling force over an external load. The most well-known pneumatic muscle, the McKibben muscle, consists of an inflatable membrane surrounded by a meshed braid of inextensible fibers. When the elastic membrane is inflated it expands. The inextensible fibers resist this expansion and are stretched over the inflated tube. This causes the overall length of the muscle to decrease. **Figure 1-17** shows the internal structure and the functioning mechanism of the PAM. In the functioning mechanism diagram it is shown that the angle of the fibers in the mesh changes with the contraction of the muscle but the length of the fibers stays the same.

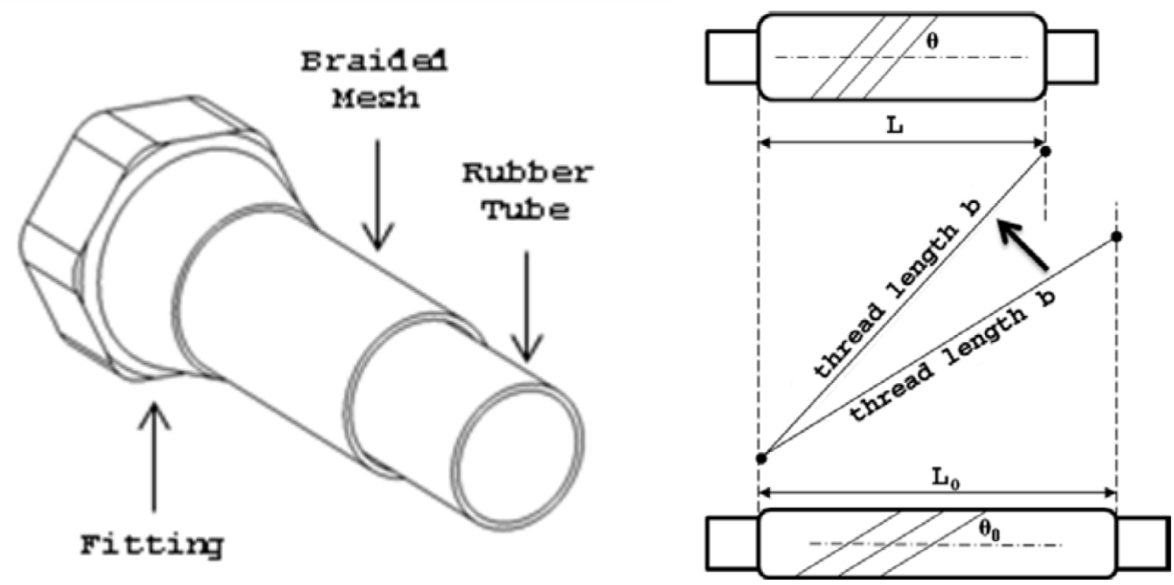

Figure 1-17: Structure (left) and Functioning Mechanism (right) of the Pneumatic Artificial Muscle.

Compared with other types of actuators, PAMs possess two outstanding features: (I) High power density: Researchers have reported the values of power density for PAMs ranging from 1.5 kW/kg at 200 kPa, 3kW/kg at 400 kPa [32] to 5 kW/kg [25], even up to 10kW/kg [33]. Compared with a DC motor, which has a power density of about 0.1 kW/kg [34], PAMs possess

a 10 to 100 times advantage in power density, and thus offer a potential for dramatically improving the performance of robotic systems. (II) Similar elastic characteristics to biological muscles: Like a biological muscle, a PAM is essentially a contractile element, with the pulling force related to the length of the muscle. Furthermore, the force-length relation of the PAM is very close to the biological muscle [35], making it an excellent choice for bio-robotic systems, especially prosthetic and orthotic devices.

1.3.3 APPLICATIONS OF PAMS

This type of actuator is first developed as an orthotic power source, leveraging its similar length-load characteristics to the biological muscle [23, 24]. Later PAMs have been used to power a variety of robotic systems, mainly those mimicking human limb functions, including robotic arms [25-27] and biped walking robots [28, 29]. Some other robotic applications have emerged as well, including a linear drive [30] and a parallel manipulator [31].

1.3.4 DRAWBACKS OF THE PAM

Although PAMs are very competitive as an actuation means for robotic systems, especially mobile robotic systems which have strict weight and volume constraints, the majority of PAM-driven robotic systems are either stationary or tethered. Like all other pneumatic actuators, the PAM relies on traditional pneumatic supplies as energy sources. Typical pneumatic supplies either directly store compressed air in a high-pressure reservoir or generate compressed air from other energy sources (chemical or electrical) through a compressor. The former suffers from a low energy density, while the latter involves complex devices and thus suffers from a large weight and volume as well as low conversion efficiency. Lack of appropriate pneumatic supply poses the biggest hurdle for the further development of PAMs as

promising robotic actuators. The Chemo-Muscle Actuation System, discussed in Chapter 2, addresses this issue.

REFERENCES

1. National Limb Loss Information Center. 2007 Fact sheet: Limb loss in the United States. Knoxville (TN): Amputee Coalition of America; (2011) Retrieved from: *http://www.amputee-coalition.org/*

2. Ziegler-Graham K, MacKenzie EJ, Ephraim PL, Travison TG , Brookmeyer R. Estimating the prevalence of limb loss in the United States: 2005 to 2050. *Arch Phys Med Rehabil.* 2008;89(3):422–29. [PMID: 18295618] DOI:10.1016/j.apmr.2007.11.005

3. McFarland L., Winkler S., Heinemann A., Jones M., Esquenazi A. Unilateral upper-limb loss: Satisfaction and prosthetic-device use in veterans and servicemembers from Vietnam and OIF/OEF conflicts. *JRRD 2010*, 47(4): 299-316

4. Adee S. Dean Kamen's "Luke Arm" Prosthesis Readies for Clinical Trials. *IEEE Spectrum*. Feb. 2008. *http://spectrum.ieee.org/biomedical/bionics/dean-kamens-luke-arm-prosthesis-readies-for-clinical-trials/0*

5. Lake C, Dodson R. Progressive Upper Limb Prosthetics. *Phys Med Rehabil Clin N Am* 17 (2006) 49–72. DOI:10.1016/j.pmr.2005.10.004

6. Cupo M, Sheredos S. Clinical evaluation of a new, above-elbow, body-powered prosthetic arm. *Journal of Rehabilitation Research and Development*; Oct 1998; 35, 4; Research Library pg. 431

7. Kuniholm J. Open Arms: What prosthetic-arm engineering is learning from open source, crowd sourcing, and the video-game industry. *IEEE Spectrum*. Mar. 2009

8. Toledo C, Leija L, Muñoz R, Vera A, Ramírez A. Upper Limb Prostheses for Amputations Above Elbow: A Review. *PAHCE 2009, IEEE* Cat#: CFP0918G

9. Vermed, Medical Sensors. *http://www.vermed.com/electrodes.php?cat=3&subcat=25,* January 2011

10. Mann R, Rimers S. Kinesthetic Sensing for the EMG Controlled "Boston Arm." *IEEE Transactions On Man-Machine Systems*, March 1970 Pg. 110-115

11. Jacobsen S, Knutti D, Johnson R, Sears H. Development of The Utah Artificial Arm. *IEEE Transactions on Biomedical Engineering*, Vol. BME-29, No. 4, April 1982

12. Guinnessy P. DARPA joins industry, academia to build better prosthetic arms. *Physics Today*, September 2006 Pg. 24-25

13. Adee S. Winner: The Revolution Will Be Prosthetized, Darpa's prosthetic arm gives amputees new hope. *IEEE Spectrum*, Jan. 2009. *http://spectrum.ieee.org/robotics/medical-robots/winner-the-revolution-will-be-prosthetized/0*

14. Otto Bock, Dynamic arm. *http://www.ottobock.com/cps/rde/xchg/ob_us_en/hs.xsl/6905.html?id=10038#t10038,* Jan 2011

15. Hsu J. "Luke" Arm Begins Widespread Testing Among Veterans. *PopSci.com* June 2009. *http://www.popsci.com/scitech/article/2009-06/luke-arm-begins-widespread-testing-among-veterans*

16. Applied Physics Laboratory, Revolutionizing Prosthetics 2009. Viewed Jan 2011 *http://www.jhuapl.edu/ourwork/stories/st090829.asp*

17. Fite K, Withrow T, Wait K, Goldfarb M. Liquid-Fueled Actuation for an Anthropomorphic Upper Extremity Prosthesis. *Proceedings from IEEE EMSB* Sept. 2006, 5638-5642

18. Fite K, Withrow T, Shen X, Wait K, Mitchell J, Goldfarb M. A Gas-Actuated Anthropomorphic Prosthesis for Transhumeral Amputees. *IEEE Transactions On Robotics*, Vol. 24, No. 1, February 2008, 159-169

19. Withrow T, Shen X, Mitchell J, Goldfarb M. A Forearm Actuation Unit for an Upper Extremity Prosthesis. *IEEE International Conference on Robotics and Automatio*n 2008, Pg. 2456-2464

20. Dalley S, Wiste T, Withrow T, Goldfarb M. Design of a Multifunctional Anthropomorphic Prosthetic Hand with Extrinsic Actuation. *IEEE/ASME Transactions on Mechatroni*cs 2009

21. Takeda H, Tsujiuchi N, Koizumi T, Kan H, Hirano M, Nakamura Y. Development of Prosthetic Arm with Pneumatic Prosthetic Hand and Tendon-Driven Wrist. *Proceedings of the 31st Annual International Conference of the IEEE EMBS*, 2009, 5048-5051.

22. Tortora, G. *Principles of Human Anatomy*, Fifth Edition. New York, 1989, Harper & Row, Publishers, Inc.

23. Schulte, H.F. "The characteristics of the McKibben artificial muscle." *The Application of External Power in Prosthetics and Orthotics,* Washington, DC., National Academy of Sciences – National Research Council, 1961.

24. Gavrilovic, M.M. and Maric, M.R. "Positional servo-mechanism activated by artificial muscles." *Medical and Biological Engineering*, vol. 7, pp. 77-82, 1969.

25. Hannaford, B., Winters, J.M., Chou, C.-P., and Marbot, P.-H. "The anthroform biorobotic arm: a system for the study of spinal circuits." *Annals of biomedical engineering*, vol. 23, pp. 399-408, 1995.

26. Bowler, C.J., Caldwell, D.G., and Medrano-Cerda, G.A. "Pneumatic muscle actuators: musculature for an anthropomorphicrobot arm." *IEE Colloquium on Actuator Technology: Current Practice and New Developments*, pp. 8/1-8/6, 1996.

27. Tondu, B. and Lopez, P. "Modeling and control of McKibben artificial muscle robot actuators." *IEEE Control Systems Magazine*, vol. 20, no. 2, pp. 15-38, 2000.

28. Hosoda, K., Takuma, T., and Nakamoto, A. "Design and control of 2D biped that can walk and run with pneumatic artificial muscles." *IEEE-RAS International Conference on Humanoid Robots*, pp. 284-289, 2006.

29. Vanderborght, B., Verrelst, B., Van Ham, R., and Lefeber, D. "Controlling a bipedal walking robot actuated by pleated pneumatic artificial muscles." *Robotica*, vol. 24, no. 4, pp. 401-410, 2006.

30. Aschemann, H. and Schindele, D. "Sliding-mode control of a high-speed linear axis driven by pneumatic muscle actuators." *IEEE Transactions on Industrial Electronics*, vol. 55, no. 11, pp. 3855-3864, 2008.

31. Zhu, X., Tao, G., Yao, B., and Cao, J. "Adaptive robust posture control of a parallel manipulator driven by pneumatic muscles." *Automatica*, vol. 44, no. 9, pp. 2248-2257, 2008.

32. Caldwell, D.G., Razak, A., and Goodwin, M.J. "Braided pneumatic muscle actuators." *IFAC Conference on Intelligent Autonomous Vehicles*, pp. 507-512, 1993.

33. Hannaford, B. and Winters, J.M. "Actuator properties and movement control: biological and technological models." in *Multiple Muscle Systems: Biomechanics and Movement Organization*, chapter 7, pp. 101-120, Springer-Verlag, New York, 1990.

34. Isermann, R. and Raab, U. "Intelligent actuators – Ways to autonomous systems." *Automatica*, vol. 29, no. 5, pp. 1315-1331, 1993.

35. Klute, G.K., Czerniecki, J.M., and Hannaford, B. "Artificial muscles: Actuators for biorobotic systems." *The International Journal of Robotics Research*, vol. 21, no. 4, pp. 295-309, 2002.

CHAPTER 2:

THE CHEMO-MUSCLE ACTUATION SYSTEM

2.1 CHAPTER ABSTRACT

This chapter describes the design and control of a new monopropellant-powered muscle actuation system for robotic systems, especially the mobile systems inspired by biological principles. Based on the pneumatic artificial muscle, this system features a high power density, as well as characteristics similar to biological muscles. By introducing the monopropellant as the energy storage media, this system utilizes the high energy density of liquid fuel and provides a high-pressure gas supply with a simple structure in a compact form. This addresses the limitations of pneumatic supplies on mobile devices and thus is expected to facilitate the future application of artificial muscles on bio-robotic systems. In this chapter, design of the monopropellant–powered muscle actuation system is presented as well as a robust controller design that provides effective control for this highly nonlinear system. To demonstrate the proposed muscle actuation system, an experimental prototype was constructed on which the proposed control algorithm provides good tracking performance.

2.2 INTRODUCTION

The approach presented in this chapter seeks to overcome the lack of a high pressure gas supply by using a special type of liquid fuel, namely monopropellant (such as hydrogen peroxide), as an energy-storing media. This type of liquid fuel can be directly converted into high-pressure hot gas through simple catalytic decomposition. Generally, liquid fuels possess significantly higher energy densities than electrochemical batteries, the most common energy source in mobile robotics. The traditional means of converting chemical energy into useable work often involves heat release through combustion, a process that is inefficient, hard to control, and involves complex hardware. Monopropellants, however, decompose rapidly in the presence of a catalytic material:

$$2H_2O_2 \xrightarrow{catalyst} 2H_2O + O_2 + Heat \quad (2.1)$$

This reaction is strongly exothermic and thus generates a large amount of heat, which, in turn, vaporizes the water and converts the reaction products into a gaseous mixture of steam and oxygen. This gaseous mixture, or hot gas, can be used directly to drive the PAMs in a robotic system. As such, the monopropellant, combined with the catalyst, essentially functions as a compact gas supply with an extremely simple structure and high energy conversion efficiency. Using a monopropellant as a compact form of gas supply was first proposed by Goldfarb et al. [1-4] as a means to drive cylinder-type pneumatic actuators. This technology has been successfully applied to the actuation of robotic arm prostheses [5, 6]. Combining a monopropellant system with the PAM, the new actuation system leverages the high energy density provided by the liquid fuel and the high power density provided by the PAM, and thus offers the potential to improve the performance of mobile robotic systems, especially the bio-robotic systems such as humanoid robots and robotic prostheses/orthoses.

2.3 SYSTEM DESIGN

For a monopropellant-powered muscle actuation system, the original form of energy is essentially the chemical energy stored in the liquid fuel. This chemical energy storage replaces the pressure-related internal energy stored in the compressed air for a traditional PAM actuation system. To reflect this change, this new actuation system is named 'Chemo-muscle' actuation system to distinguish it from the traditional PAM system. A schematic of the Chemo-muscle actuation system is shown in **Figures 2-1 and 2-2** in a rotational and translational setup respectively.

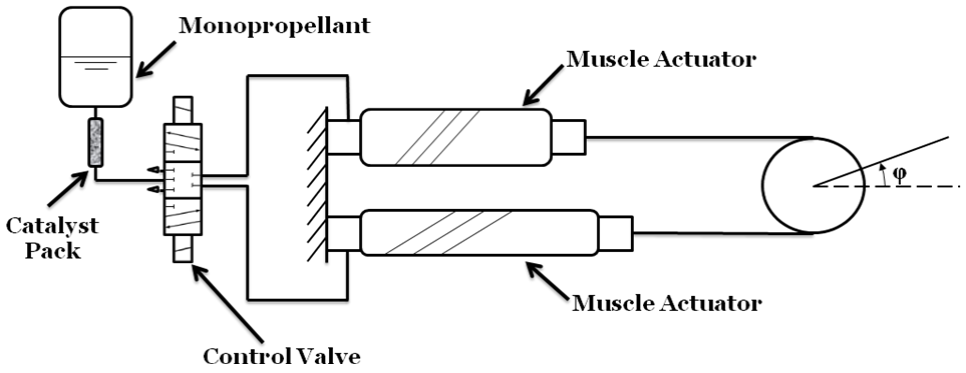

Figure 2-1: Chemo-Muscle Actuation System in a rotational antagonist setup

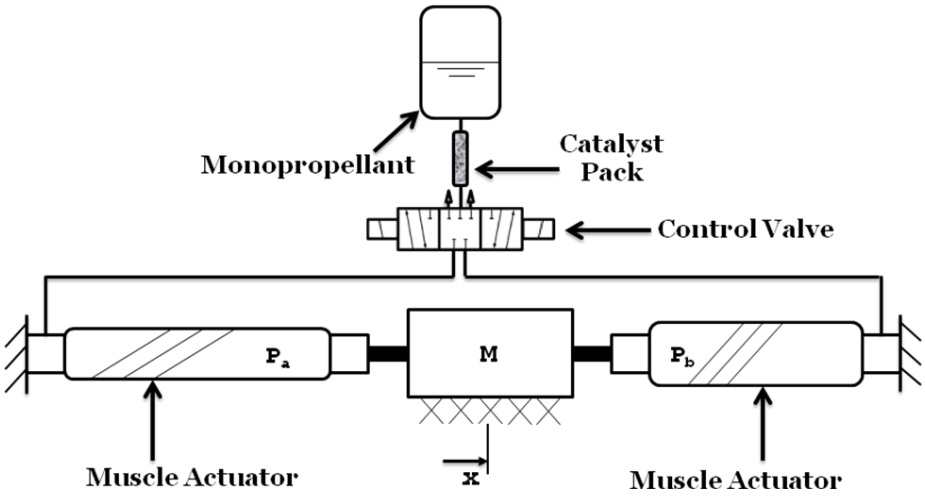

Figure 2-2: The Chemo-Muscle Actuation System in a translational antagonistic setup

In this system, monopropellant is stored in a liquid fuel tank which is pressurized with compressed nitrogen at a constant pressure. This serves as a stable fuel supply without the mechanical complexity of a fuel pump. The outlet of the fuel tank is connected to a catalyst pack, where the monopropellant decomposes upon contact with a certain catalyst and generates hot gas for the purpose of actuation. The outlet of the catalyst pack, in turn, is connected to a hot-gas servo valve that regulates the gas flows to the muscle actuators. With this configuration, a stable supply of pressurized gas can be obtained with minimum hardware requirements.

The pressurized gas in this system is supplied on an on-demand basis. When there is no demand for the hot gas (control valve closed), the downstream impedance can be assumed to be

infinite, and thus the actuator will not draw any flow from the monopropellant tank. When hot gas is needed (control valve opened), the downstream impedance will be lowered correspondingly, and the resulted monopropellant flow will generate the required hot gas through the reaction in the catalyst pack. Such an on-demand supply eliminates the need for hot gas storage through a reservoir, and thus significantly reduces the energy loss through heat dissipation.

Compared with a traditional PAM actuation system, the Chemo-muscle system in **Figures 2-1** and **2-2** only involves modifying the pneumatic supply. As such, a chemo-muscle actuation system can be easily constructed with existing components (PAM, servo valve, and sensors) that have a high temperature rating. Despite its simple construction, the advantages of the Chemo-muscle system are significant. Hydrogen peroxide, a common type of monopropellant, features an energy density of 503 kJ/kg at the concentration of 99%, which is an order of magnitude higher than that of a CO2 cartridge (56 kJ/kg), a typical compressed gas source for mobile applications. To make use of the commercial components, especially the available high-temperature seals and flexible tubing, the concentration of hydrogen peroxide can be lowered to 70% with a corresponding adiabatic decomposition temperature of 232 ºC. Even with the lowered concentration, the corresponding energy density (210 kJ/kg) is still four times that of a CO2 cartridge. This high energy density gas source enables the storage of a large amount of energy in a compact form. Therefore, integrating this source significantly enhances the practicality of an artificial muscle actuation system in mobile robotic systems such as powered prosthetics.

2.4 MODELING THE CHEMO-MUSCLE ACTUATION SYSTEM

To make full use of the potential of the proposed Chemo-muscle actuation system, the control of such systems deserves special attention, not only because of its importance in robotic applications, but also because of the difficulty in the controller design. For the traditional PAM actuation systems, servo control is always considered a challenging problem due primarily to the highly nonlinear nature of these systems. Compared with the traditional system, a Chemo-muscle actuation system utilizes the hot gas from the catalytic reaction of a monopropellant as the working fluid, and thus introduces extra complexity to the control problem. To form a solid foundation for the development of a robust controller a full nonlinear model is presented in this section encompassing all the major nonlinearities of the system. Specifically, a Chemo-muscle actuation system takes the servo valve command (opening area) as the input, and the position of the external load as the output. The whole system involves four major processes: (I) valve flow dynamics, from the valve command to the gas flow rates to the muscle actuators; (II) pressure dynamics, from the gas flow rates to pressure variations; (III) pressure-force relations, from the internal pressure to the corresponding output force; and (IV) load dynamics, from the forces of muscle actuators to load position. Each process will be studied and combined to form a complete dynamic model.

From the control point of view, the total dynamic model takes the form of:

$$x^{(n)} = f(\mathrm{x}, \mathbf{u}) \tag{2.2}$$

where $x^{(n)}$ is the nth derivative of x (the position of the load), x is a vector of the continuous states of the system, and $\mathbf{u}$ is the control input to the system. As such, the development of the nonlinear model starts from the load dynamics, which provides an expression of the second-order derivative of the load position.

2.4.1 LOAD DYNAMICS

To simplify the analysis, a translational system (**Figure 2-2**) is considered in this chapter, and the load dynamics derived accordingly. Note that the methodology proposed in this chapter can be easily extended to a rotational system as shown in **Figure 2-1**. Assuming a combined inertia and viscous load, the load dynamics can be expressed by the following equation:

$$M\ddot{x} + B\dot{x} = F_b - F_a \tag{2.3}$$

where M is the total payload, B is the viscous friction coefficient, Fa and Fb are the actuation forces of the two muscles. Equation (2.3) can be rearranged to obtain the expression of $\ddot{x}$:

$$\ddot{x} = \frac{1}{M}(F_b - F_a - B\dot{x}) \tag{2.4}$$

2.4.2 PRESSURE-FORCE RELATIONS

The dynamics from the pressure in the muscle to the force output is complicated by the unique structure. The specific form of force dynamics used in this chapter is proposed by Chou and Hannaford [7]:

$$F = [\frac{3L^2 - b^2}{4\pi n^2}] \cdot (P - P_{atm}) \tag{2.5}$$

where L is the length of the elastic part of the muscle, b is the length of the inextensible thread in the braided shell, n is the number of turns of the thread over the full length, Patm is the atmosphere pressure, and P is the absolute pressure in the muscle. Also, the lengths of the two opposing muscles can be expressed in terms of the load position x:

$$L_{a,b} = \begin{cases} L_0 + x & \text{for muscle } a \\ L_0 - x & \text{for muscle } b \end{cases} \tag{2.6}$$

where L_0 is the initial length of the muscles. Substituting (2.6) into (2.5), the muscle forces can be obtained as

$$F_{a,b} = [\frac{3(L_{a,b})^2 - b^2}{4\pi n^2}] \cdot (P_{a,b} - P_{atm}) \tag{2.7-2.8}$$

where P_a and P_b are the absolute pressures in the muscles a and b, respectively. Equations (2.7) and (2.8) can be substituted into (2.4) to obtain the expression of $\ddot{x}$ in terms of muscle pressures:

$$\begin{aligned} \ddot{x} = & [\frac{3(L_0 - x)^2 - b^2}{4\pi n^2 M}] \cdot (P_b - P_{atm}) \\ & - [\frac{3(L_0 + x)^2 - b^2}{4\pi n^2 M}] \cdot (P_a - P_{atm}) - \frac{B}{M}\dot{x} \end{aligned} \tag{2.9}$$

2.4.3 PRESSURE DYNAMICS

Based on Equation (2.9), the pressure dynamics are incorporated by differentiating this equation with respect to time.

$$\begin{aligned} \dddot{x} = & [\frac{3(L_0 - x)^2 - b^2}{4\pi n^2 M}] \cdot \dot{P}_b - [\frac{3(L_0 + x)^2 - b^2}{4\pi n^2 M}] \cdot \dot{P}_a \\ & - \frac{3[(L_0 - x)(P_b - P_{atm}) + (L_0 + x)(P_a - P_{atm})]}{2\pi n^2 M}\dot{x} - \frac{B}{M}\ddot{x} \end{aligned} \tag{2.10}$$

To recover the mass flow rates into the muscles, $\dot{P}_a$ and $\dot{P}_b$ can be obtained by studying the thermodynamic process in the muscle actuator. The hot gas generated by the catalytic decomposition of the monopropellant is a mixture of water, steam, and oxygen, which can be considered an ideal gas in the modeling process. Assuming an adiabatic process, the rate of change of the muscle pressure can be expressed by the following equation:

$$\dot{P} = \begin{cases} \dfrac{\gamma R T_{in} \dot{m}_{in}}{V} - \dfrac{\gamma P}{V}\dot{V} & \text{Charging} \\ \dfrac{\gamma R T \dot{m}_{out}}{V} - \dfrac{\gamma P}{V}\dot{V} & \text{Discharging} \end{cases} \tag{2.11}$$

where γ is the ratio of specific heats, R is the universal gas constant, T is the temperature of the gas in the muscle, Tin is the temperature of the gas entering the muscle, V is the volume inside each muscle, and $\dot{m}_{in}$ and $\dot{m}_{out}$ are the mass flow rates entering and leaving the muscle, respectively. The inflow gas temperature Tin can be assumed to be the adiabatic decomposition temperature of the monopropellant. Note that the mass flow rates can be positive (inflow) or negative (outflow). In equation (2.11), the volume V is a function of the muscle length L:

$$V = \frac{L\left(b^2 - L^2\right)}{4\pi n^2} \tag{2.12}$$

which, in turn, is determined by the load position according to (2.6). Substituting (2.6) into (2.12) yields

$$V_{a,b} = \frac{(L_{a,b})\left[b^2 - (L_{a,b})^2\right]}{4\pi n^2} \tag{2.13-2.14}$$

and the corresponding rates of change are:

$$\dot{V}_a = \frac{b^2 - 3(L_0 + x)^2}{4\pi n^2} \cdot \dot{x} \tag{2.15}$$

$$\dot{V}_b = \frac{-b^2 + 3(L_0 - x)^2}{4\pi n^2} \cdot \dot{x} \tag{2.16}$$

As can be seen from the pressure dynamics in equation (2.11), the charging and discharging dynamics are slightly different. This is due to the different temperatures of the charging and discharging mass flows. Note that a single 4-way servo valve is used to regulate

the mass flows, and thus the charging of one muscle is always accompanied by the discharging of the other. As such, substituting (2.11-2.16) into (2.10) gives

$$\ddot{x} = \begin{cases} \dfrac{C_b^+}{M} \cdot \dot{m}_{b,in} - \dfrac{C_a^+}{M} \cdot \dot{m}_{a,out} - \dfrac{K}{M}\dot{x} - \dfrac{B}{M}\ddot{x} \\ \text{Charging b, discharging a} \\ \dfrac{C_b^-}{M} \cdot \dot{m}_{b,out} - \dfrac{C_a^-}{M} \cdot \dot{m}_{a,in} - \dfrac{K}{M}\dot{x} - \dfrac{B}{M}\ddot{x} \\ \text{Charging a, discharging b} \end{cases} \tag{2.17}$$

where

$$C_a^+ = \frac{\gamma RT\left[3(L_0 + x)^2 - b^2\right]}{(L_0 + x)\left[b^2 - (L_0 + x)^2\right]} \tag{2.18}$$

$$C_b^+ = \frac{\gamma RT_{in}\left[3(L_0 - x)^2 - b^2\right]}{(L_0 - x)\left[b^2 - (L_0 - x)^2\right]} \tag{2.19}$$

$$C_a^- = \frac{\gamma RT_{in}\left[3(L_0 + x)^2 - b^2\right]}{(L_0 + x)\left[b^2 - (L_0 + x)^2\right]} \tag{2.20}$$

$$C_b^- = \frac{\gamma RT\left[3(L_0 - x)^2 - b^2\right]}{(L_0 - x)\left[b^2 - (L_0 - x)^2\right]} \tag{2.21}$$

$$\begin{aligned} K = {} & \frac{3\left[(L_0 - x)(P_b - P_{atm}) + (L_0 + x)(P_a - P_{atm})\right]}{2\pi n^2} \\ & + \frac{\gamma\left[3(L_0 + x)^2 - b^2\right]^2 P_a}{4\pi n^2 (L_0 + x)\left[b^2 - (L_0 + x)^2\right]} \\ & + \frac{\gamma\left[3(L_0 - x)^2 - b^2\right]^2 P_b}{4\pi n^2 (L_0 - x)\left[b^2 - (L_0 - x)^2\right]} \end{aligned} \tag{2.22}$$

2.4.4 VALVE FLOW DYNAMICS

The final step in the modeling is to incorporate the valve flow dynamics by expressing the mass flow rates as functions of the valve command (opening area). Assuming the gas flows

are isentropic flows of an ideal gas through a converging nozzle, the mass flow rate is related to the valve command by the following relation:

$$\dot{m}(P_u, P_d, T_u) = A_{v,e}\,\Psi(P_u, P_d, T_u) \tag{2.23}$$

where

$$\Psi(P_u, P_d, T_u) = \begin{cases} \sqrt{\frac{\gamma}{RT_u}\left(\frac{2}{\gamma+1}\right)^{(\gamma+1)/(\gamma-1)}}\, C_f P_u \\ \quad \text{if} \quad \frac{P_d}{P_u} \le C_r \quad \text{(choked)} \\ \sqrt{\frac{2\gamma}{RT_u(\gamma-1)}}\sqrt{1-\left(\frac{P_d}{P_u}\right)^{(\gamma-1)/\gamma}}\left(\frac{P_d}{P_u}\right)^{(1/\gamma)} C_f P_u \\ \quad \text{otherwise (unchoked)} \end{cases} \tag{2.24}$$

In (2.23-2.24), Av,e is the effective valve opening area, Pu and Pd are the upstream and downstream pressures, respectively, T_u is the upstream gas temperature, C_f is the discharge coefficient of the valve (which accounts for irreversible flow conditions), and Cr is the pressure ratio that divides the flow regimes into unchoked (sub-sonic) and choked (sonic) flow through the orifice. Note that with the use of a single servo valve the effective opening areas to the two muscles are related with the following equation:

$$-A_{v,a} = A_{v,b} = A_v \tag{2.25}$$

where A_v is the valve command. According to this equation, a positive command corresponds to the charging of muscle b and the discharging of muscle a, while a negative command corresponds to the opposite. Therefore, the mass flow rates can be expressed as

$$\dot{m}_{a,in} = \begin{cases} 0 & if\ A_v \ge 0 \\ -A_v \cdot \Psi(P_s, P_a, T_{in}) & if\ A_v < 0 \end{cases} \tag{2.26}$$

$$\dot{m}_{a,out} = \begin{cases} -A_v \cdot \Psi(P_a, P_{atm}, T) & if\ A_v \ge 0 \\ 0 & if\ A_v < 0 \end{cases} \tag{2.27}$$

$$\dot{m}_{b,in} = \begin{cases} A_v \cdot \Psi(P_s, P_b, T_{in}) & if\ A_v \geq 0 \\ 0 & if\ A_v < 0 \end{cases} \tag{2.28}$$

$$\dot{m}_{b,out} = \begin{cases} 0 & if\ A_v \geq 0 \\ A_v \cdot \Psi(P_b, P_{atm}, T) & if\ A_v < 0 \end{cases} \tag{2.29}$$

where P_s and P_{atm} are the supply pressure and the atmospheric pressure respectively. Substituting (2.26-2.29) into (2.17) gives

$$\dddot{x} = \begin{cases} \dfrac{C_b^+ \cdot \Psi(P_s, P_b, T_{in}) + C_a^+ \cdot \Psi(P_a, P_{atm}, T)}{M} \cdot A_v - \dfrac{K}{M}\dot{x} - \dfrac{B}{M}\ddot{x} \\ \qquad if\ A_v \geq 0 \\ \dfrac{C_b^- \cdot \Psi(P_b, P_{atm}, T) + C_a^- \cdot \Psi(P_s, P_a, T_{in})}{M} \cdot A_v - \dfrac{K}{M}\dot{x} - \dfrac{B}{M}\ddot{x} \\ \qquad if\ A_v < 0 \end{cases} \tag{2.30}$$

Equation (2.30), with the included functions defined by Equations (2.18-2.22) and (2.24), is the full nonlinear model of the Chemo-muscle system. It can be further rewritten in the following control canonical form:

$$\dddot{x} = \begin{cases} f(\mathbf{x}) + p^+(\mathbf{x}) A_v & if\ A_v \geq 0 \\ f(\mathbf{x}) + p^-(\mathbf{x}) A_v & if\ A_v < 0 \end{cases} \tag{2.31}$$

where

$$f(\mathbf{x}) = -\frac{K}{M}\dot{x} - \frac{B}{M}\ddot{x} \tag{2.32}$$

$$p^+(\mathbf{x}) = \frac{C_b^+ \cdot \Psi(P_s, P_b, T_{in}) + C_a^+ \cdot \Psi(P_a, P_{atm}, T)}{M} \tag{2.33}$$

$$p^-(\mathbf{x}) = \frac{C_b^- \cdot \Psi(P_b, P_{atm}, T) + C_a^- \cdot \Psi(P_s, P_a, T_{in})}{M} \tag{2.34}$$

The state vector $\mathbf{x}$ consists of the pressure in each PAM, along with the position, velocity, and acceleration of the load:

$$\mathbf{x} = \begin{bmatrix} x & \dot{x} & \ddot{x} & P_a & P_b \end{bmatrix}^T \tag{2.35}$$

Note that, in order to simplify the dynamic model as well as the following controller design, the system is assumed to have reached a thermal steady state, i.e. the temperature in the muscles, T, is constant. The small variation in the temperature can be taken as a disturbance, and the corresponding model uncertainty will be addressed by the robust controller in the following section.

2.5 CONTROLLER DESIGN

Based on the full nonlinear model, a robust control approach is developed. The specific control methodology chosen in this work is the sliding mode control [8], which is capable of maintaining control stability and providing a consistent control performance in the presence of model uncertainties and disturbances. First, an integral sliding surface is selected:

$$s = (\frac{d}{dt} + \lambda)^3 \int_0^t e d\tau \tag{2.36}$$

where λ is the positive constant known as the control bandwidth, e is the position error,

$$e = x - x_d \tag{2.37}$$

and x_d is the desired position. A robust control law can be obtained correspondingly:

$$A_v = \begin{cases} \frac{1}{p^+(x)} \left[u_{eq} + u_{rb} \right] & if\ A_v \geq 0 \\ \frac{1}{p^-(x)} \left[u_{eq} + u_{rb} \right] & if\ A_v < 0 \end{cases} \tag{2.38}$$

where u_{eq} is the equivalent control component and u_{rb} is the robustness control component. Note that the control law takes a slightly different form for the positive and negative valve commands due to the discontinuity of the model at $A_v = 0$. Note also that both $p^+(x)$ and $p^-(x)$ are positive, and thus the sign of Av can be solely determined by the sign of $\lfloor u_{eq} + u_{rb} \rfloor$, which is unaffected by the choice between $p^+(x)$ and $p^-(x)$. The expression for the robustness component u_{eq} is derived to achieve the desired motion on the sliding surface $\dot{s} = 0$:

$$u_{eq} = x_d - \hat{f}(\mathbf{x}) - 3\lambda\ddot{e} - 3\lambda^2\dot{e} - \lambda^3 e \tag{2.39}$$

The robustness control component is used to accommodate the model uncertainties and disturbances, which takes the following form:

$$u_{rb} = -G \cdot \mathrm{sgn}(s) \tag{2.40}$$

where G is the robustness gain. In the implementation of the control algorithm, the robustness component (2.40) is slightly modified to introduce a boundary layer for the purpose of reducing chatter in the control signal:

$$u_{rb} = -G \cdot \mathrm{sat}(\frac{s}{\Phi}) \tag{2.41}$$

where Φ is the thickness of the boundary layer. Based on the derivations above, a complete control algorithm is obtained by combining Equation (2.38) with (2.39) and (2.41), which can be used to calculate for the valve command based on the system states (2.35) in real-time implementation.

2.6 EXPERIMENTAL RESULTS

An experimental setup described in **Figure 2-2** was constructed to demonstrate the effectiveness of the proposed Chemo-muscle actuation system. A photo of the setup is shown in **Figure 2-3**. Note that most components in the system are commercially available, including the artificial muscles (FESTO DMSP-20-150N-RM-CM) and the 4-way proportional servo valve (FESTO MPYE-5-M5-010-B). In the experiments these components functioned reliably under repeated testing.

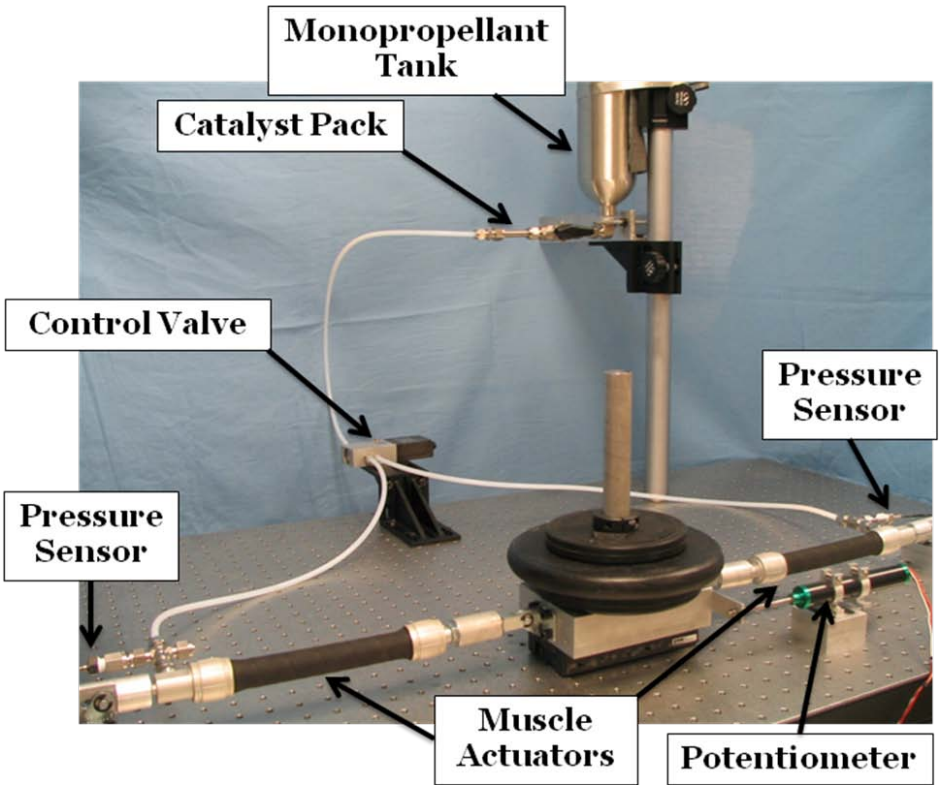

Figure 2-3: Experimental setup of The Chemo-Muscle Actuation System.

As the fuel source, hydrogen peroxide was stored in a stainless steel tank, which was pressurized with nitrogen at an absolute pressure of 653 kPa (94.7 psi). The concentration of the hydrogen peroxide is limited to 70% so that the corresponding adiabatic decomposition

temperature (232 ºC) does not exceed the thermal limit of the flexible components such as the PTFE tubing.

The outlet of the fuel tank is connected to a catalyst pack consisting of a 5-cm (2 in) long, 1-cm (3/8 in) diameter stainless steel tube packed with catalytic particles (iridium). The catalyst pack, in turn, is connected to the servo valve through flexible tubing to provide a steady supply of hot gas. For the power output of this actuation system, a pair of PAMs are used to drive a 10.8 kg mass, which is supported on a linear stage (Parker 4606) for a one-dimensional linear motion.

For the implementation of the control algorithm, the system states as defined by (35), including the pressures in the muscles and the position, velocity, and acceleration of the load, are required. To obtain the values of these state variables, a pair of high-temperature pressure sensors (Measurement Specialties EPXO-X01-300P-/Z38) were used to measure the pressures and a linear potentiometer (Midori LP-100F) was used to measure the position. The velocity and acceleration were obtained via filtered differentiation of the position signal with a cut-off frequency of 25 Hz.

The control performance was characterized by the sinusoidal tracking at different frequencies. **Figures 2-4 and 2-5** show the sinusoidal tracking performances of the Chemo-muscle actuation system at 0.5 Hz and 1.0 Hz respectively. The close match between the commanded and measured motions indicates the effectiveness of this actuation system. Note that the tracking performance degraded at higher frequencies, especially at motion reversals (i.e., near zero velocity). The possible reasons include the choked flow through the proportional valve, which limits the actuation power, and the hysteresis and friction/stiction in the actuator,

the effect of which becomes more significant in high-frequency motions. To provide more insight on the control algorithm, the valve commands are also included in **Figures 2-4** and **2-5**. As the plots of the valve commands indicate, the high-frequency switching in the command is small in magnitude as a result of the introduction of the boundary layer in the sliding mode controller and the fine tuning of the control parameters in Equation (2.41).

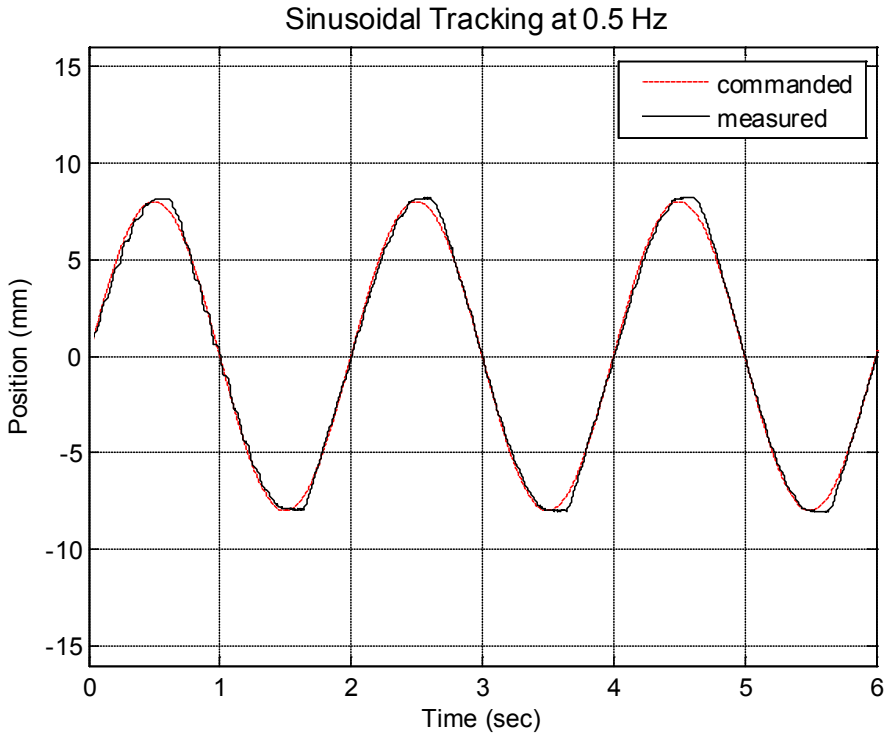

(a)

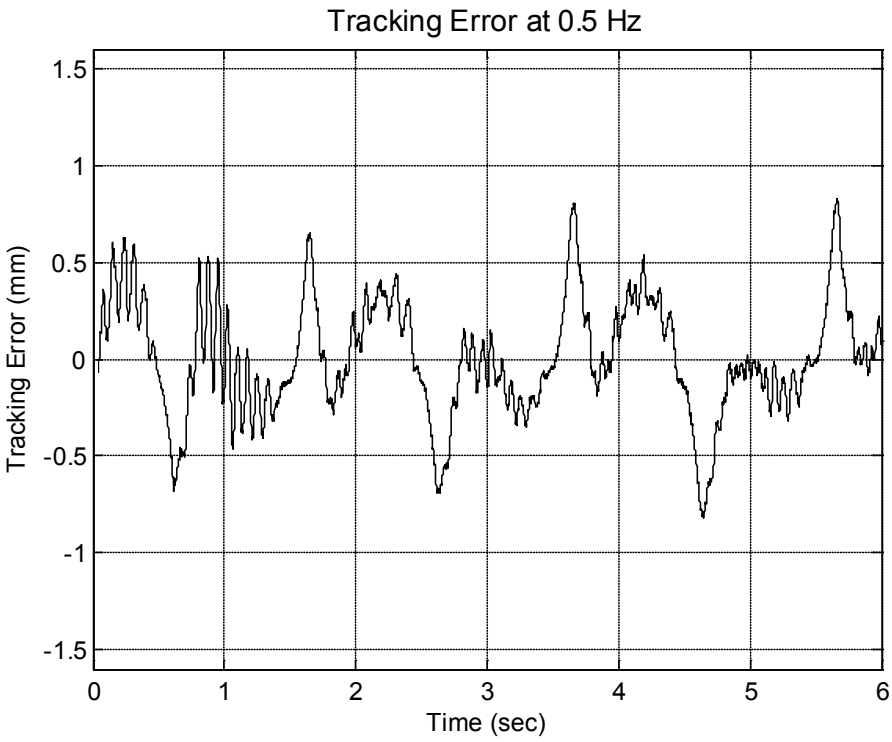

(b)

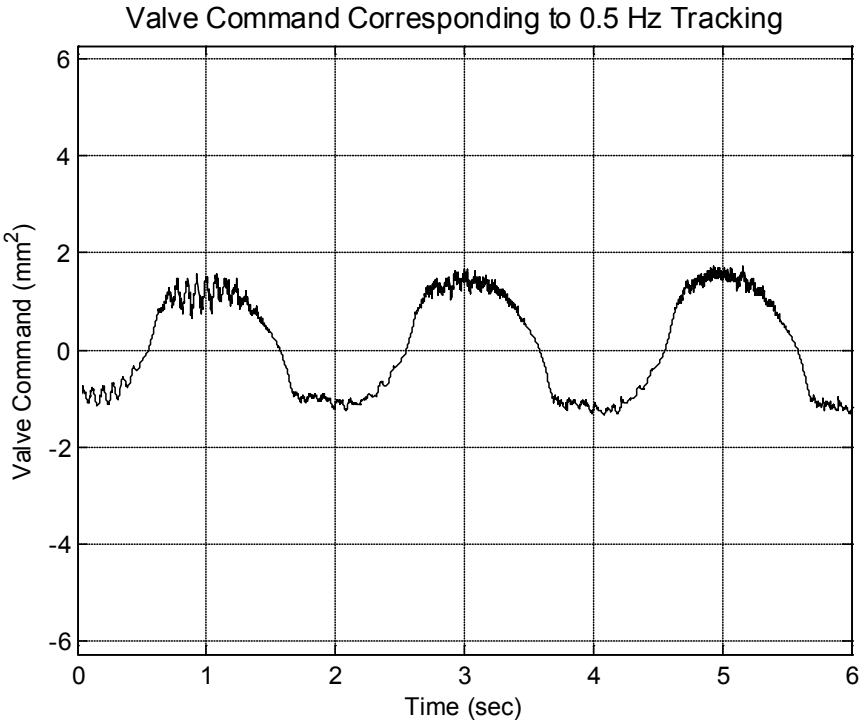

(c)

Figure 2-4: Control performance in the 0.5 Hz sinusoidal tracking: (a) commanded and measured motion; (b) tracking error; and (c) valve command.

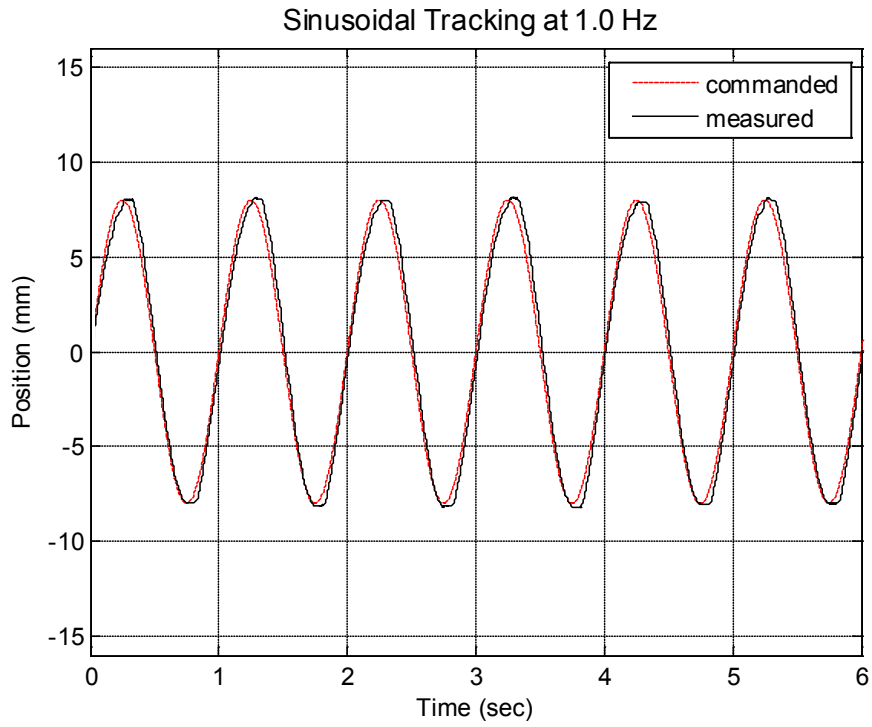
Sinusoidal Tracking at 1.0 Hz
commanded
measured
Position (mm)
Time (sec)
15
10
5
0
-5
-10
-15
0
1
2
3
4
5
6

(a)

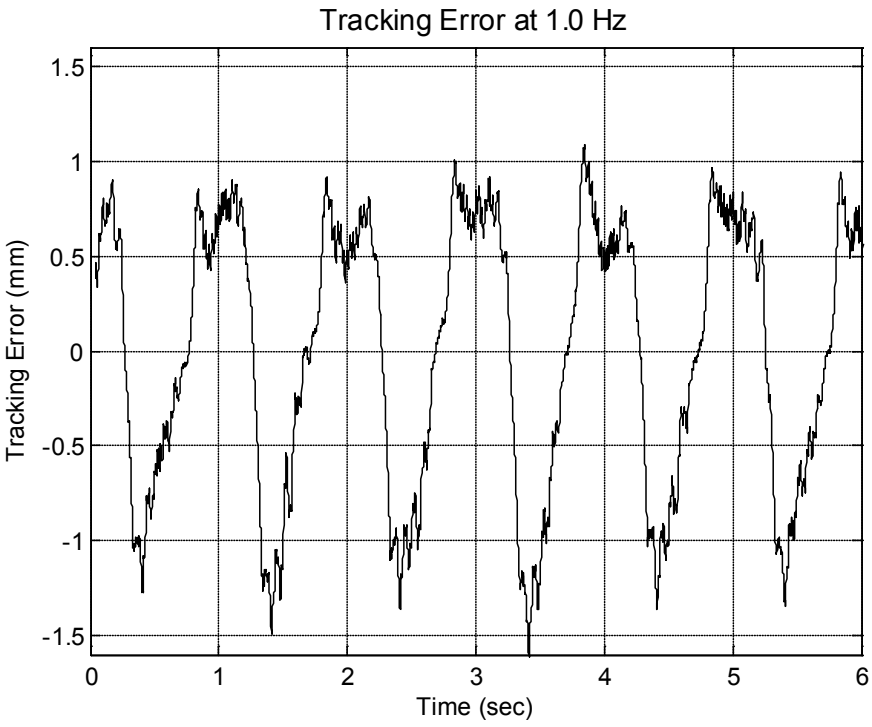
Tracking Error at 1.0 Hz
Tracking Error (mm)
Time (sec)
1.5
1
0.5
0
-0.5
-1
-1.5
0
1
2
3
4
5
6

(b)

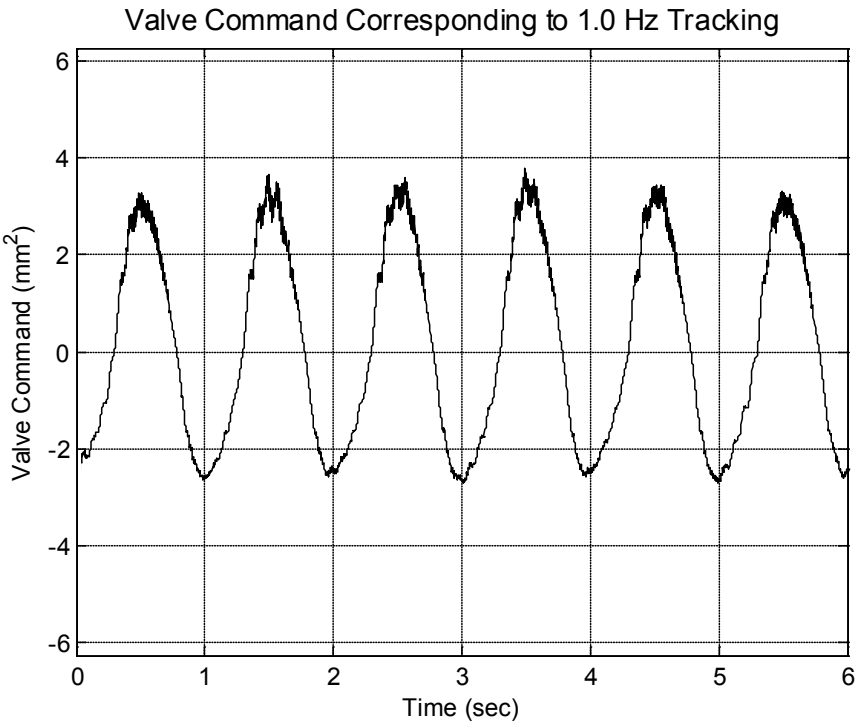

(c)

Figure 2-5: Control performance in the 1.0 Hz sinusoidal tracking: (a) commanded and measured motion; (b) tracking error; and (c) valve command.

2.7 CONCLUSIONS

This chapter presents the design and control of the Chemo-muscle actuation system, a new actuation system for robotic applications. In this system, a special type of liquid fuel, a monopropellant, functions as the energy storage media decomposing instantaneously upon contact with certain catalytic materials to generate a large amount of gaseous product used to power the artificial muscle actuators. Therefore, the proposed system leverages the high energy density of the liquid fuel combining it with the pneumatic artificial muscle actuator, which features a high power density and similar characteristics to biological muscles. The result is an actuation system that provides excellent performance with a compact package and simple structure. For the design of the system, a configuration was proposed that provides a stable gas supply with minimum hardware required. Based on this configuration, a dynamic model was

developed that encompasses all the major nonlinearities in the system and forms the foundation of the subsequent controller design. The controller for this system was developed with the standard sliding mode control approach which provides robust control in the presence of model uncertainties and disturbances. To demonstrate the Chemo-muscle actuation system, an experimental prototype was constructed. This prototype functioned reliably under repeated testing, and the effectiveness of the robust controller was demonstrated with results in sinusoidal tracking at different frequencies.

REFERENCES

1. Gogola, M.A., Barth, E.J., and Goldfarb, M. "Monopropellant powered actuators for use in autonomous human-scaled robotics." in *Proceedings of the 2002 IEEE International Conference on Robotics & Automation*, pp. 2357-2362.

2. Goldfarb, M., Barth, E.J., Gogola, M.A., and Wehrmeyer, J.A. "Design and energetic characterization of a liquid-propellant-powered actuator for self-powered robots." *IEEE/ASME Transactions on Mechatronics*, vol. 8, no. 2, 2003.

3. Fite, K.B. and Goldfarb, M. "Design and energetic characterization of a proportional-injector monopropellant-powered actuator." *IEEE/ASME Transactions on Mechatronics*, vol. 11, no. 2, 2006.

4. Shields, B.L., Fite, K.B., and Goldfarb, M. "Design, control, and energetic characterization of a solenoid-injected monopropellant-powered actuator." *IEEE/ASME Transactions on Mechatronics,* vol. 11, no. 4, 2006.

5. Fite, K.B., Withrow, T.J., Shen, X., Wait, K.W., Mitchell, J.E., and Goldfarb, M. " A gas-actuated anthropomorphic prosthesis for transhumeral amputees." *IEEE Transaction on Robotics,* vol. 24, no. 1, pp. 159-169, 2008.

6. Withrow, T.J., Shen, X., Mitchell, J.E., and Goldfarb, M. "A forearm actuation unit for an upper extremity prosthesis." *IEEE International Conference on Robotics and Automation*, pp. 2459-2464, 2008.

7. Chou C.-P. and Hannaford, B., "Measurement and modeling of McKibben pneumatic artificial muscles," *IEEE Transactions on Robotics and Automation*, vol. 12, no. 1, pp. 90 – 102, 1996.

8. Slotine, J.J.E., and Li, W. *Applied Nonlinear Control.* Prentice-Hall, Inc., New Jersey, 1991.

CHAPTER 3:

REDUCING EFFECTIVE VOLUME OF PNEUMATIC ARTIFICIAL MUSCLE WITH COMPONENT INTEGRATION

3.1 ABSTRACT

Pneumatic artificial muscle (PAM) is a class of flexible muscle-like actuator with a low structure weight and high power density. With its high performance, the PAM can be used to power robotic systems with strict weight and volume limitation, such as the mobile robots. In this paper, an integrated PAM design is presented, which incorporates peripheral elements, especially the control valves, in the interior space of the actuator to reduce the complexity and volumetric profiles of PAM-actuated robotic systems. More importantly, the incorporated components are expected to largely eliminate the dead volume in the PAM actuator, and improve the energy efficiency in the operation. An energy consumption analysis is presented, which provides an estimation of the maximum percentage of energy saving that can be achieved with the integrated design. A practical design of the integrated PAM actuator is presented as well, incorporating the standard poppet valves to control the mass flow from the supply to the PAM, or that from the PAM to the atmosphere. To demonstrate the energy saving effect of the proposed integrated PAM actuator, experiments were conducted with a commercial PAM actuator, which was modified to incorporate a solid bar to simulate the integrated components. Experimental results indicated an energy saving effect of up to 13%, which is expected to increase significantly with the custom-made integrated PAM actuators in the future.

3.2 INTRODUCTION

Mimicking the biological principles has been a major trend in modern robotics research [1,2]. Leveraging the underlying biological principles, a biorobotic system is expected to enjoy the similar advantages to its biological counterparts. In the biorobotics research, a fundamental challenge is to develop a robotic counterpart for skeletal muscles, not only for the output of force and power, but also for the implementation of biological control strategies for a safe and natural interaction with the environment [3,4]. To address this challenge, researchers have investigated a variety of technical routes, including the modification of traditional actuators (e.g. DC motors) to introduce controllable compliance [5-7], and the exploration of new actuation principles to simulate skeletal muscle characteristics (e.g. piezoelectric and shape memory alloy actuators [8-9]).

Among these efforts, pneumatic artificial muscle (PAM) stands out as a high competitive approach. As discussed in Section 1.3.2, a PAM is composed of an air-tight tube surrounded by an inextensible mesh. When the interior volume is pressurized, the tube expands in the radial direction and shortens in the axial direction, generating a pulling force to the external load. As determined by this process, the PAM has a very simple structure, and its power density (power output per unit of weight) is considerably higher than other actuators due to the light-weight nonmetal structure. Moreover, the actuation force decreases with the shortening in length, which can be utilized to simulate the elastic behavior of biological skeletal muscles [10]. With these unique characteristics, PAM has seen extensive use in robotics, including humanoid robots [11-13] and robotic rehabilitation devices [14-16].

Utilizing compressed air as the working fluid, PAM is a pneumatic actuator per se. However, the kinetic characteristics of PAM are fundamentally different from traditional pneumatic

actuators. Specifically, traditional pneumatic actuators generate power output with a moving piston or vane driven with gas pressure. The PAM, on the other hand, generates power output through the inflation – contraction of the flexible membrane. Without the moving elements sweeping through the internal space, the PAM contains a dead space at 60% ~ 75% of the equilibrium internal space (depending on the maximum percentage of shortening), which provides a potential for integrating the peripheral components (control valve and various sensors) and obtaining an encapsulated actuation package (**Figure 3-1**). Furthermore, by eliminating this dead space with integrated components, the resulted PAM design can provide additional benefits in actuator performance, especially the significantly reduced energy consumption. In the existing literature, Davis and Caldwell proposed the integration of valves and sensors into the PAM design to better fit into a humanoid robotic system [17]. However, the potential benefits associated with the reduction of the dead space were not realized or discussed.

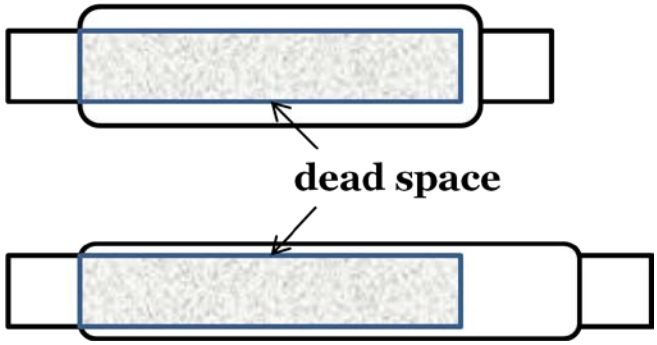

Figure 3-1: Dead space in the PAM.

In this chapter, we propose the concept of integrating peripheral components into the PAM design to obtain a more compact and high-performance encapsulated actuator. Such integrated design eliminates the need of adding peripheral components, and thus reduces the weight, volume, and complexity of the whole robotic system. More importantly, the integrated

components occupy the unused dead space in the PAM, thus reduces the energy consumption by decreasing the internal volume for pressurizing and depressurizing. In the subsequent sections, the energy-saving mechanism with the proposed integrated PAM design will be analyzed. To realize the potential energy saving, we propose an integrated PAM actuator design, which incorporates control valves into the dead volume to modulate the gas flows into and out of the actuator. For the last part of the paper, experiments were conducted to demonstrate the benefits with the proposed integrated PAM actuator design, and conclusions were presented based on these results.

3.3 ENERGY-SAVING MECHANISM

The PAM features a light-weight structure and high output force, and thus has a potential to be used in mobile robotic systems, which have strict weight and volume limitations. For a mobile robotic system, energy consumption of the actuator directly affects the duration of operation, and thus has a significant effect on the performance. As such, reducing the energy consumption makes an important research topic in the effort of improving the practicality of mobile robotic systems.

The proposed integrated design reduces the energy (i.e. compressed air) consumption by decreasing the effective volume to be pressurized and depressurized. For a quantitative analysis, consider a traditional PAM actuator and an identical PAM actuator in the integrated design are utilized to generate the same force trajectory over a certain period of time:

$$F_{tr} = F_{in} = F(t),\ t = 0 \sim T \tag{3.1}$$

where the subscripts '*tr*' and '*in*' represents the traditional and integrated designs, respectively. According to the existing results on the pressure-force relation, such as the model by Chou and

Hannaford [18], the actuation force generated by a PAM can be expressed as a function of the internal pressure in the PAM and the rate of change of the internal volume:

$$F = -(P - P_{atm})\frac{dV}{dL} \tag{3.2}$$

In the proposed integrated design, the components are of a constant volume, and thus the rate of change of the internal volume will not be affected. Accordingly, the same force trajectory requires the same pressure trajectory as well:

$$P_{tr}(t) = P_{in}(t) = P(t),\ t = 0 \sim T \tag{3.3}$$

For the simplicity of the analysis, an isothermal assumption is adopted, which assumes that the air mass in the actuator can be expressed as a function of the pressure and volume:

$$m = \frac{PV}{RT} \tag{3.4}$$

Define the internal volume of the traditional design as V_{tr}, and assume that the integrated components occupy a fixed volume of V_c, and thus the internal volume of the integrated design V_{in} can be expressed as:

$$V_{in} = V_{tr} - V_C \tag{3.5}$$

Furthermore, to facilitate the comparison between the two designs, a volumetric ratio between V_C and V_{tr} is defined as

$$\alpha = \frac{V_C}{V_{tr}} \tag{3.6}$$

As such, V_{in} can be expressed as a function of V_{tr}:

$$V_{in} = (1-\alpha)V_{tr} \tag{3.7}$$

Note the ratio α is not a constant, but instead is a function of V_{tr}, which in turn is a function of the length of the PAM. Combining (3.4) and (3.7), the following relation between the air mass values can be obtained:

$$m_{in} = \frac{PV_{in}}{RT} = (1-\alpha)\frac{PV_{tr}}{RT} = (1-\alpha)m_{tr} \tag{3.8}$$

where m_{in} and m_{tr} are the air masses in the integrated PAM and the traditional PAM, respectively. The equation above can be differentiated to obtain the mass flow rate:

$$\dot{m}_{in} = (1-\alpha)\dot{m}_{tr} - \dot{\alpha}\, m_{tr} \tag{3.9}$$

Note that, since the ratio α is a function of the PAM length, and thus the rate of change of α is determined by the load dynamics, which is usually significantly slower than the pressure dynamics. As such, in Eq. (3.9), the first term dominates, and thus the equation can be approximated by the following equation:

$$\dot{m}_{in} = (1-\alpha)\dot{m}_{tr} \tag{3.10}$$

To calculate the cumulative energy consumption, the pressurizing gas flow rate can be integrated over the period of time:

$$E_{in} = \int_0^T pos(\dot{m}_{in})dt = \int_0^T (1-\alpha)\cdot pos(\dot{m}_{tr})dt \tag{3.11}$$

where the function *pos(x)* is defined as

$$pos(x) = \begin{cases} x & when\ x \geq 0 \\ 0 & when\ x < 0 \end{cases} \tag{3.12}$$

To obtain a simplified conclusion, assuming the range of motion is small, and thus the volume ratio α can be assumed to be nearly constant:

$$E_{in} = \int_0^T (1-\alpha) \cdot pos(\dot{m}_{tr}) dt = (1-\alpha) \cdot \int_0^T pos(\dot{m}_{tr}) dt = (1-\alpha) E_{tr} \tag{3.13}$$

Equation (3.13) essentially provides an approximate estimation of the maximum energy saving effect by the proposed integrated PAM design, with the value of α as the percentage of the energy saving. As shown in **Figure 3-1**, the maximum allowable space for the integrated components is a cylindrical space, whose length is determined by the maximum shortening. Take the commercially available FESTO PAMs (DMSP/MAS series, FESTO, Germany) as an example. With a maximum shortening at 25%, the integrated components can be as long as 75% of the initial length of the internal space. As such, the maximum value of α (without shortening) can be as high as 0.75, representing a 75% decrease in energy consumption according to (3.13). With the increase of the shortening, the total volume in the PAM increases, which results in a smaller value of α and thus a lower percentage of energy saving. In spite of this, the integrated design still has a potential to generate a considerable amount of energy saving, and thus significantly improve the performance of the PAM actuated robotic systems.

3.4 A PRACTICAL DESIGN WITH VALVE INTEGRATION

To obtain a complete PAM actuation system for robotic applications, multiple peripheral components are required to provide essential sensing and control capabilities. The components include the sensors (e.g. potentiometers and pressure transducers) to provide system state feedback, and the control valves to regulate the mass flow into and out of the actuator. Note that,

to achieve the potential energy saving as shown in the preceding section, the integrated components are expected to take a significant portion of the internal space of the PAM. As such, in the design presented in this section, only the control valves are considered, primarily due to the larger volume as compared with sensors. Furthermore, with the valve integrated into the PAM, it eliminates the need for the connection pipelines, and thus minimizes the time delay in the mass flow control.

Figure 3.2 shows the structure of the valve. For the simplicity of the design, on each end of the PAM, a two-way poppet valve is attached to control the pressurizing flow from the gas supply, or the depressurizing flow to the atmosphere. With this structure, the position of the valve body can be easily adjusted in the axial direction, for the purpose of adjusting the internal volume to be occupied. Furthermore, the independent pressurizing/depressurizing valves allow a higher level of flexibility in determining the inflow-outflow capabilities. The internal structure of the valve is shown in **Figure 3.3**. Leveraging the standard 2-way poppet valve design, the valve spool is driven with a solenoid for the on-off control. With this standard design, the existing poppet valves can be easily incorporated in the design and fabrication of the proposed integrated PAM actuator. Also, on the inner end of the valve, a soft bumper is attached to absorb the possible shock load during contact, and the adjustable length of the bumper provides extra flexibility in occupying the internal volume to obtain the greatest possible energy saving effect. Note that the design can be easily modified to obtain a proportional control capability by utilizing a voice coil instead of the solenoid for the actuation of the valve spool.

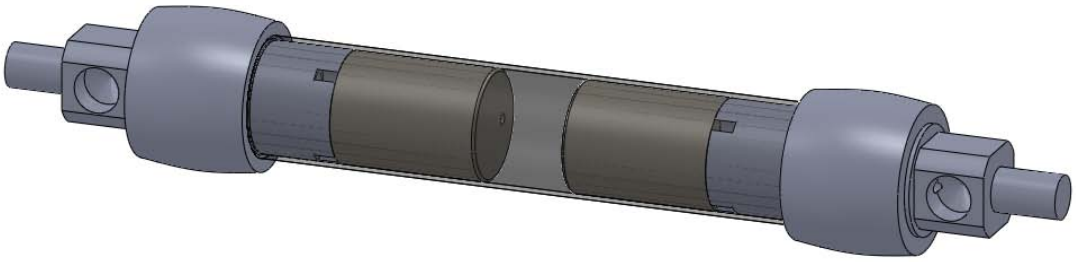

(a)

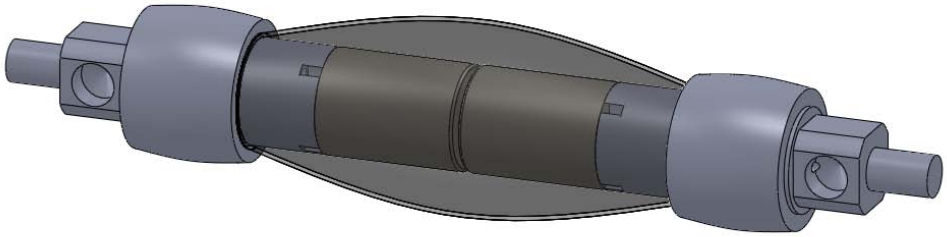

(b)

Figure 3-2: The overall structure of the integrated PAM design: (a) At-rest state; (b) Inflated state.

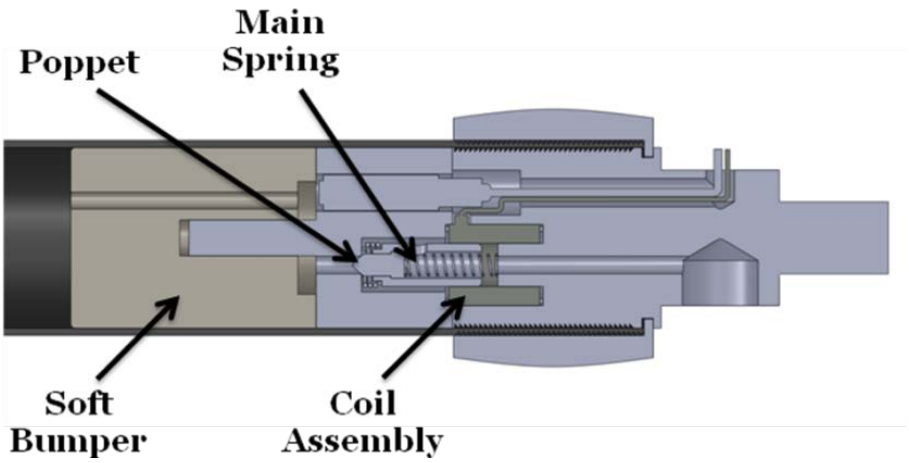

(a)

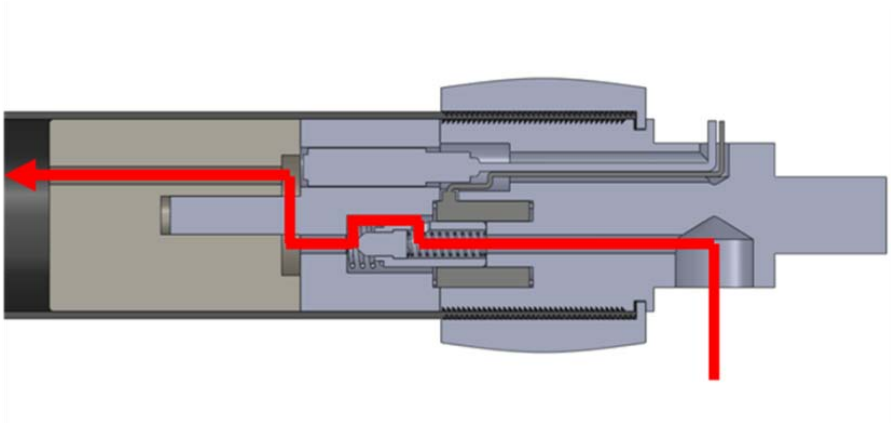

(b)

Figure 3-3: The internal structure of the poppet valve incorporated into the PAM actuator (a) and the pathway for the air flow (b) when the valve is switched on.

3.5 SIMULATED EXPERIMENTS

To demonstrate the energy saving effect provided by the integrated PAM design, experiments were conducted with a simulated integrated PAM actuator. Due to the considerable amount of effort involved in manufacturing an integrated PAM actuator (such as the design as shown in **Figures 3-2** and **3-3**), a commercial PAM actuator (Model DMSP-20-150N-RM-CM, FESTO, Germany) was modified to include a solid cylindrical bar, which simulates the components integrated in the PAM. **Figure 3-4** shows the comparison of the original PAM actuator and the integrated solid bar. The design parameters are summarized in **Table 3-1**.

Table 3-1. Design parameters for the simulated PAM actuator with the integrated bar.

Parameter	Description	Value	Unit
L_0	PAM at-rest length	150	mm
D_0	PAM at-rest diameter	20	mm
L_B	Bar length	112.5	mm
D_B	Bar diameter	16	mm
α_0	At-rest volumetric ratio	0.48	

Figure 3-4: The PAM actuator and the incorporated solid bar for the simulated experiments.

The PAM actuator is essentially a single-acting actuator, which only generates a pulling force in the actuation. To enable a reciprocating motion without the complexity of an antagonistic configuration, a vertical weight-lifting experimental setup was constructed (**Figure 3-5**). In this system, the PAM actuator, suspended from a fixed socket, drives the motion of the attached 10 lb (4.5 kg) weight. To measure the cumulative energy consumption, a 1-gallon (3.785 L) air tank was utilized as the pneumatic supply, which was pressurized to 70 psig (552 kPag) before running each experiment. During the experiment, the pressure in the tank was measured as an indication of the cumulative energy consumption. Specifically, assuming the air in the supply tank is an ideal gas undergoing an isothermal process, the energy in the fixed-volume tank is proportional to the mass, which is in turn proportional to the pressure in the tank. As such, the pressure drop in the supply tank is proportional to the cumulative energy supply in the experiment. In the experiments, a pair of pressure transducers (SDET-22T-D25-G14-U-M12, FESTO, Germany) was used to measure the pressures in the supply tank and the PAM actuator, and a linear potentiometer (LP-100F, Midori, Japan) was used to measure the displacement of the load. Also, a 4-way proportional control valve (MPYE-5-M5-010-B,

FESTO, Germany) was used to modulate the airflow into or out of the PAM actuator for the servo control purpose.

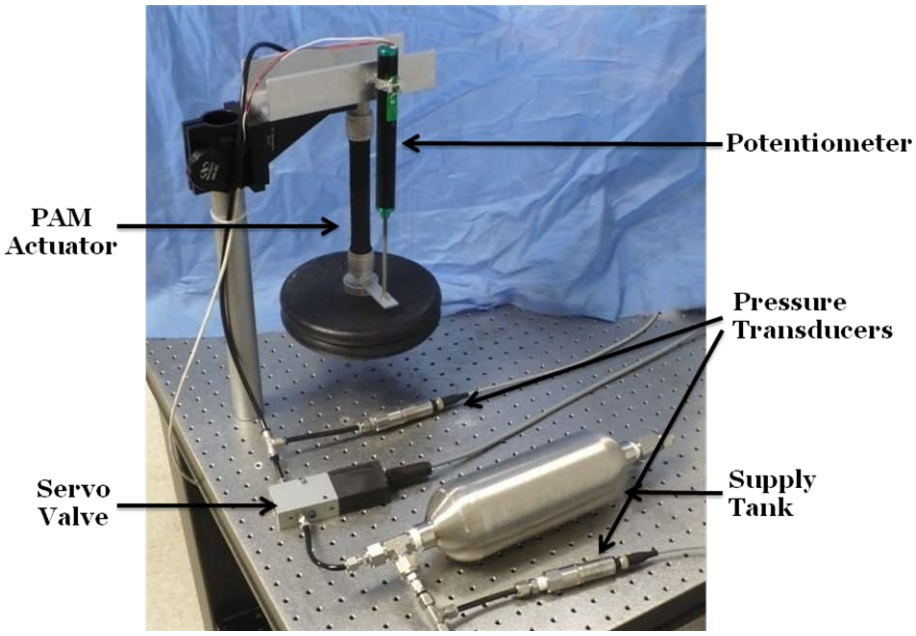

Figure 3-5: The experimental setup.

In the experiments, both the original unmodified PAM actuator and the modified PAM actuator (with the solid bar simulating the integrated components) were tested. The PAM actuators were controlled to track a square-wave reference signal, which essential provides step inputs in both directions. The control signal to the servo valve was generated with a standard proportional controller. A typical control performance is shown in **Figure 3-6**. Note that, since the control performance is not the emphasis of this work, the control gain was tuned to obtain an acceptable performance without excessive oscillation. As shown in **Figure 3-6**, the tracking performances of the original and modified PAM actuators are essentially unchanged. The energy consumption, as indicated by the pressure drop in the supply tank, was also recorded and is shown in **Figure 3-7**. As shown in this figure, the pressure drop associated with the original

PAM actuator is always greater than that associated with the modified PAM actuator, demonstrating the energy saving effect provided by the integrated design.

Note that the energy saving effect is determined by the volumetric ratio α, according to Eq. (3.13). Also, the internal volume of the actuator increases with the contraction, which results in a reduction of α, as indicated by Eq. (3.6). As such, the energy saving effect is highly related to the contraction of the PAM actuator. For a comprehensive evaluation of the energy saving effect, square input tracking experiments at different percentages of contraction was conducted, with the results shown in **Figure 3-8**. As can be observed in this figure, the energy saving is most significant when the contraction is small, and gradually reduces with the increase of the contraction. Note that there is a discrepancy between the largest energy saving obtained in the experiments (13%) and the theoretical prediction according the value of α_0 (48%). The primary reason, presumably, is that there is a significant volume associated with the tubing between the servo valve and the PAM actuator, essentially increasing the total internal volume and reducing the effective volumetric ratio α. Furthermore, the prediction by Equation (3.13) is accurate only when the contraction is minimal (close to 0), and thus the volume increase associated with the smallest contraction in the experiments (3%) also contributes to the deviation from the predicted value. Note that, in a custom-designed PAM actuator with integrated components, the volume associated with the connection tubing will be completely eliminated. Also, a custom-designed actuator is expected to occupy a higher percentage of the internal volume, and thus provide a more significant energy saving effect.

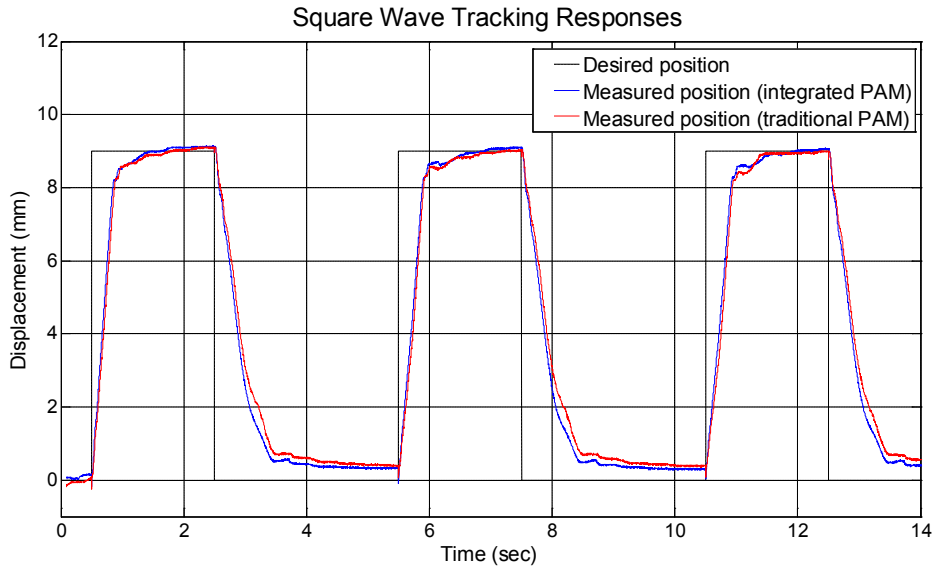

(a)

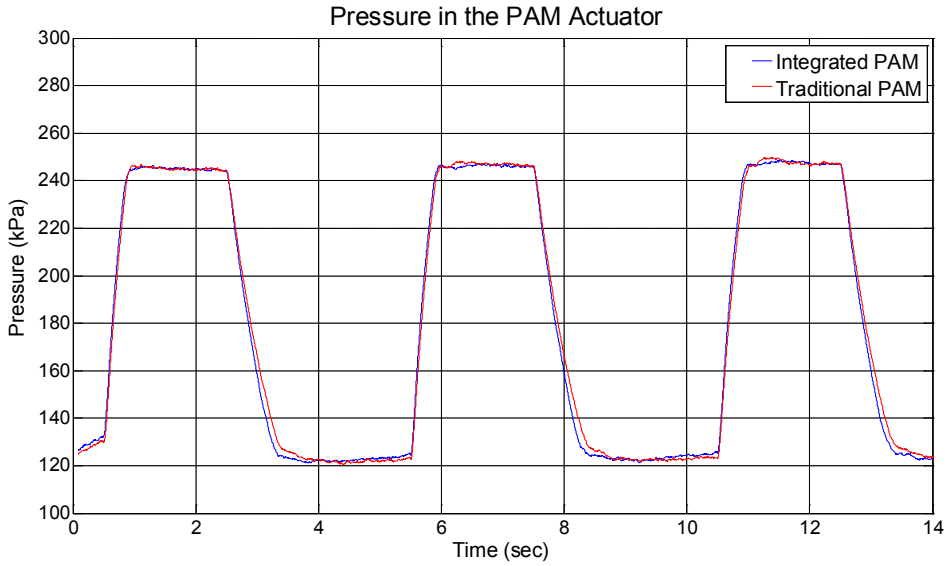

(b)

Figure 3-6: Comparison of tracking performance (a) and pressure change in the actuator (b) of the integrated PAM actuator versus the traditional PAM actuator.

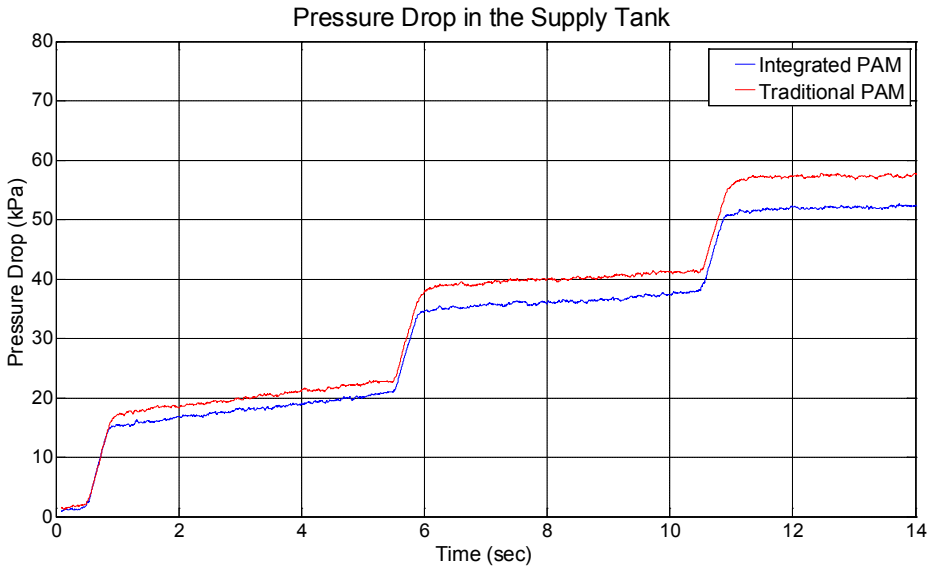

Figure 3-7: The pressure drop in the supply tank, indicating the energy consumption in the experiment.

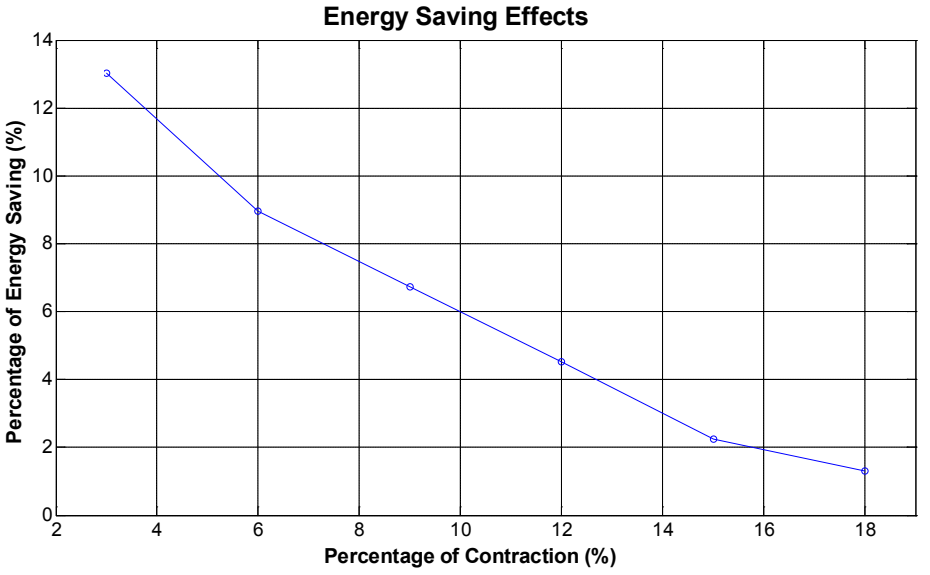

Figure 3-8: Energy saving effects provided by the integrated design.

3.6 CONCLUSIONS

This paper presents a novel PAM actuator design that eliminates the unaffected dead space in the internal volume by integrating the peripheral elements (especially the control valves). Such integrated design not only reduces the complexity and volumetric profiles of PAM-actuated robotic systems, but also generates a considerable amount of energy saving by decreasing the internal volume for pressurizing/depressurizing. An energy consumption analysis was conducted to provide an estimate of the maximum percentage of energy saving. A practical PAM design was presented, incorporating the standard poppet valves to control the mass flow from the supply to the PAM, or that from the PAM to the atmosphere. Finally, experiments were conducted to demonstrate the energy saving effects of the proposed integrated PAM actuator, which was simulated with a commercial PAM actuator modified with a solid bar to simulate the integrated components. Experimental results indicated an energy saving effect of up to 13%, which is expected to increase significantly with the custom-made integrated PAM actuators in the future.

REFERENCES

1. Beer, R.D., Quinn, R.D., Chiel, H.J., and Ritzmann, R.E. (1997) "Biologically inspired approaches to robotics." *Communications of the ACM*, vol. 40, no. 3, pp. 31-38.

2. Sharkey, N.E. (2002) "Biologically inspired robotics." *Handbook of Brain Theory and Neural Networks*, 2002.

3. Hogan, N. (1984) "Adaptive control of mechanical impedance by coactivation of antagonist muscles." *IEEE Transactions on Automatic Control*, vol. 29, no. 8, pp. 681-690.

4. Hogan, N. (1985) "The mechanics of multi-joint posture and movement control." *Biological Cybernetics*, vol. 52, pp. 315-331.

5. Koganezawa, K. and Yamazaki, M., 1999, "Mechanical stiffness control of tendon-driven joints," in *Proceedings of the IEEE/RSJ International Conference on Intelligent Robots and Systems*, pp. 818–825.
6. Koganezawa, K. and Ban, S., 2002, "Stiffness Control of Antagonistically Driven Redundant DOF Manipulator," in *Proceedings of the IEEE/RSJ International Conference on Intelligent Robots and Systems*, pp. 2280-2285.

7. English, C.E. and Russell, D., 1999, "Implementation of variable joint stiffness through antagonistic actuation using rolamite springs," *Mechanism and Machine Theory*, vol. 34, no. 1, pp. 27-40.

8. Secord, T.W., Ueda, J., and Asada, H.H. (2008) "Dynamic analysis of a high-bandwidth, large-strain, PZT cellular muscle actuator with layered strain amplification." *Proceedings of IEEE International Conference on Robotics and Automation*, pp. 761-766.

9. Ikuta, K. (1990) "Micro/miniature shape memory alloy actuator." *Proceedings of the IEEE/RSJ International Conference on Intelligent Robots and Systems*, pp. 2156-2161.

10. Klute, G.K., Czerniecki, J.M., and Hannaford, B. (2002) "Artificial Muscles: Actuators for Biorobotic Systems." *The International Journal of Robotics Research*, vol. 21, no. 4, pp. 295-309.

11. Caldwell, D.G., Medrano-Cerda, G.A., and Bowler, C.J. (1997) "Investigation of bipedal robot locomotion using pneumatic muscle actuators." *IEEE International Conference on Robotics and Automation*, Albuquerque, NM, pp. 799-804.

12. van der Linde, R.Q. (1998) "Active leg compliance for passive walking." *IEEE International Conference on Robotics and Automation*, San Antonio, TX, pp. 2635-2640.

13. Hosoda, K., Takuma, T., and Nakamoto, A. (2006) "Design and control of 2D biped that can walk and run with pneumatic artificial muscles." *IEEE-RAS International Conference on Humanoid Robots*, pp. 284-289.

14. Klute, G., Czerniecki, J., and Hannaford, B. (1998) "Development of powered prosthetic lower limb." in Proceedings of *the First National Meeting, Veterans Affairs Rehabilitation Research and Development Service*, Washington, DC.

15. Klute, G., Czerniecki, J., and Hannaford, B. (2000) "Muscle-like pneumatic actuators for below-knee prostheses." in Proceedings of *the 7th International Conference on New Actuators*, Bremen, Germany, pp. 289-292.

16. Versluys, R., Desomer, A., Lenaerts, G., Van Damme, M., Berl, P., Van der Perre, G., Peeraer, L., and Lefeber, D. (2008) "A pneumatically powered below-knee prosthesis: Design specifications and first experiments with an amputee." in Proceedings of the *Second Biennial IEEE/RAS-EMBS International Conference on Biomedical Robotics and Biomechatronics*, Arizona, USA, pp. 19-22.

17. Davis, S. and Caldwell, D.G. (2006) "Pneumatic muscle actuators for humanoid applications – Sensor and valve integration." *IEEE-RAS International Conference on Humanoid Robots*, pp. 456-461.

18. Chou C.-P. and Hannaford, B. (1996) "Measurement and modeling of McKibben pneumatic artificial muscles." *IEEE Transactions on Robotics and Automation*, vol. 12, no. 1, pp. 90 – 102.

CHAPTER 4:

PROSTHETIC PROTOTYPE DESIGN

4.1 INTRODUCTION

In the previous chapters the Pneumatic Artificial Muscle was introduced and some improvements to the standard McKibben type PAM are discussed. The Chemo-Muscle Actuation system provides increased functionality and strength and allows for the use of PAMs in mobile applications such as prosthetics. The efficiency of the PAM was improved by inserting an incompressible volume into the muscle chamber. It was shown that this volume could also be utilized to hold other required components reducing the overall required size of the system. The third and final level of innovation for this project focuses on the design of the prosthetic arm's functioning mechanism. This chapter discusses the design of each of the components and how they function as a working assembly. The manufacturing of a prototype will also be discussed. Testing and control of the prototype will be discussed in Chapter 5.

4.2 ARM STRUCTURE

4.2.1 BIOLOGICAL ARM STRUCTURE

In order to better compare the functionality of the prosthetic prototype, first it is important to understand how a biological arm functions. The proximal side of the elbow joint, the side closest to the center of the body, is one large long bone called the humerus. The distal end of the humerus, the furthest end from the body, consists of two sliding joints that make up the elbow. These two different sections of the elbow joint correspond to the two long bones in the forearm, the radius and the ulna.

The radius is the lateral bone of the forearm, meaning it runs between the humerus and the thumb side of the wrist. The proximal side of the radius is essentially a mobile pivot joint. It is able to rotate, sliding on the distal surface of the humerus and on the side of the ulna. This

connection allows the radius to rotate but keeps it aligned with the ulna. The distal end of the radius consists of a styloid process, the connection to the carpal bones of the wrist, and also an ulnar notch that mates with the distal end of the ulna. This connection is very similar to the proximal connection between the radius and the ulna, with the roles reversed.

The Ulna is the medial, or pinky finger side, bone in the forearm. It contains the main flexing joint in the elbow. Its connection to the humerus, called the trochlear notch, is basically a hinge joint. The proximal end of the ulna also contains a radial notch that guides the rotation of the radius. The distal, wrist end of the ulna consists of a styloid process, similar to that of the radius, and is free to rotate within the ulnar notch of the radius.

The radial and ulnar notches allow for what most refer to as the rotation of the wrist. The wrist is rotated by this movement, but the rotation actually takes place throughout the forearm. As the proximal end of the radius and the distal end of the ulna rotate, the forearm twists. The slight outward curves of the radius and ulna wrap around each other as the proximal ends and the wrist are rotated. This rotational motion of the forearm is called pronation and supination with pronation turning the palm posterior or inferior and supination turning the palm anterior or superior.

The ranges of human arm motions are discussed in Luttgens & Hamilton's 1997 text [1]. The range of elbow flexion is said to have a maximum of 140 degrees as shown in Figure 4-1. The range of wrist rotation is said to be approximately ±85 degrees from the neutral position for a range of around 170 degrees. The approximate envelope of the human forearm was given previously in Figure 1-13.

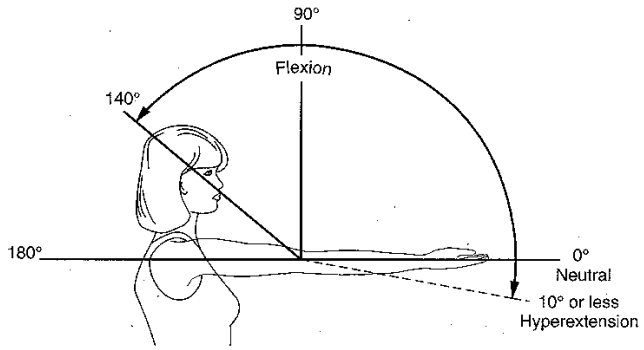

Figure 4-1: Range of human arm flexion [1]

4.2.2 STRUCTURE OF PROSTHETIC PROTOTYPE

Like a biological arm the prosthetic prototype is designed with an internal skeleton for structural support the forearm. However the prototype's skeleton has only one rigid bar in the forearm region, not the two that allow the biological forearm to twist. Since the one metal bar is replacing the radius and the ulna of a biological arm it is aptly named the radiulna. The ends of the radiulna provide an anchoring location for the PAMs. The PAMs attach with the body of the PAM running along the radiulna and alternate directions around its surface. This is all shown in **Figures 4-2 & 4-3.**

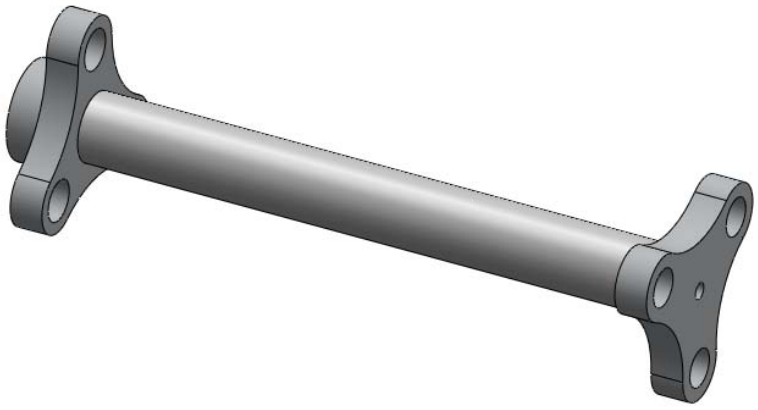

Figure 4-2: Forearm section, call the radilulna, with out PAMs

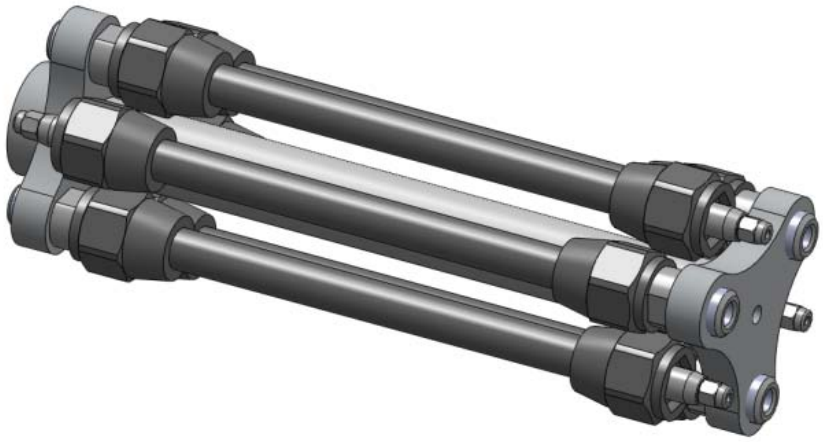

Figure 4-3: Forearm section, call the radiulna, with PAMs

The wrist rotation degree of freedom is replaced by a structure that allows the entire forearm region, including the radiulna and PAMs, to rotate freely. This structure is made up of a coupling that attaches to the proximal end of the radiulna, the end closer to the elbow. The coupling encloses a chamber containing a thrust bearing, a bolt that acts as the axle for the pronation/supination called the pronation pin, and a potentiometer that measures such motion. The coupling and the components it encloses are shown in **Figure 4-4** and in cross section in **Figure 4-5.** On the proximal end of the coupling, another thrust bearing mates the coupling to the elbow bracket, freely allowing rotation between the two of them.

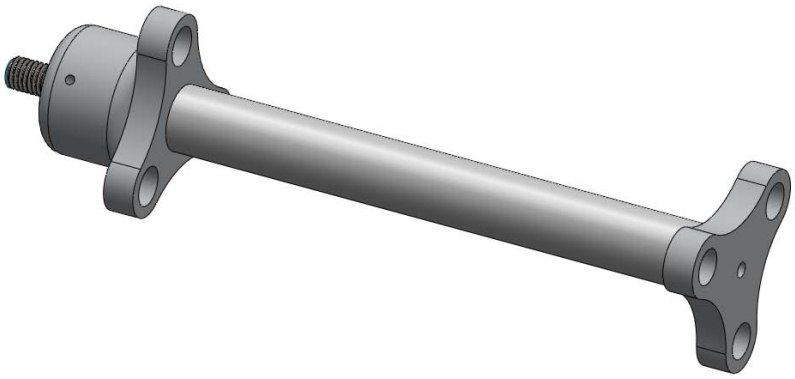

Figure 4-4: Forearm section, call the radiulna, with proximal coupling attached

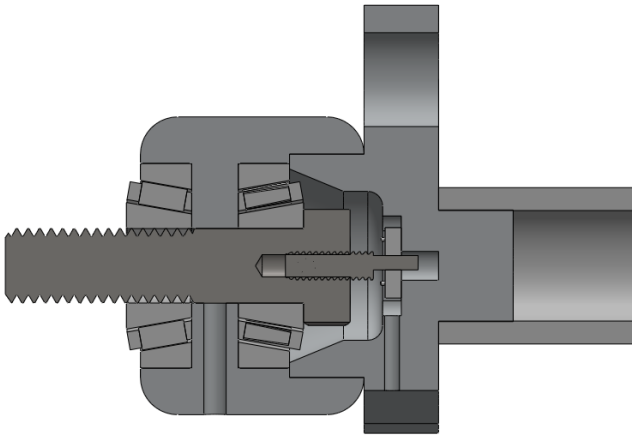

Figure 4-5: Cross section of coupling and internal components

The elbow bracket makes up the main structure of the distal portion of the elbow joint. It also is the anchor point for a plastic cover that mounts the potentiometer that measures elbow rotation. A bolt provides the pin about which the elbow joint hinges and also provides the input for the potentiometer. The bolt is covered by a copper sleeve to reduce rotational friction. These are shown in **Figure 4-6**

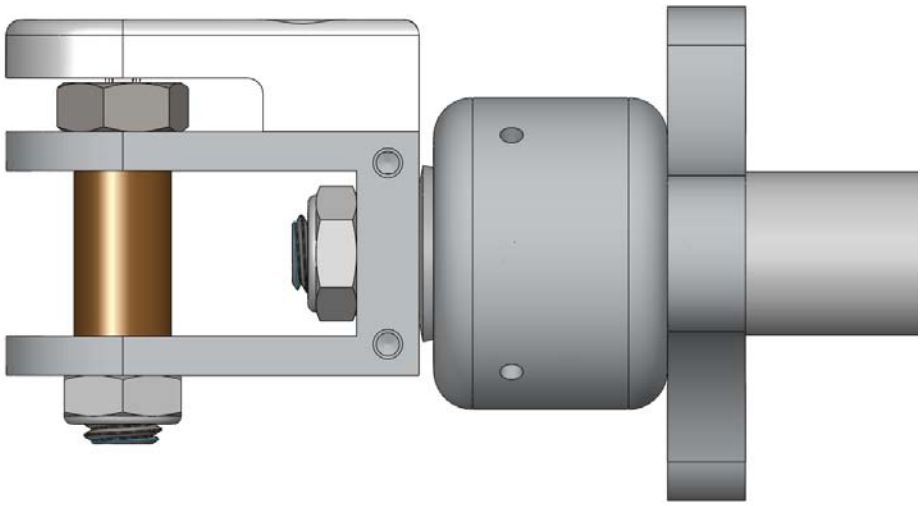

Figure 4-6: Elbow bracket and attached components, top view

The proximal portion of the elbow joint is made of a complex set of pulleys and spacer plates that are attached to an aluminums block called the anchor block. On the proximal end of the anchor block is a pyramid connector that is a common type of connector in current prosthetics. This would connect to a socket and harness worn by the amputee. These components are shown in **Figure 4-7** below and will be discussed in more detail in Section 4.3.

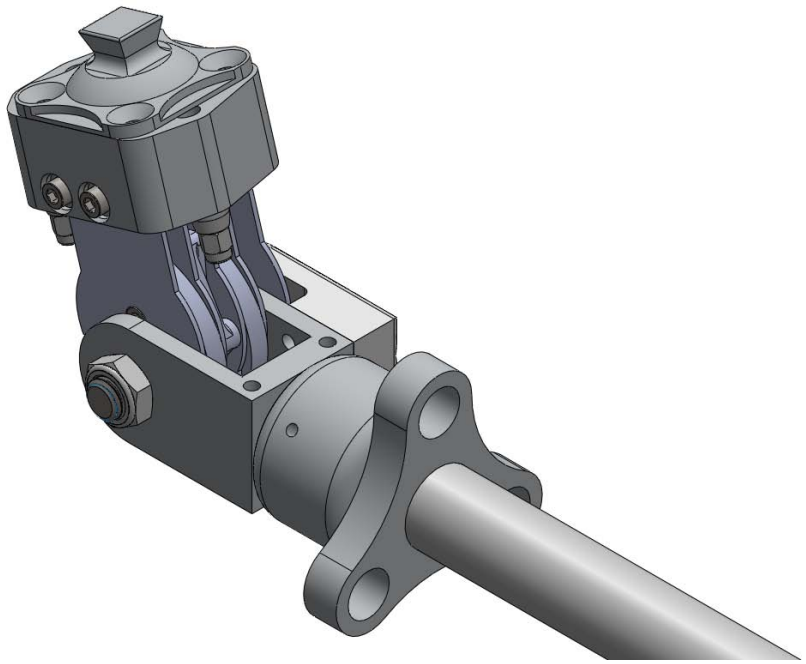

Figure 4- 7: Attached proximal portion of the elbow joint, also known as the elbow pulley assembly

4.2.3 MOTIONS AND ACTUATIONS OF THE PROSTHETIC PROTOTYPE

The three motions of a biological forearm are the bending of the elbow, the rotation of the wrist, and the bending of the wrist. In the human body these motions are controlled by many muscles of varying sizes that participate in multiple different motions and work collectively to perform specific motions. In other words, many of the muscles share the same duties. Traditional prosthetics, on the other hand, simplifies this by using a single bi-directional actuator or a pair of mono-directional actuators for each DOF. This prototype seeks to take the advantages of both approaches, providing the same functionality as a complex biological system, by utilizing groups of smaller actuators to control multiple degrees of freedom while still simplifying the system so that there are no redundant actuators. This allows for the design to use a minimum number of actuators and therefore be conservative in both the energy use and the size and weight of the prosthetic.

There are six PAM actuators in the prosthetic prototype design. Three are fixed at the distal end of the radiulna and point towards the elbow joint. They are arranged with two of the muscles on the anterior sides of the arm and one centered on the posterior of the arm. These three muscles are attached to the elbow joint by steel cables that are routed through a system of pulleys. The anterior muscles, actuated together, provide the torque required for the largest gross movement of the forearm, the flexion of the elbow. The posterior muscle is the antagonist for the two anterior muscles, providing the ability to hold the joint at a specific angle. It also extends the elbow joint, which requires much less force than flexion since it does not typically carry an extra load. The model is shown in the fully flexed and fully extended elbow positions in **Figures 4-8 & 4-9** respectively.

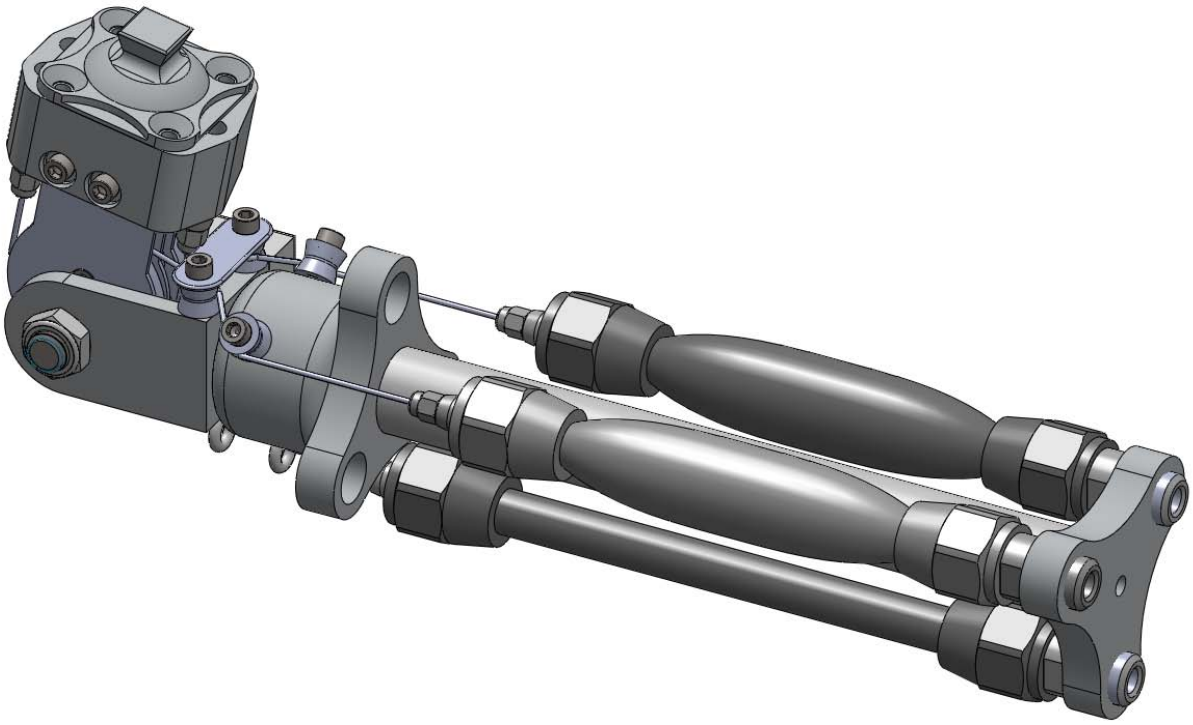

Figure 4-8: Elbow joint in the fully flexed position

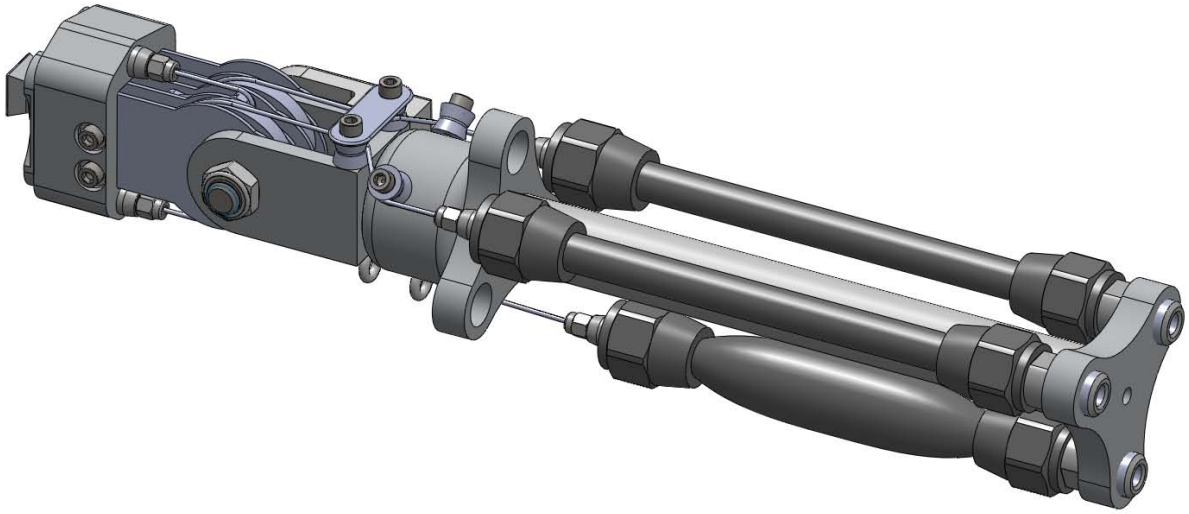

Figure 4-9: Elbow Joint in fully extended position

These same three muscles are also what control the forearm pronation and supination, or the rotation of the wrist. The cables from the anterior muscles are routed through a system of pulleys before reaching the elbow joint. When one of the anterior muscles is actuated to a greater degree than the other, that cable has greater tension in it. Since both cables are anchored at the same fixed length in the proximal end of the elbow joint, the forearm is forced to rotate to compensate for and eliminate the tension difference. The muscle that is providing the greater cable tension forces the wrist/forearm to rotate in the opposite direction. With one anterior muscle fully contracted and the other fully relaxed the wrist will be at its maximum rotation in that direction. This rotation is expected to reach around 60 degrees. With the same amount of rotation possible in the opposite direction, the design provides a theoretical wrist rotation range of 120 degrees. The model is shown in a pronated position in **Figure 4.10**. Note that the posterior muscle is also contracted to secure the elbow angle in place. The same degree of supination is possible in the opposite direction.

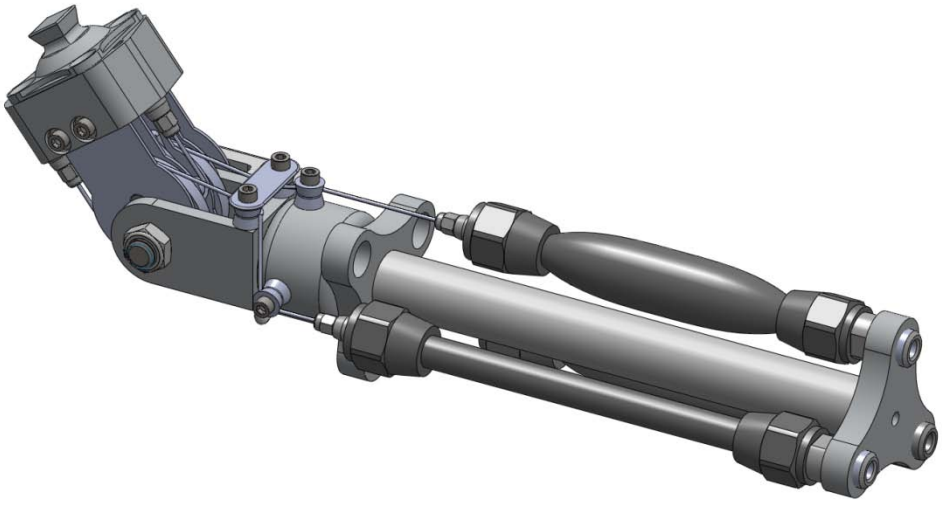

Figure 4-10: Forearm in pronated position

The positioning of the wrist is also addressed. The three remaining muscles are fixed at the proximal end of the radiulna running parallel to and in between the muscles used for the elbow joint, but in the opposite direction. This is shown in **Figure 4-11**. These three muscles are attached by cables to a plate that is mounted on the distal end of a ball joint wrist. This 'wrist' is a simple proof of concept design that works on the principle that a plane's position can be given by three points in space. In this case, the three point's positions are controlled by the muscle actuators. The muscles start in a partially contracted state and therefore can be shortened or lengthened to allow a full range of motion in all directions for the wrist. This essentially mimics the four motions of the biological wrist, Flexion, Extension, Ulnar deviation and Radial deviation, with only three muscle actuators.

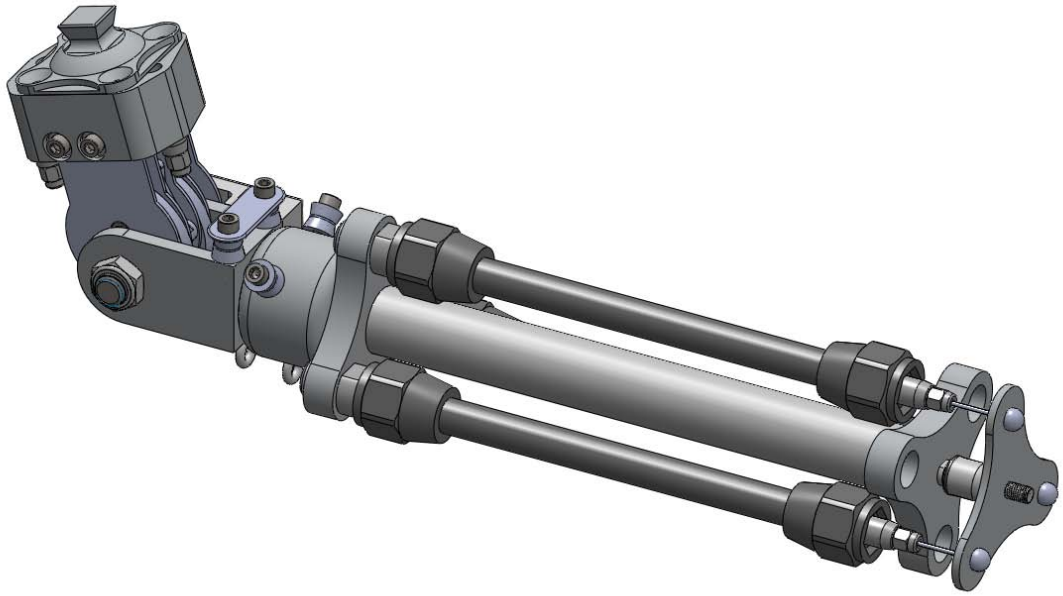

Figure 4-11: Prosthetic model with wrist control components

4.3 DESIGN DETAILS

The detailed drawings for all machined components are provided in **Appendix A**. This section contains detailed descriptions of the design of each component and the methodology behind these designs.

4.3.1 RADIULNA

The radiulna is the main skeletal structure for the forearm of the prototype. It is made up of three components that are mounted together to form the bone-like shape. The central portion is an aluminum pipe, ¾" ID schedule 80 and 9in. in length. The insides of the two ends are threaded to connect the end pieces. It was later realized that this could cause misalignment due to thread variations, so it is recommended that this be modified to a keyed slot design or a solid surface with multiple threaded connectors. This will insure that the end mounts are oriented properly and make them easier to mass produce. These three components are shown in **Figure 4-12**.

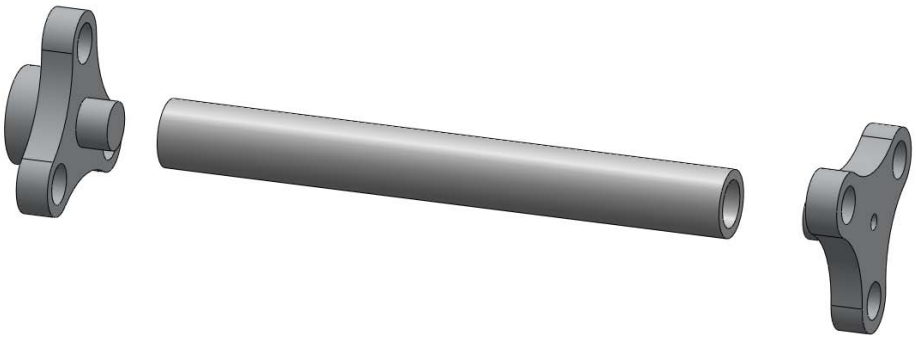

Figure 4-12: Three components of radiulna separated

The end mounts are basically rounded triangular shaped pieces that provide three equally spaced mounting holes for the PAMs. Each end mount also has a threaded stud that is used, in the manufactured version of the prototype, to connect them to the central pipe. The two end mounts also have features that allow them to connect to the next adjacent component. For the distal end mount, this is just a tapped hole for the wrist ball joint to attach to. This could also be modified to connect any type of prosthetic hand or wrist as necessary in later versions of this design.

For the proximal end mount, shown in **Figure 4-13**, the connection is a good deal more complex. The outside of the connection is threaded to link to the next component, the pronation coupling, while the inside of the connection is carved out to allow space for internal components. This carved out portion has a tapered section that provides space for the head of the pronation pin. After the tapered section, there is a flat that has a custom slot sized to fit the rotational potentiometer that will be used to read the pronation angle. The electrical cables for the potentiometer are fed out through a small hole that penetrates the chamber.

Figure 4-13: Proximal end mount for radiulna internal structure including potentiometer slot

4.3.2 PRONATION COUPLING

The pronation coupling attaches to the proximal end of the radiulna. In doing so in encloses the head of the pronation pin and the potentiometer it attaches to. It also encloses one of the thrust bearings that provide the ability for the forearm to rotate. These bearings are tapered roller bearings made for a ½" shaft diameter. The second thrust bearing is press fit into a hole on the proximal end of the pronation coupling with its proximal face flush on the distal face of the elbow bracket. The pronation pin holds these two faces together. This portion of the assembly was shown previously in cross section in **Figure 4-5,** but is also shown in an exploded view in **Figure 4-14**.

The exterior of the pronation coupling is 2" in diameter. On this outer surface are three #10-24 tapped holes. They are the anchor points for two pulleys, on the anterior, and an eye loop, on the posterior. These act as cable guides keeping the muscles relatively strait throughout the contraction and extension process. They are also the components that facilitate the

pronation/supination motion using the flexion/extension muscles. These are shown in position in **Figure 4-14** on the left.

Figure 4-14: Assembled (left) and exploded views (right) of pronation coupling and inner workings

4.3.3 PRONATION PIN

The pronation pin is a ½" zinc plated steel cap screw with a 2" bolt length. A nylon patch is applied to keep the connecting nut from slipping. The head end of the pronation pin is modified by tapping a #10-24 hole 0.4" deep on center. A #10-24 bold is modified such that the bolt head is removed and the remaining end is machined into the D-shaped insert for the pronation potentiometer. This piece is threaded into the end of the pronation pin. This allows for an adjustable connection between the pronation pin and the potentiometer. These components are shown in **Figure 4-15**. The pronation pin is fed through the pronation coupling with the thrust bearings and then through the elbow bracket. A nut is fixed in a slot in the elbow bracket so that it both allows the pronation pin to hold the pronation coupling and the elbow

bracket together tightly and keeps the pronation pin in rotational alignment with the elbow bracket. This alignment allows the forearm rotation to be measured by the pronation potentiometer.

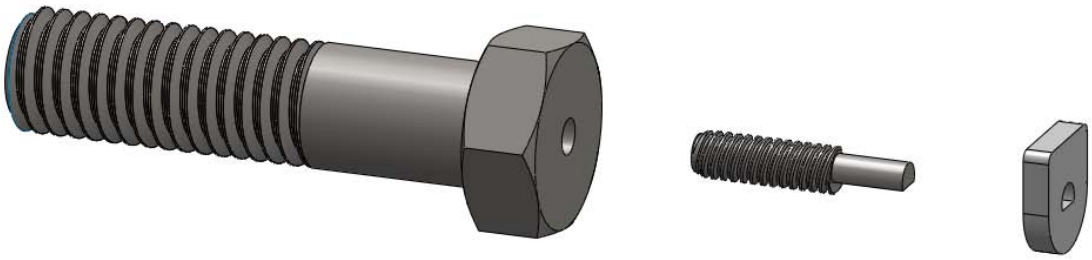

Figure 4-15: Pronation pin components with potentiometer

4.3.4 ELBOW BRACKET

The elbow bracket, shown in **Figure 4-16**, is the main structural piece distal to the elbow joint. The forearm connects to the distal end of the bracket through the pronation pin. The elbow control cables are routed through pulleys on the anterior of the distal end of the bracket and an eye loop on the posterior side. These correspond to the similar pulleys on the pronation coupling and are mounted in the same way, #10-24 bolts. The exterior side of the elbow bracket is the mounting place for the plastic elbow potentiometer mount. This mount is strong enough to protect the potentiometer and hold it in place, while still being lightweight. It is anchored to the elbow bracket by four bolts to prevent twisting or other misalignment of the potentiometer due to inadvertent contact.

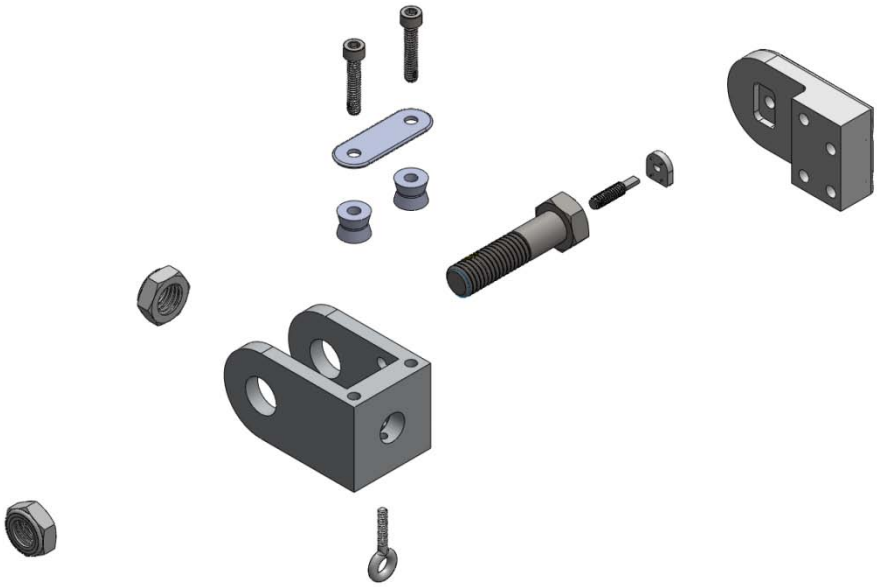

Figure 4-16: Exploded view of elbow bracket components

The elbow joint is hinged about a bolt identical to the pronation pin, including the D-shaped potentiometer insert. This bolt is covered by a copper sleeve to reduce elbow joint friction. The sleeve is loosely fit into the hinge holes of the elbow bracket and press fit into the proximal portion of the elbow joint. The copper sleeve therefore moves with the elbow pulley assembly.

4.3.5 ELBOW PULLEY ASSEMBLY

The elbow pulley assembly, shown in **Figure 4-17**, is the most complicated portion of the prototype. It consists of three variable radius pulleys, four spacer plates, three spacer blocks, an elbow pin guide plate, an anchor block, Electroline cable end fittings, and a pyramid connector. These components are shown in an exploded view in **Figure 4-18**.

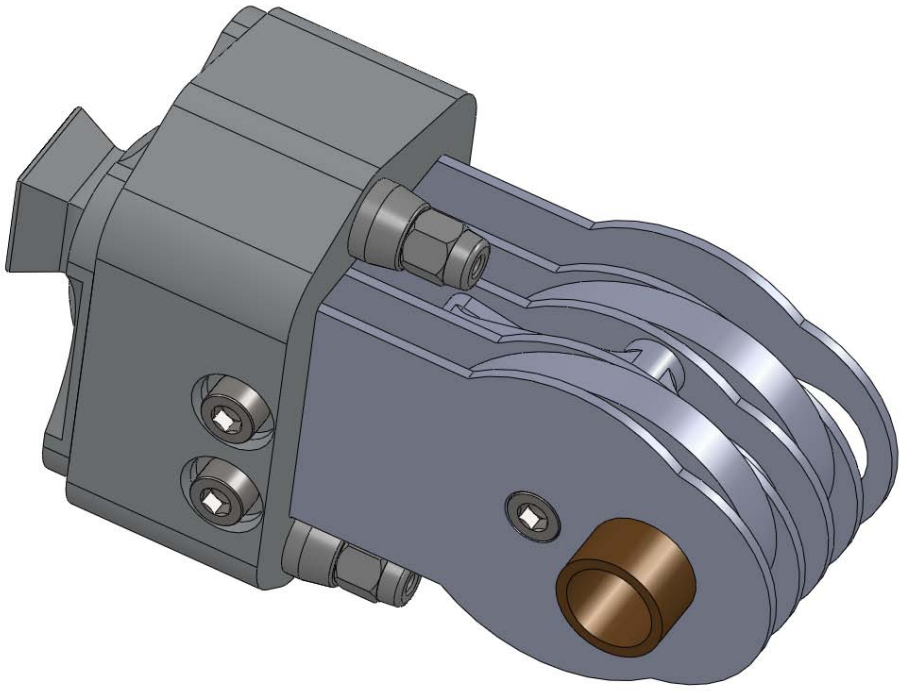

Figure 4-17: Elbow pulley assembly

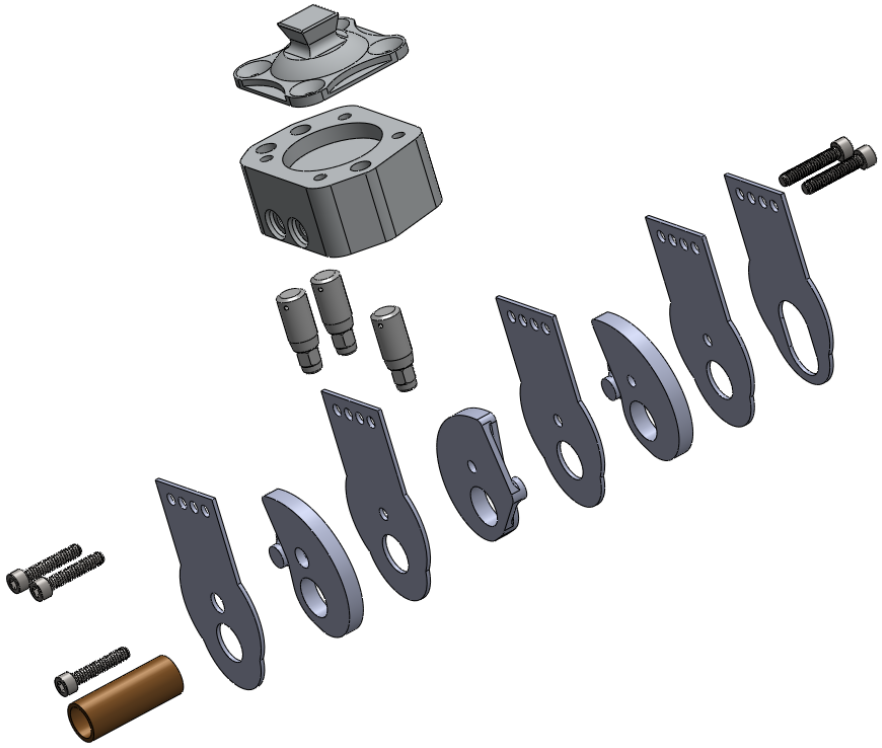

Figure 4-18: Exploded view of the elbow pulley assembly

4.3.5.a VARIABLE RADIUS PULLEYS

The most important component of the elbow pulley assembly is the pulleys. They are optimized variable radius pulleys that were designed to mimic the torque curve of the human elbow. Using Matlab's Optimtool as a local optimizer with the fmincon solver and GlobalSearch as a global optimizer, a code was developed that calculated the torque of the prosthetic arm and compared it to an approximate human elbow joint torque curve. This code is provided in its entirety in **Appendix B**. The resulting optimized inputs are also provided along with the output they achieve. Both Optimtool and GlobalSearch attempt to optimize a given function by adjusting the inputs of the function to minimize the output. The function, therefore, must take the given inputs and calculate an amount of error that is to be minimized.

In this case, the input variables were the coefficients of a quadratic function that represented the radius of the pulley. A quadratic function was chosen because the approximation for the human elbow joint torque is hyperbolic in shape. This approximation is taken form Khalaf and Parnianpour's database of normative joint strengths [2]. Their surface plot and the estimated maximum curve are shown in **Figure 4-19**. This maximum curve was reduced by 25% in order to make a desired torque that was achievable in the size constraints. 75% human strength is still a 50% improvement even over other experimental research prosthetics such as Withrow et al's forearm unit. [3]

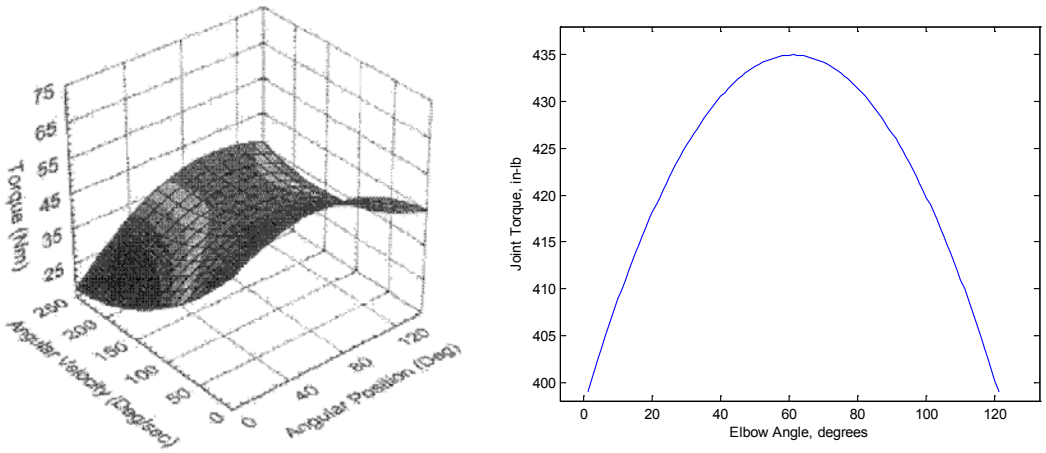

Figure 4-19: Surface plot of human elbow torque (left) [2] and estimated maximum joint torque plot (right)

The quadratic function coefficients are plugged into an equation for the radius of the pulley. The radius is calculated for every tenth of a degree for a range of 0 to 240 degrees. The radius is then checked to see that it fits within the physical size constraints. If the size constraints are satisfied, the code determines the effective point of the pulley and the tangent line associated with that point for each degree of elbow joint rotation, 0 to 120 degrees. This is done by finding a line from each point on the pulley surface and connecting it to a known fixed point on the body of the forearm. The slopes of these lines are compared. The line with the minimum slope is the tangent line and the corresponding point on the pulley surface is the effective point.

Once the effective point is known the effective radius can be determined. First, however, other checks now can, and should, be performed. Knowing the initial length of the muscles, we can calculate the percent contraction at each degree as well as the required tendon cable length at each degree. If either of these exceeds their maximums, a large amount of error is induced and the function outputs this large error, just as it does for the size constraints. The limits for the muscle are a maximum of 25% contraction at an actuation (max tendon cable) length of about 1.5 in. These would change for a different size or type of muscles. If all constraints are met, the

effective radius is used to calculate the torque for each degree of rotation. The force output by the muscles, F_i, is given in terms of percent contraction, h_i, in Equation (4.1) which is approximated from a curve in the muscle manufacturer documentation [4], shown in **Figure 4-20**. In this figure, 1 is the min theoretical force at the max operating pressure, 2 is the max operating pressure, 4 is the max pretensioning, and the grey region is the operating range. The force, F_i, generated by Equation (4.1) is calculated in Newtons, but is later converted to in-lbs in the code.

$$F_i = 0.6058 \cdot h_i^2 - 39.598 \cdot h_i + 630 \tag{4.1}$$

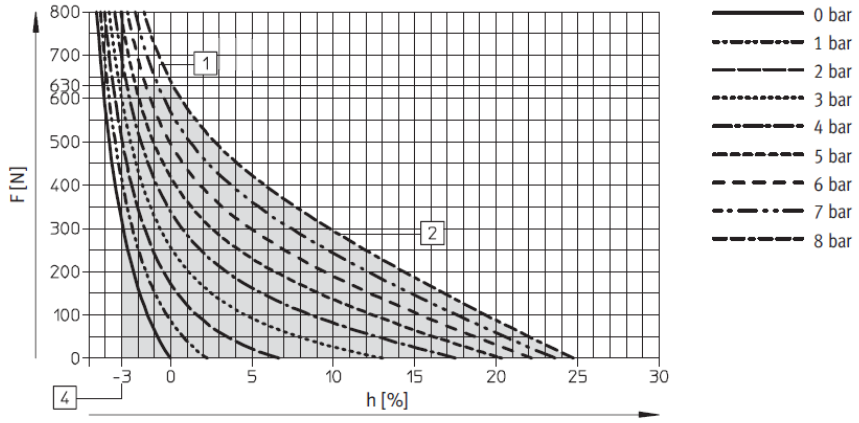

Figure 4-20: Festo muscle documentation on DMSP 10mm PAM. [4]

This calculated torque curve corresponds specifically to the variable radius pulley chosen for that iteration of the function. This desired torque curve is subtracted from the calculated curve and the error from each point is summed into a total error for that design iteration. This total error is output to the optimizer and is minimized based on adjustments to the input coefficients. The local optimizer took approximately 15-20 minutes to run and had approximately 12 iterations for each run. The global optimizer took the better part of a day to run, but proved that a minimum found by manually iterating the local optimizer was in fact the

global minimum. The remaining code, which was not run during iteration, plots the actual and desired torque curves for comparison and also generates a movie that shows the pulley shape and the tangent line for each angle of elbow rotation. These were used as visual checks for the optimized results. The torque curves for the optimized variable radius pulley are shown in **Figure 4-21** below. The resulting shape of the variable radius pulleys were imported into Solid Works and a model was generated and is shown in **Figure 4-22**.

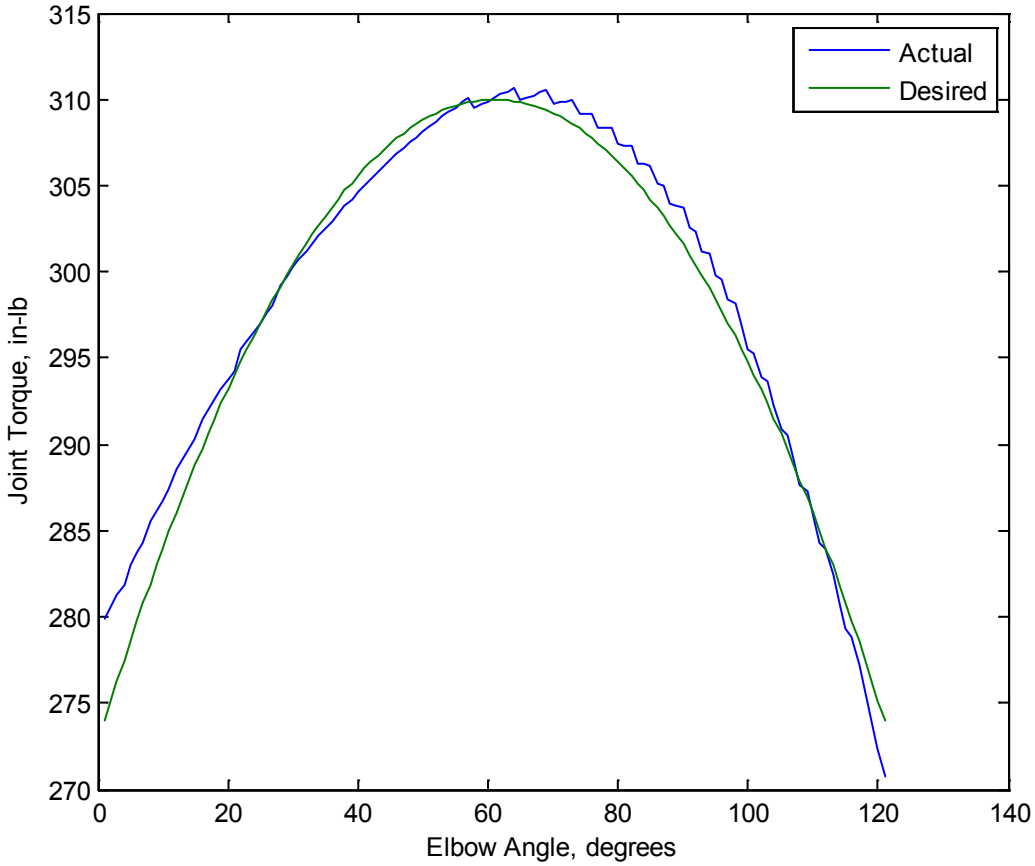

Figure 4-21: Actual and desired joint torque curves for optimized variable radius pulleys in the elbow

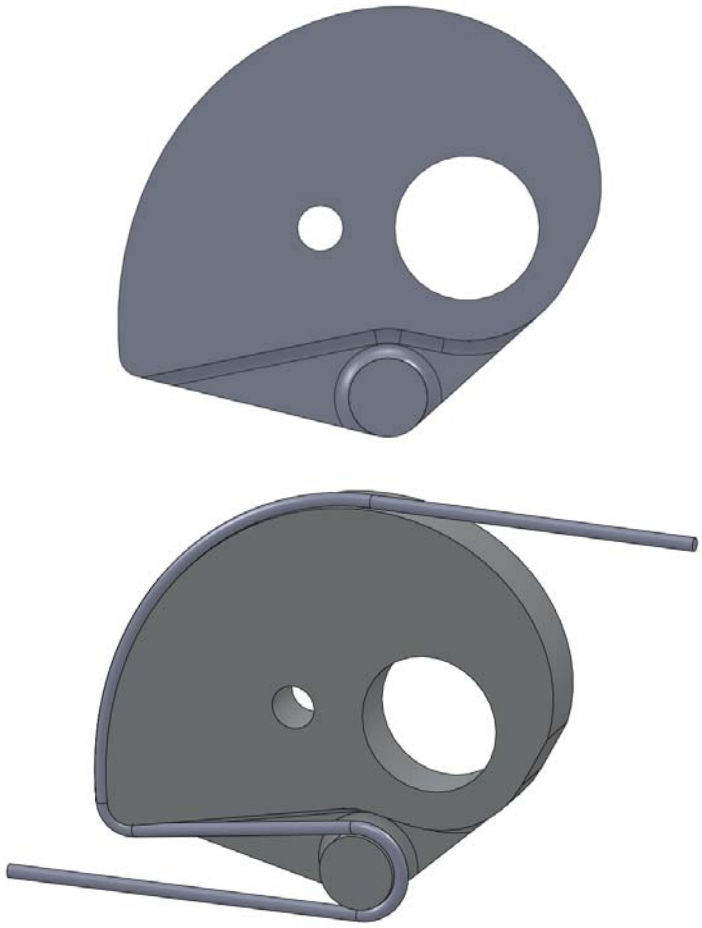

Figure 4-22: Optimized variable radius pulley shape (left) and example of cable routing (right)

These pulleys were inserted into the upper portion of the elbow joint and are separated by spacer plates. These plates are 1/16" thick and hold the pulleys in place with a #10-24 bolt that is countersunk so it does not impede the elbow joint rotation. The two outer pulleys link to the two anterior muscles. The middle pulley is inverted so that it can be connected to the posterior muscle. The pulleys also have a cable routing section on the opposite side of the working surface. This allows the cable to double back and anchor into the anchor block rather than elsewhere in the assembly. This is shown in **Figure 4-22** also.

4.3.5.b ANCHOR BLOCK

The anchor block performs exactly the function it is named for. It provides a, attachment point for the spacer plates, the elbow pin guide plate, the pyramid connector, and the drive cables from the PAMs. It was originally designed as a single block with slots and holes drilled into it, but at the suggestion of the machinist, it was redesigned into an anchor block with one rectangular abscess instead of slots and intermediate spacer blocks. This design performs the same function, but is significantly easier to machine. The slots were the problematic feature. Since they are narrow and deep it is likely that the tool bit would be broken in the process. Also this size slot required a nonstandard size bit which would further increase the time and monetary costs.

Three of the four spacer blocks are the same thickness as the pulleys and are placed in between the spacer plates containing the pulleys but on the proximal end near the anchor block. The fourth spacer block is slightly thicker than the others, 0.3in rather than .25in, and separates the elbow pin guide plate from the other spacer plates. This guide plate keeps the elbow pin oriented with the upper portion of the elbow allowing the elbow potentiometer to properly read the elbows rotation. The spacer blocks and spacer plates are held together and attached to the anchor block by four #10-24 bolts that are inserted into the sides of the anchor blocks. The pyramid connector is mounted to the proximal end of the anchor block by four more #10-24 bolts.

4.4.5.c ELECTROLINE CABLE END FITTINGS

Electroline cable end fittings are made by Esmet, Inc. [5]. These cable end fittings attach to the ends of wire rope and provide a secure threaded mounting end for any size cable. An Electroline wire rope fitting is installed much like a compression fitting in a plumbing

application as shown in **Figure 4-23**. The wire rope passes through a sleeve. The strands are fanned-out and a plug is inserted. As the plug is driven into the fanned end of the rope, the diameter of the end increases so that the rope can't dislodge itself. Finally, a socket is placed over the sleeve and threaded on tight. It is this socket that has been modified for use in this prototype as described in the next section.

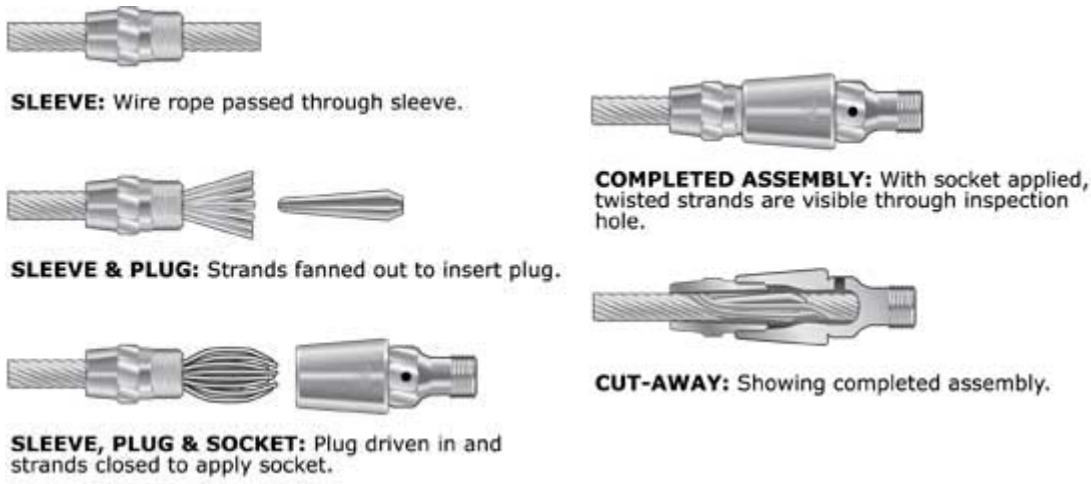

Figure 4-23: Esmet Electroline cable end fitting assembly diagram [5]

4.4 PROTOTYPE MANUFACTURING AND ASSEMBLY

4.4.1 PROTOTYPE MANUFACTURING

The prototype was constructed by The University of Alabama Mechanical Engineering Department Machine Shop. Most of the parts were made using a computer numerically controlled (CNC) milling machine. Some were made entirely by the programmed machine, but other, more complicated parts were completed by hand. The manufactured parts are shown in **Figures 4-24** through **4-28**.

Figure 4-24: Prototype modified anchor block, top (left) and bottom (right)

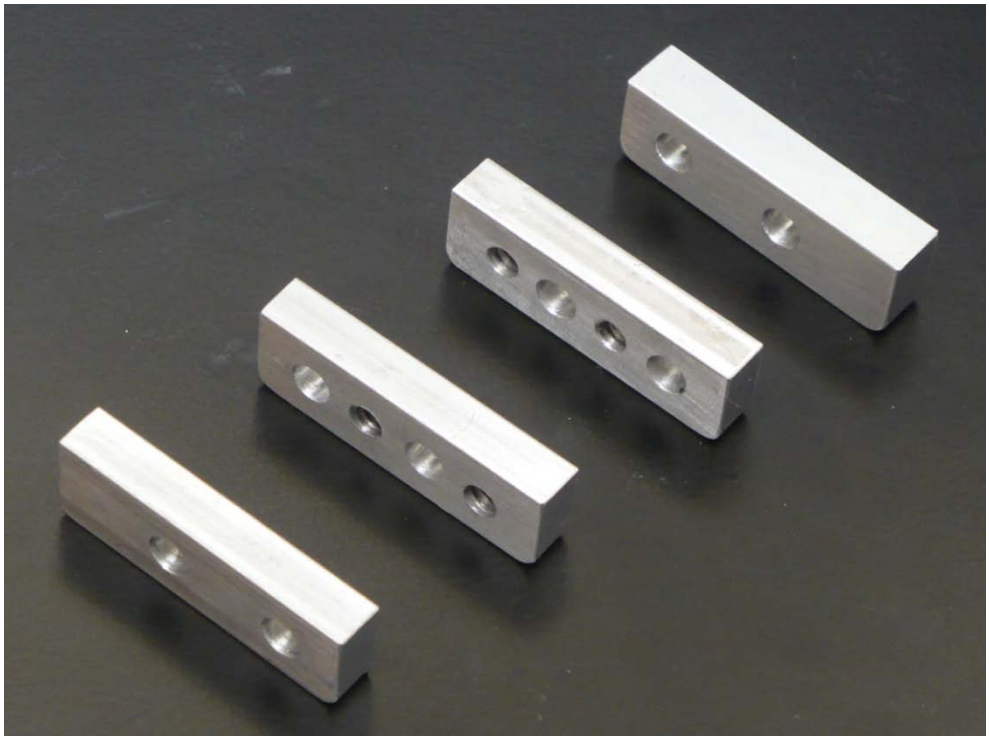

Figure 4-25: Prototype anchor block spacers

Figure 4-26: Prototype elbow pulley spacer plates, three standard (right) and one with cap screw head clearance (left)

Figure 4-27: Prototype elbow potentiometer guide plate

Figure 4-28: Unassembled prototype radiulna components

This process took a couple of months and included multiple design adjustments. One such change to the anchor block was mentioned in 4.3.5.b and shown in **Figure 4-24**. Another change was to the cable attachment method. The original design included a hole in the anchor block that mimicked the internal structure of the Electroline socket shown in the cut away in **Figure 4-23**. This complex geometry was determined to be too difficult to reproduce at such a small size without special tools. It was decided that it would be much simpler to increase the overall size of the anchor block, thread the outside of the existing socket and mount them into the block. This also allowed the connection to the PAMs to be much simpler. The cable mounting end of the muscle was drilled out and retreaded to fit the external thread of the modified Electroline socket. The original Electroline socket, the modified socket and the adjustments to the PAMs are shown in **Figures 4-29, 4-30** and **4-31** respectively.

Figure 4-29: Electroline fittings, original

Figure 4-30: Electroline fittings, modified

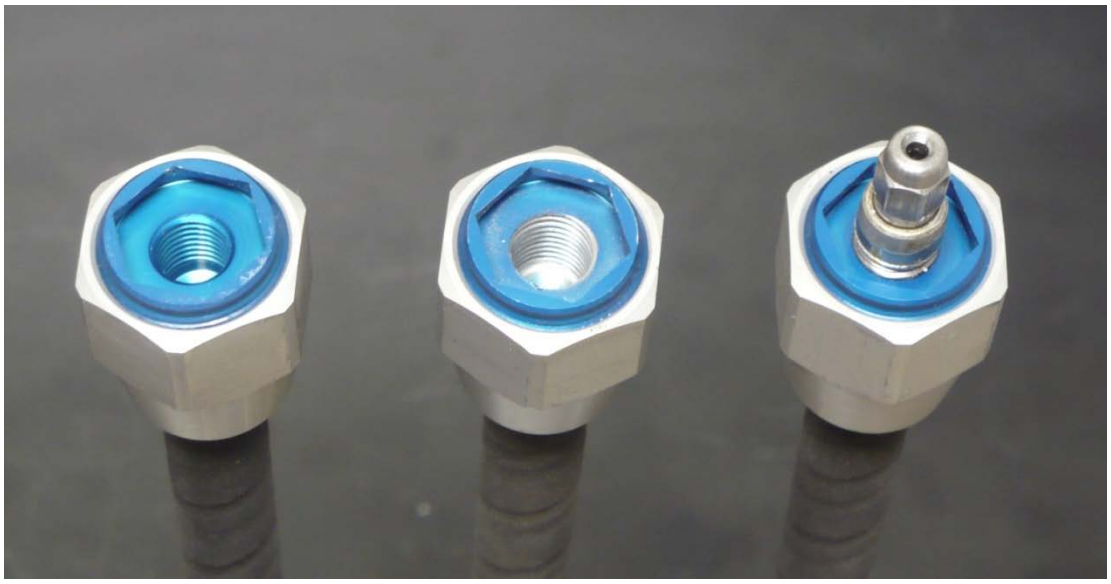

Figure 4-31: Muscle modifications, original (left), re-tapped (center) and with cable fitting (right)

4.4.2 PROTOTYPE ASSEMBLY

The assembly process took place in specific steps. First the radiulna and the elbow pulley assembly were put together as individual subassemblies. These are shown in **Figures 4-32** and **4-33**. Note that the pronation potentiometer must be wired before connecting the pronation coupling to the radiulna.

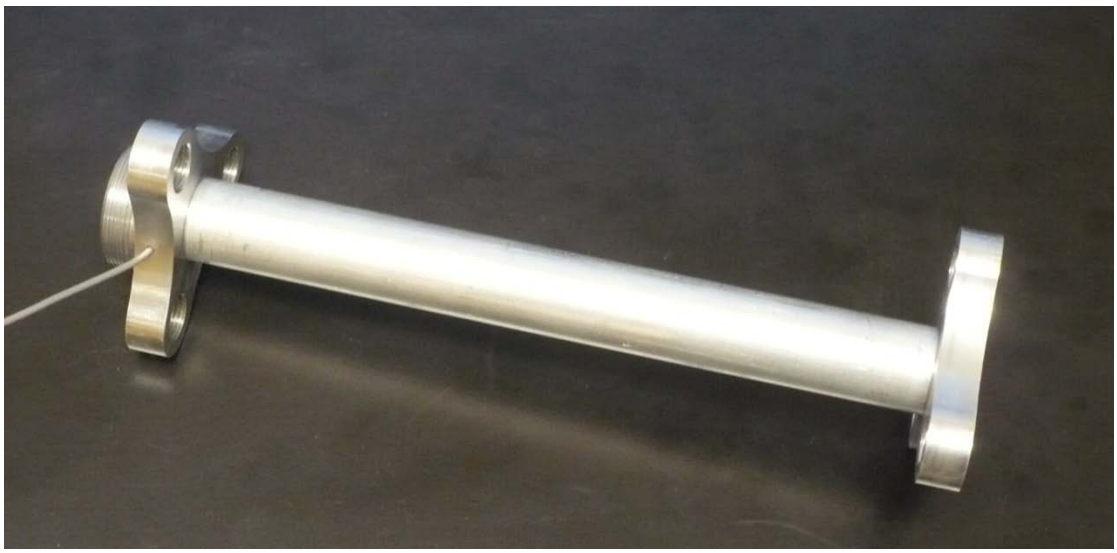

Figure 4-32: Assembled radiulna

Figure 4-33: Elbow pulley assembly steps: Insert spacer blocks (top left), insert spacer plates (top right), insert pulleys and copper collar, bolt subassembly together, attach pyramid connector (bottom center)

Then the elbow bracket and the pronation coupling were connected along with their corresponding internal bearings and external pulleys. These are shown in **Figures 4-34** and **4-35**.

These three sections were then combined together. First the pronation coupling and the radiulna are attached as shown in **Figure 4-36**.

Figure 4-34: Assembled elbow bracket and pronation coupling, side view

Figure 4-35: Assembled elbow bracket and pronation coupling, end view showing internal bearings and pronation pin

Figure 4-36: Forearm assembly without muscles

Then the elbow pulley sub assembly is attached as shown in **Figure 4-37**.

Figure 4-37: Full assembly without muscles

The muscles were installed and the elbow potentiometer was installed and wired. The elbow potentiometer mount is shown in **Figure 4-38**.

Figure 4-38: Elbow potentiometer mount with components

Finally the tendon cables were strung and the prototype was ready for testing. The final pretesting construction of the arm is shown in **Figure 4-39** below.

Figure 4-39: Final prototype with elbow control muscles attached and ready for testing

4.4.3 ADJUSTMENTS MADE DURING ASSEMBLY

The major components assembled fairly easily with only minor adjustments to improve fit. For example, the copper sleeve in the elbow joint was meant to have an easy press fit into the elbow pulley assembly and have a loose fit with the elbow bracket. However the low tolerances of the sleeves caused it to be too tight in the elbow bracket and restrict movement. The size of the elbow bracket holes was increased slightly by sanding the inside of the hole until the proper fit was achieved.

The elbow potentiometer guide plate, shown in **Figure 4-27,** was designed for simplified manufacturing. The size and shape of the plate is similar to the other plates so that they could all be made with the same CNC program. However, the unnecessary outer shape of the plate makes contact with the elbow potentiometer mount and limits the elbow flexion range. By cutting one of the rounded bumps off of the side of the plate the interaction with the potentiometer mount is eliminated and the elbow flexion has the range of approximately 110 degrees from fully extended to fully contracted. The plate was also bent slightly outward so that it did not slip under the elbow pin. The modified plate is shown in **Figure 4-40**.

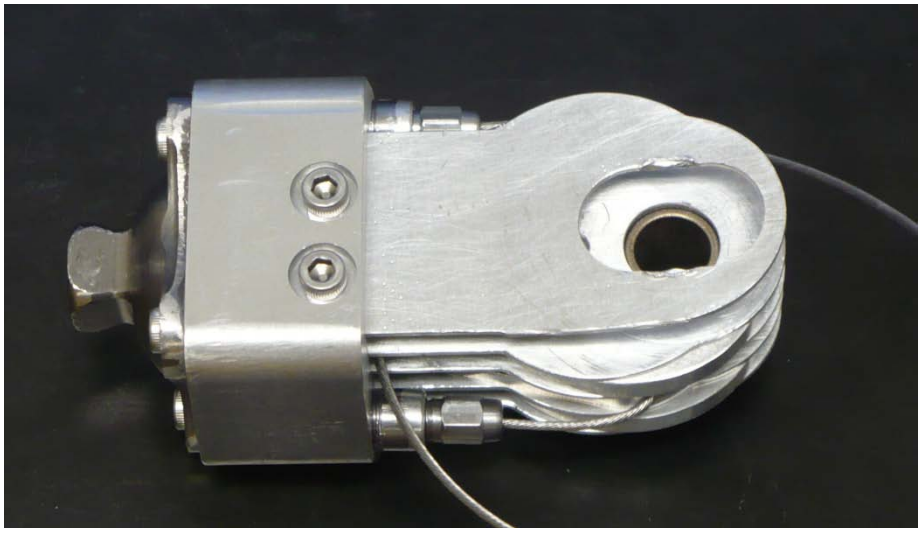

Figure 4-40: Assembled and modified elbow potentiometer plate

The two most difficult tasks during the assembly process were the installation of the internal potentiometer and the 1/16th in steel cable tendons. The pronation pin's D-shaped portion was difficult to align with the internal potentiometer for multiple reasons. At first, the pin was aligned in such a way that the potentiometers motion caused it to move through its "dead spot" where the rotational potentiometer transitions from minimum to maximum resistance (0 to 10 kΩ). This was corrected by adjusting the D-pins relation to the bolt it threads into. This adjustment however also changed the overall length of the pronation pin making it either too long, damaging the potentiometer and not allowing the pronation coupling to fully seat, or too short, making it imposable to insert the D-pin into the potentiometer before connecting the pronation coupling. The D-pin and the potentiometer could still connect properly once the pronation coupling was assembled; however the assembly was only able to be done by feel, with no visual reference. In the future, a solution to this would be to make the D-shaped part of the pin longer and the size clearance hole in the proximal part of the radiulna accordingly. This would allow the pin to be inserted before moving out of visual range.

The steel cables were also particularly difficult to install. The Electroline fittings work well, but the assembly process was painful. With the 1/16th in. steel cables in a 1x19 strand construction you are able to achieve good strength, but the many individual wires are quite small and stiff. This made them difficult to unwind and to keep form twist around each other even after being unwound. They were also quite sharp, easily cutting or poking through the latex gloves worn during assembly. These cables also had to be pre-stretched in order to get the slack out and make them fit well around the pulleys. If the cables were cut to size and installed in the muscles without being pre-stretched the muscles would pull the cables tighter around the pulleys and cause excess slack in the lines that would affect performance.

The cables were also difficult to install because they needed to thread in on both ends. So as the second end was being attached, the first was unscrewing itself. The cable had to be twisted before assembly which could decrease its strength and durability. To avoid this in the future, muscle anchor points should not be threaded but rather attached with a nut. This would make the installation and tightening of the cable easier and not require the cable to be twisted.

4.5 CONCLUSION

The prototype discussed in this chapter is the final level of innovation for this project. It provides a novel approach for using Pneumatic Muscle Actuators to actuate an AE prosthetic arm with nearly the full range in all degrees of freedom for the elbow and wrist, as compared to a biological arm. It is able to provide 110 of the 140 degrees of biological flexion and 120 of the 170 degrees of forearm rotation. This design is also able to provide over 75% the power of a biological arm, which is an over 50% improvement from other available prosthetic arms.

REFERENCES

1. Luttgens, K. & Hamilton, N. (1997). *Kinesiology: Scientific Basis of Human Motion, 9th Ed.*, Madison, WI: Brown & Benchmark.
2. Khalaf, K.A., Parnianpour, M. "A Normative Database of Isokinetic Upper-Estremity Joint Strengths: Towards the Evaluation of Dynamic Human Performance." *Biomed Eng Appl Basis Comm*, 2001(April); 13:79-92
3. Withrow T, Shen X, Mitchell J, Goldfarb M. A Forearm Actuation Unit for an Upper Extremity Prosthesis. *IEEE International Conference on Robotics and Automation* 2008, Pg. 2456-2464
4. FESTO. (2011). Retrieved from *http://www.festo.com/cms/en-us_us/index.htm*
5. Esmet Electroline. (2011) Retrieved from *http://www.esmet.com/electroline.html*

CHAPTER 5:

PROTOTYPE TESTING AND CONTROL

5.1 ABSTRACT

The prototype discussed in Chapter 4 offers the potential to improve the functionality of upper limb prosthetics, especially for the above elbow level of amputation. This design must first be proven to provide the functionality for which it was designed. It must also be shown to be controllable. This is shown in a series of tests that results in some further modifications to the design. The design is then shown to be controllable with a simple control system.

5.2 EXPERIMENTAL SETUP

For the purposes of testing, the pyramid bracket was removed and a section of channel was attached in its place which in turn was mounted to the table. Once the assembled arm was mounted the pneumatic tubing was run and tied to the radiulna to maintain the envelope of the forearm. These were both shown previously in **Figure 4-29**. The muscles that power the elbow and forearm are each controlled by a 3-port solenoid valve (SMC). These normally closed solenoid valves open the gas flow from the storage tank to each muscle or exhausts each muscle independently. A pressure sensor is placed between each valve and their corresponding muscle actuator to measure the pressure in the muscle. The table surface components are shown in **Figure 5-1**. Note that these components would all be contained in the inclusive volume muscle discussed in Chapter 3 and would significantly decrease the overall size of the device.

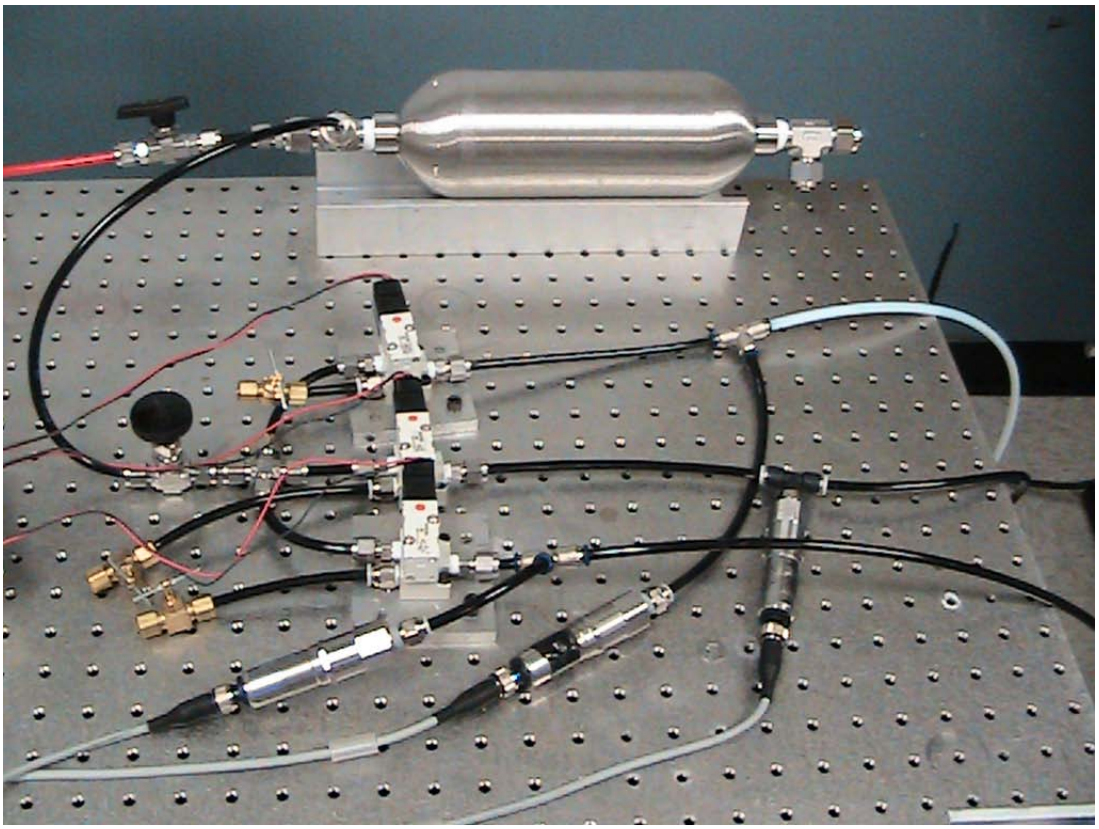

Figure 5-1: Table components of the experimental setup used to test the prosthetic prototype

The valves, pressure sensors, and the joint potentiometers are powered by an external power supply. The control signals come from a computer data acquisition board. This card also collects the data from the sensors. It can also be seen in **Figure 5-1** that regulators are used to control the flow rates of the inlet and each exhaust. This will be discussed in the next section along with the other modifications made to the design as was necessary during the testing process.

5.3 DESIGN MODIFICATIONS DURING TESTING

There were many modifications made to the prototype during the testing phase. These modifications helped overcome hurtles that impeded the testing process or the performance of the prototype

5.3.1 SIMPLE MODIFICATIONS

There were some simple modifications made that helped improve the performance or functionality of the prototype. The first was the machining of a notch in the stop plate that is mounted on the top of the anterior pulleys of the elbow bracket. This notch was made to keep the Electroline fitting in the anchor block, the one for the posterior/extension muscle, from being an early point of contact and bearing a lot of load in the fully flexed arm position. This also increased the maximum flexion angle to 110 degrees. This notch is shown in **Figure 5-2**.

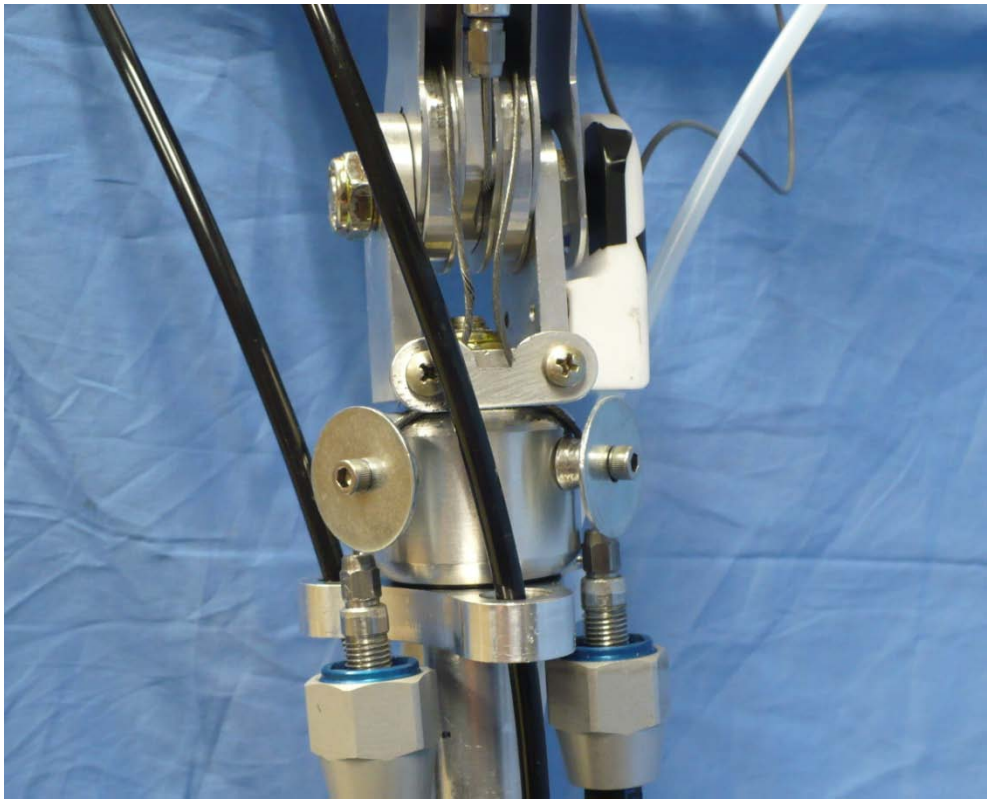

Figure 5- 2: Simple modifications made to the prototype during testing

The other simple modification was the addition of washers on top of the pronation pulleys of the pronation coupling. These washers acted as cable guides. When in full pronation or full supination one anterior muscle is fully contracted and the other is fully exhausted. The rotation also tends towards the exhausted muscle increasing the slack in the corresponding

tendon cable. This slack was sufficient enough to cause the cable to slip over the top of the pulley. The washer helps hold the cable down enough so that as the cable slack decreases the cable is able to properly reseat itself onto the pulley.

Another simple modification was the addition of regulators into the pneumatics system as shown in **Figure 5-1**. This need stemmed from issues with the control using the 3-way solenoid valves. The combination of the large flow rate of the valves, the high source pressure (110 psi) and the small internal volume of the 10mm Festo muscles caused the muscles to contract very quickly. It filled to maximum pressure so quickly, and exhausted so quickly, that it was impossible to command any motion other than that requiring maximum and minimum contractions. The regulators help by limiting the maximum flow rate while not limiting maximum pressure. This slowed the muscles to a controllable contraction rate without limiting the range of motion.

5.3.2 COMPLEX MODIFICATIONS

There were also some more complex modifications made during the testing phase. The first of these had to do with the tensioning of the tendon cables. As mentioned in Section 4.4, the threading in the prototype caused the cables to be required to twist during assembly. This not only damaged the cables, but it also made it difficult to accurately tighten the cables to adequate tension. Since the right handed threads were already in place, it was impossible to left hand thread any of the components. To allow better tensioning of the cables and easier overall assembly, the threads of the distal section of the radiulna, the ones that mounted the muscles, were manually removed. This is shown in Figure 5-3.

The resulting holes were smoothed out to allow the mounting end of the muscle to slide easily through. The job that the removed threads previously held was taken over by the nuts that

came with the muscle fittings. By loosening these nuts, the tension in the cable was easily adjustable without having to remove the muscles. The long threaded outside of the Electroline fitting served as the adjustability. The modified and assembled distal end of the radiulna is shown in **Figure 5-4**.

Figure 5-3: Distal end of the radiulna with the muscle mount threads removed

The second complex modification focuses on the pronation/supination potentiometer. This potentiometer, located inside the pronation coupling is likely the most difficult part of the prototype to access, requiring the removal of the entire distal portion of the arm including the radiulna and the muscles. Therefore, it failed multiple times during testing and needed to be replaced. After the second replacement failed, the cause of the failure was determined to be the prototype itself and not other assembly errors or mistakes. However, the cause of the problem was difficult to deduce since the potentiometer is entirely encased during operation and could not be directly viewed during assembly.

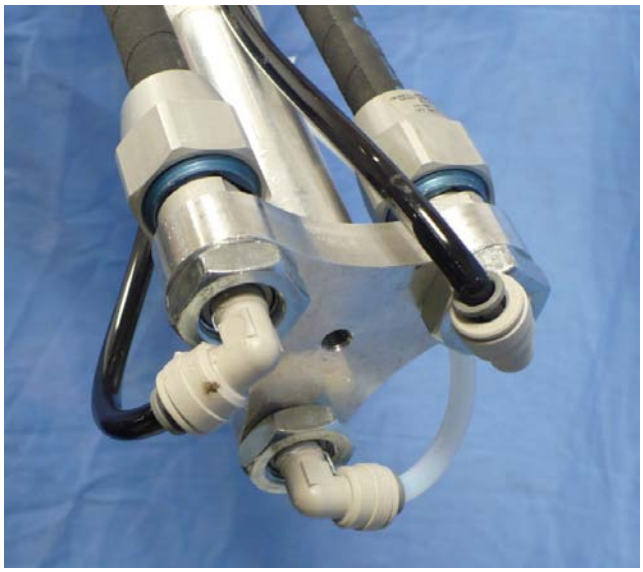

Figure 5-4: Modified, assembled end of the radiulna allowing adjustable cable tensioning

From the way the potentiometers failed, it was determined that they were being crushed. It was initially thought that the pronation pin bolt head was the culprit, with the small amount of play inherent in the thrust bearings allowing the bolt head to rock and put pressure on the potentiometer. The pronation pin was modified so that 0.2 in was removed from the bolt head, as shown in **Figure 5-5**. This thickness removed is greater than the thickness of the potentiometer and should eliminate any possibility of crushing the potentiometer. This, however, did not solve the problem.

It was then determined that the prolonged exposure of the potentiometer to side loading would also cause the potentiometer to fail. The slot that orients the potentiometer was also designed to hold it in place and therefore had a fairly tight fit. To eliminate the possibility that this fit caused damaging side loading, the sides were ground down to loosen the fit. This modification is shown in **Figure 5-6**.

Figure 5-5: Modified pronation pin bolt head

Figure 5-6: Modified potentiometer slot with loose fit

However this loose fit also allowed more flexibility in the location of the potentiometer making it harder to properly seat on the pronation pin. It was already difficult considering that it could not be seen during assembly and that the D-pin and slot needed to be rotationally oriented correctly. Now the added need for two degrees of translational orientation made the proper positioning nearly impossible. The wires that connect to the potentiometer are wrapped in electrical tape to create a conductivity barrier between the pins of the potentiometer and the metal radiulna end. The wires and tape had to be bent to fit in the space and therefore tried to push the potentiometer off center, adding another degree of difficulty. This is also shown on the inside left of the interior in **Figure 5-6**.

To amend this situation, the hole that allowed clearance for the D-pin on the far side of the potentiometer was extended to go through the radiulna end. This hole could then be an alignment inspection hole that could show a misalignment before that misalignment caused damage to the potentiometer. This modification is shown in **Figure 5-7**. A small roll of electrical tape was used to counteract the force of the wires without putting too much pressure on the potentiometer. These solutions allowed for much simpler assembly of the pronation coupling and decreased the probability of breaking the pronation potentiometer.

Figure 5-7: Modified radiulna end with potentiometer inspection hole

5.4 SIMPLE CONTROL

One of the reasons for testing the prototype was to prove that it is capable of being controlled. As a proof of concept, however, it was not necessary to provide an optimal control scheme. As already shown in Chapter 2, the muscles are capable of being well controlled despite their highly non-linear nature. Therefore, a full nonlinear control scheme was not developed, but instead a simplified control scheme was used to expedite the testing process.

This simple control scheme took the potentiometer input data (elbow flexion angle and pronation/supination angle) and compared them to a desired motion. Based on the difference between the desired and the actual angles, it could simply be determined what the action of the solenoid valves should be. Take the flexion of the arm for example. If the value of the difference was positive, that meant that the desired angle of the elbow joint was higher than the

actual angle. Therefore, the valves for the flexion muscles were opened, to make them flex more, and the extension muscle was exhausted to allow the motion. If the value of the difference was negative, then the arm flexion angle was too high and the opposite action would be taken; inflating the extension muscle and deflating the flexion muscles.

5.5 DISCUSION OF RESULTS

This simple control scheme was applied to the system through sinusoidal tracking. The tracking for the elbow flexion/extension and the forearm pronation/supination were run separately to show the full capabilities of both types of motion. The results of the flexion/extension tracking test are shown in **Figure 5-8**. Note that zero degrees is fully extended and 110 degrees would be fully flexed. The tracking results for the pronation/supination of the forearm is shown in **Figure 5-9**. In this case zero degrees represents the neutral point with a positive angle being in a pronated state and a negative angle being in a supinated state.

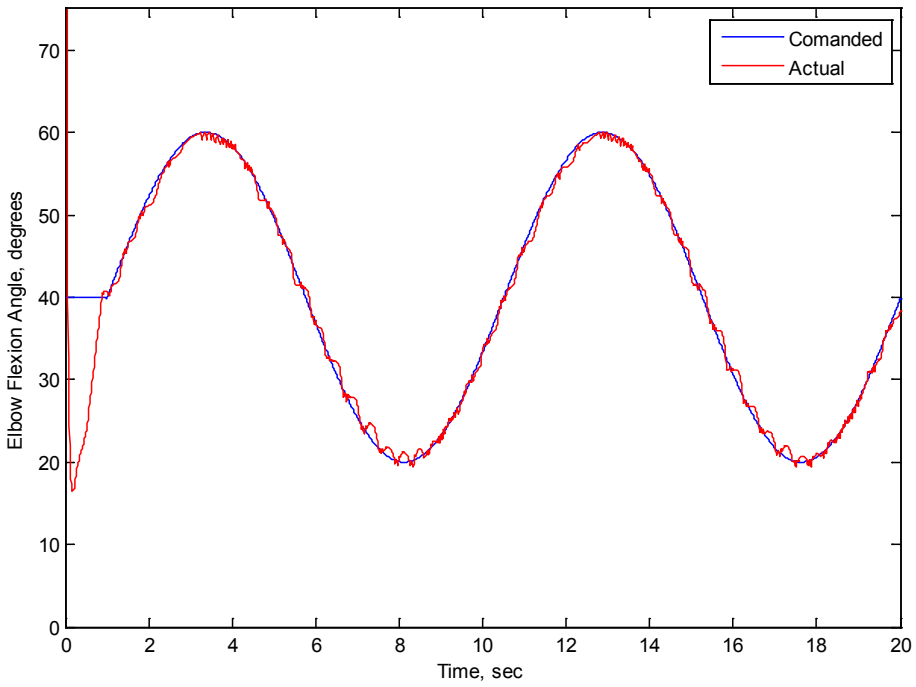

Figure 5-8: Sinusoidal tracking results for elbow flexion/extension

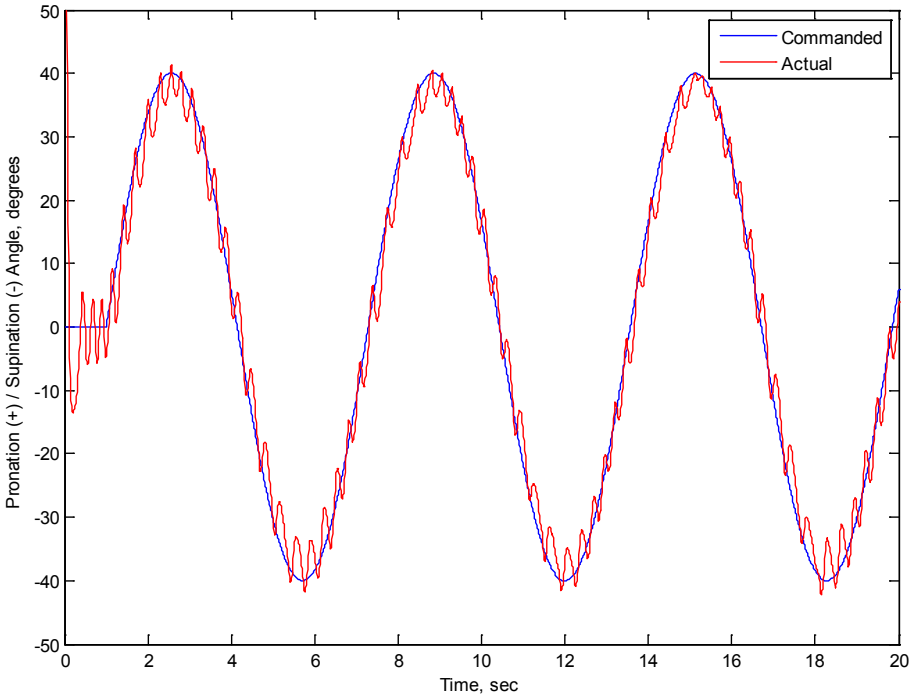

Figure 5-9: Sinusoidal tracking of the forearm

The pressure fluctuation for each muscle is also given for flexion/extension and pronation/supination tracking in **Figures 5-10** and **5-11** respectively.

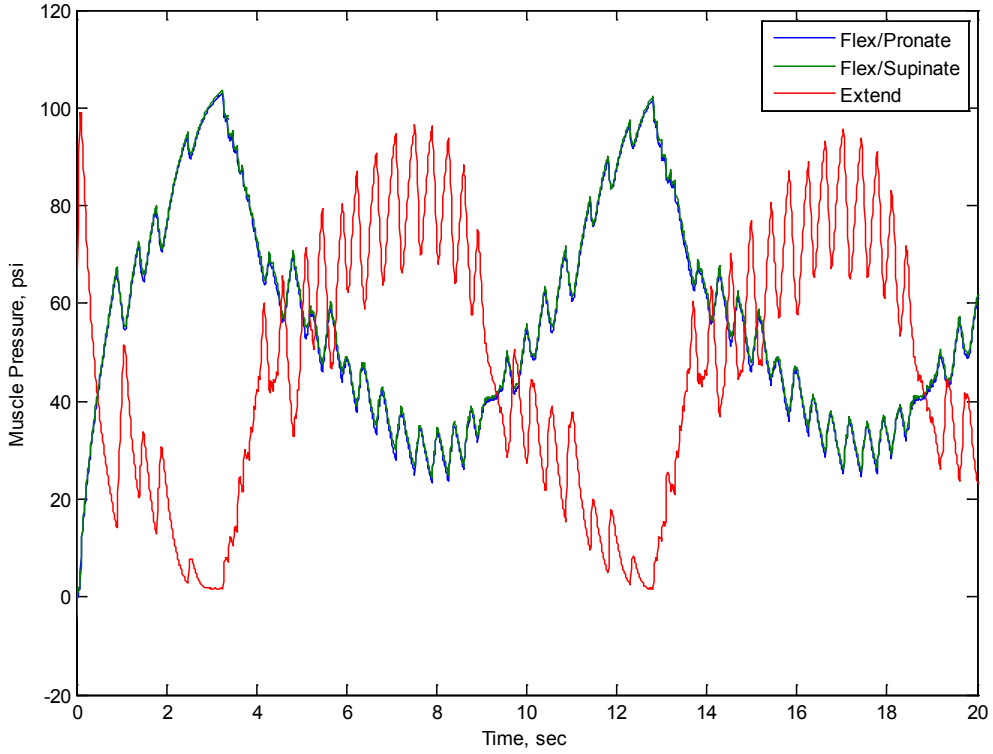

Figure 5- 10: Pressures in each muscle for the flexion/extension sinusoidal tracking

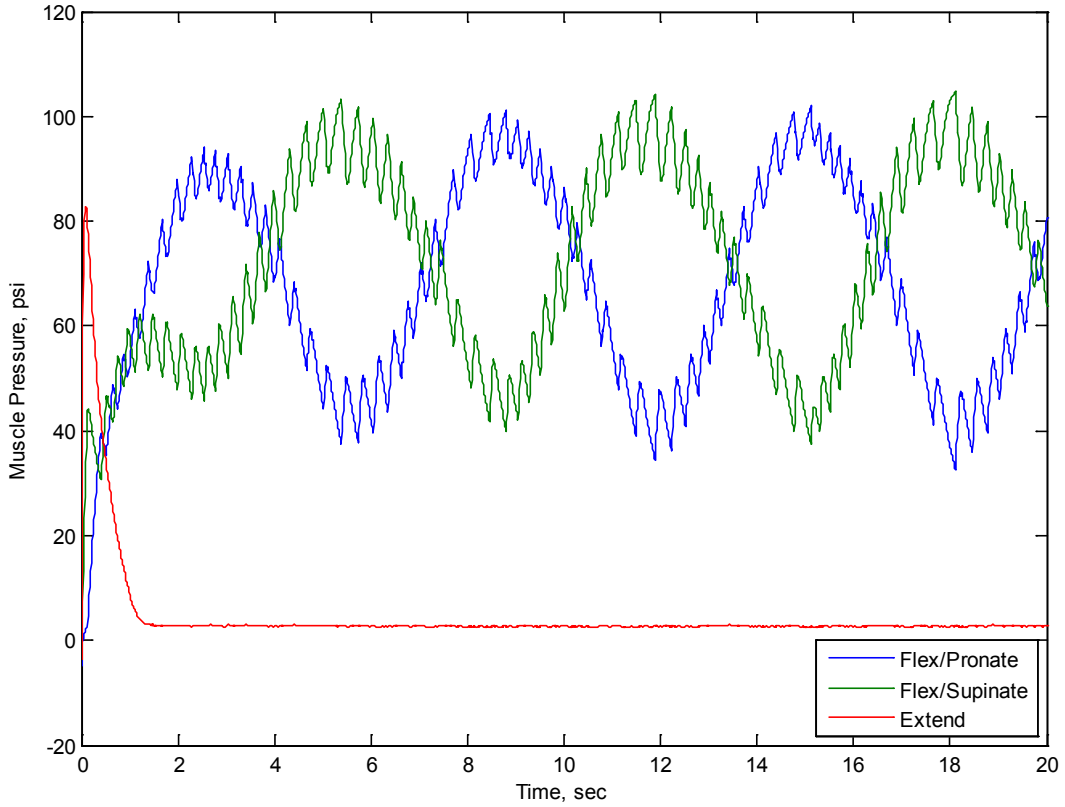

Figure 5-11: Pressures in each muscle for the pronation/supination sinusoidal tracking

These results show excellent tracking capabilities for the prototype prosthetic arm. The rapid oscillations in all the plots are inherent in the use of 3-port, on/off type valves and could be eliminated or at least diminished by using proportional valves or valves with two solenoids that provides three states; inlet, exhaust, and the neutral closed position. It can be seen that the prototype functions as it was designed. When the two anterior muscles are actuated together, as shown by the essentially identical pressure variation in **Figure 5-10**, the elbow joint flexes, as shown in **Figure 5-8**. When the two are actuated independently, as shown in the essentially opposite pressure curves in **Figure 5-11**, the pronation/supination motion is controlled as shown in **Figure 5-9**.

CHAPTER 6:

FUTURE WORK AND CONCLUSIONS

6.1 FUTURE WORK

6.1.1 CONFORMAL MULTI-UNIT ACTUATION

There are multiple future project ideas that stem from this research. The first and foremost is the conformal multi-unit design. This design takes the existing prototype and fine tunes the design by taking advantage of some rather unique properties the PAM. The design presented in Chapter 4 attempted to fit the maximum number of muscle actuators around a minimum outer radius such that none of the PAMs would interfere with each other. In other words, there is a considerable amount of underutilized space between the muscles when they are not all simultaneously actuated to their maximum s. The conformal design recognizes that this empty space that is not always necessary could allow for increased functionality.

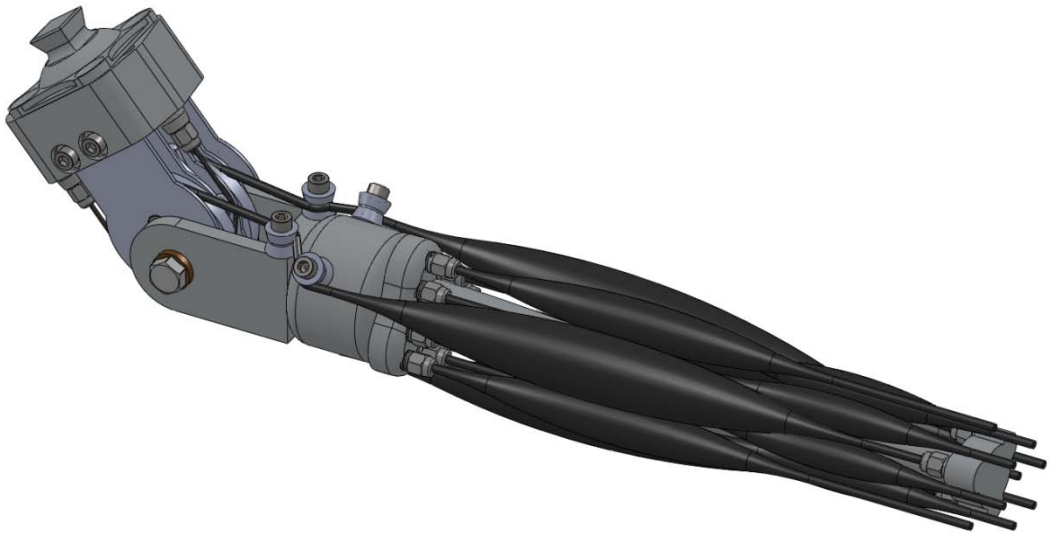

Figure 6- 1: Conformal multi-unit actuation prosthetic arm conceptual design

PAMs are a unique actuator in their flexibility. Like the human muscles they seek to replicate, they are capable of conforming to the space they are given. By eliminating the metal end connectors it is possible to create a completely flexible actuator that is more capable of conforming than any existing actuator. This would then allow for the actuators to be arranged in

such a way that their contact with each other or a central structural surface would not need to be discouraged, but could in fact be encouraged. With this in mind, the following design, shown in **Figure 6-1** was created. It expands on the design discussed in Chapter 4 and includes many changes that make it more closely resemble human anatomy.

The elbow joint structure and the pronation mechanism are largely the same. Minor changes could be made to better integrate the potentiometers. The variable radius pulleys would have to be redesigned to match the new muscle force curves. The radiulna has had many changes to make it more compact. These changes are shown in **Figure 6-2** below. The shaft or body of the radiulna is now smooth and tapered to allow more space for the PAMs that are closer to the central axis of the arm. The strength will be maintained by making it one solid piece and using FEA to optimize the design curvature. This also makes it look more like the human skeleton. The ends of the radiulna are redesigned to accommodate more muscles connections on the proximal end and to be considerably smaller on the distal end.

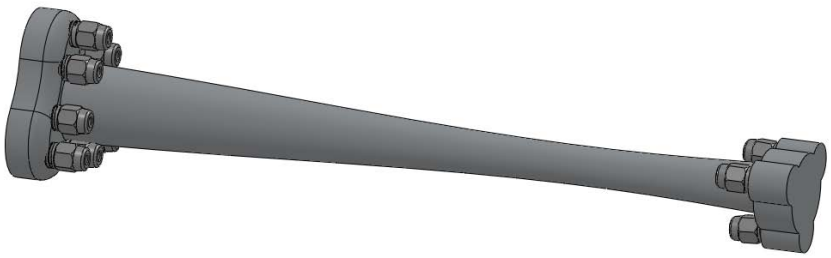

Figure 6-2: Redesigned radiulna concept for conformal muscle design

This design contains double the number muscle actuators than the design presented in Chapter 4. Three large PAMs control the elbow flexion/extension and forearm pronation/supination motions in the same way. Three intermediately spaced, medium sized muscles control the position of the wrist. Finally there are six small sized muscles located

towards the distal end of the forearm that would be used to control the motions of the hand. It has been shown that this number of actuators is adequate to control all the motions of a prosthetic hand unit. Dalley et al [1] used only five actuators in their design. These twelve actuators are radially spaced in such a way that they have minimum interaction in a resting state, but will be in contact as soon and any of the muscles is actuated.

The muscles themselves will be the most redesigned components. They would be designed to include the tendon connection directly, using the fibrous mesh wrap of the muscle section as the structural cable of the tendon section as well. The fibers would be enclosed and protected within a small layer of the rubber membrane material. The outer surface of the muscles would be coated in a lubricant to reduce friction between the muscles, and the entire arm would be covered in a flexible skin-like outer surface.

6.1.2 INTEGRATED CHEMO-MUSCLE PROSTHETIC ARM

Another goal for the future of this project would be to combine the principles discussed separately in the chapters of this thesis. Now that each level of innovation has been completed separately, a combined testing prototype is the next logical step. It is suggested that the chemo-muscle and the integrated muscle designs be combined first. This adapted inclusive chemo-muscle, proven separately, could then easily be transitioned to working with the existing prototype. Customized muscles are also the first step in the in the conformal design so the experience of developing and constructing PAMs in house would be invaluable for both projects individually and possibly in combination.

6.2 CONCLUSION

In summary, this thesis presents a design for a novel prosthetic arm, innovating on three different levels: the actuation method, system integration, and the mechanism design. The Chemo-Muscle actuation system creates the possibility of using PAMs in a mobile application by creating the high pressure gasses on demand from stored liquid fuel. The integrated muscle design makes use of the internal volume of the muscle actuator by creating an internal incompressible region which could contain other components that are typically external such as valves and pressure sensors. This is also shown to improve the efficiency of the PAM and reduce its overall consumption of its fuel source. Finally, a novel design is presented that uses multiple smaller PAMs as a group to control multiple degrees of freedom simultaneously. This design is shown to provide 50% more strength than other available prosthetic arms as well as an excellent range of motion for each degree of freedom. A simple control method is proven and the future development of this project is discussed including a conceptual design for the conformal muscle arm.

REFERENCES

1. Dalley S, Wiste T, Withrow T, Goldfarb M. Design of a Multifunctional Anthropomorphic Prosthetic Hand with Extrinsic Actuation. IEEE/ASME Transactions on Mechatronics 2009

APPENDIX A:

DETAILED DRAWINGS OF PROSTHETIC PROTOTYPE AS INITIALLY MACHINED (BEFORE MODIFICATIONS)

Pneumatic Muscle Actuated Prosthetic Arm Prototype

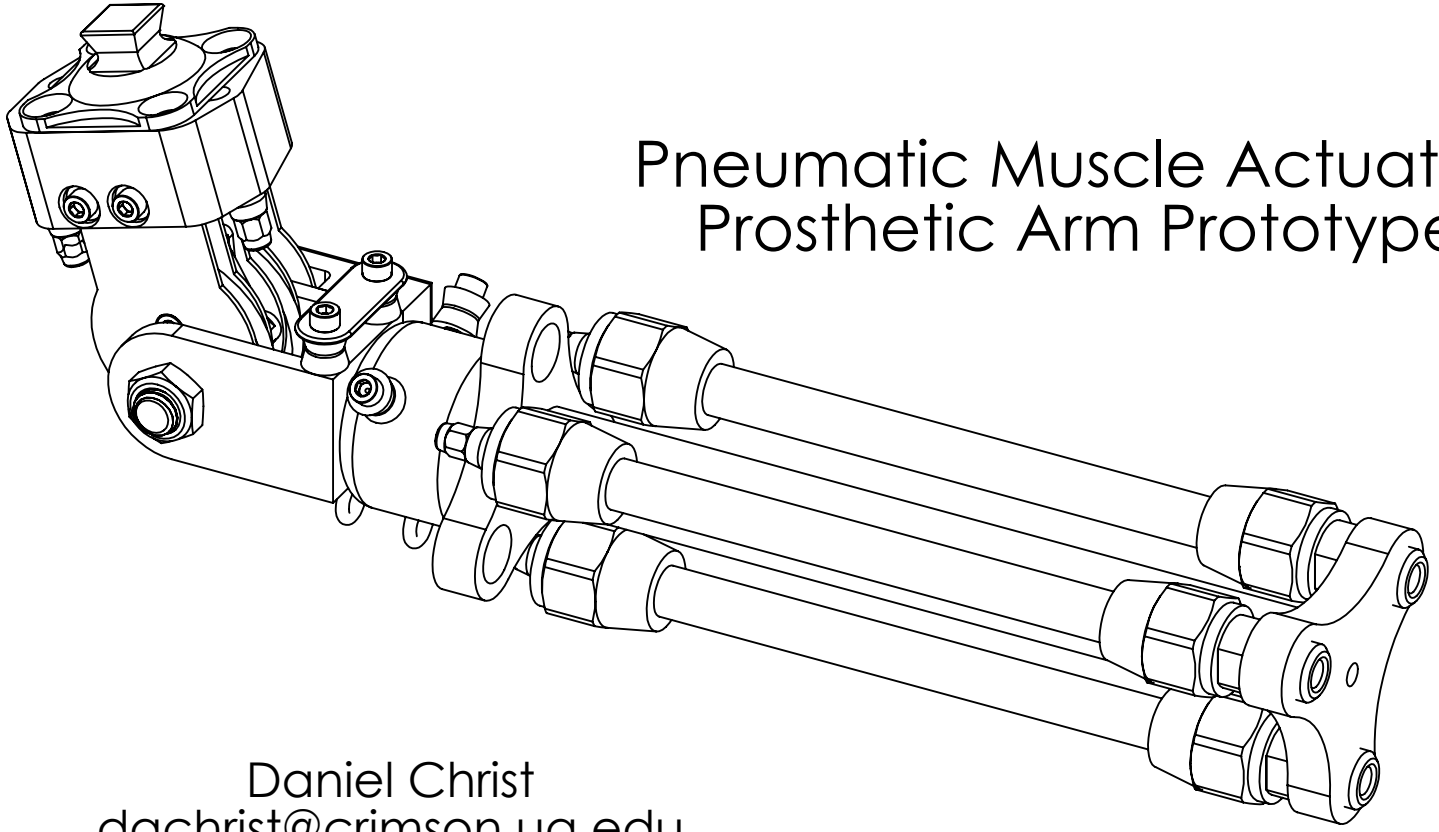

Daniel Christ
dachrist@crimson.ua.edu

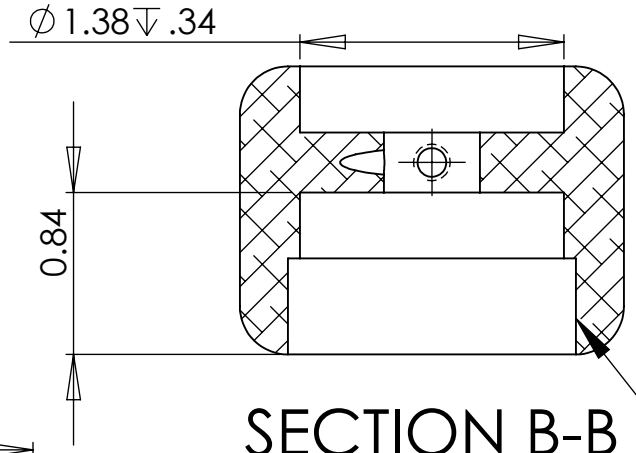

SECTION B-B

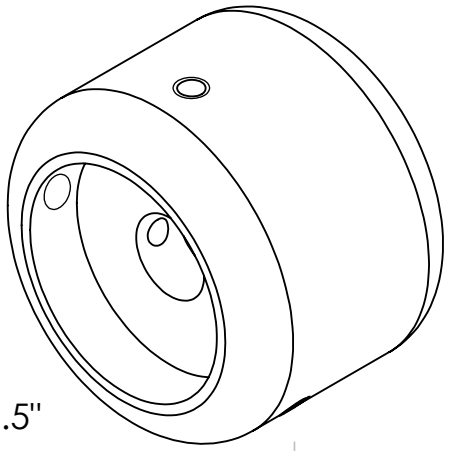

1.5"-24↧0.5"

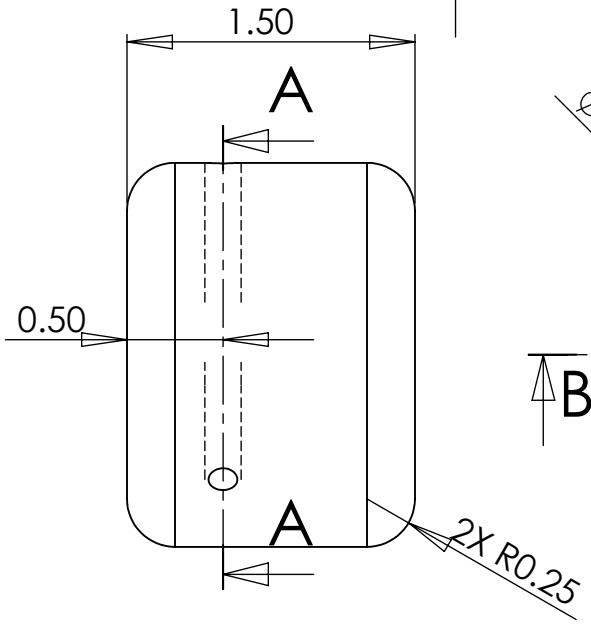

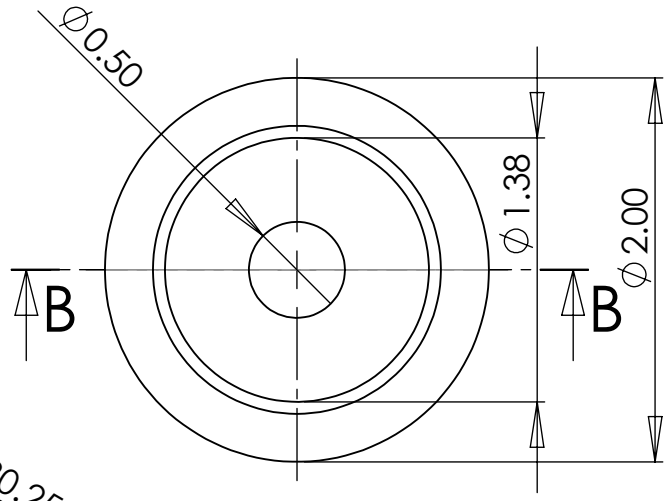

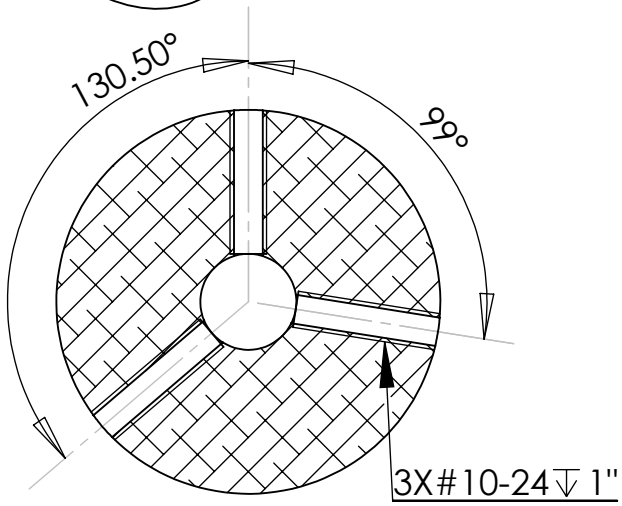

SECTION A-A

UNLESS OTHERWISE SPECIFIED:		NAME	DATE
DIMENSIONS ARE IN INCHES TOLERANCES: FRACTIONAL ± ANGULAR: MACH ± BEND ± TWO PLACE DECIMAL ± THREE PLACE DECIMAL ±	DRAWN		
	CHECKED		
	ENG APPR.		
	MFG APPR.		
INTERPRET GEOMETRIC TOLERANCING PER:	Q.A.		
MATERIAL 6061 Al	COMMENTS:		
FINISH			
DO NOT SCALE DRAWING			

TITLE:

Pronation Coupling
Proximal

SIZE	DWG. NO.	REV
A	ArmAsm3-1	

SCALE: 1:1	WEIGHT:	SHEET 2 OF 13

5 4 3 2 1

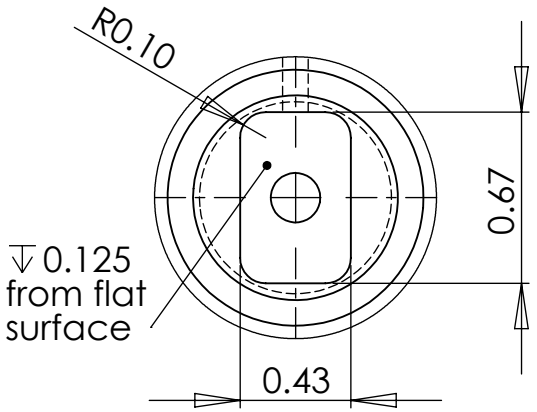

DETAIL D
SCALE 2 : 1.5

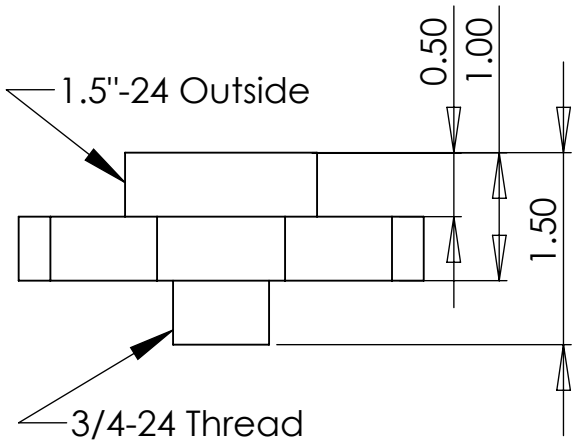

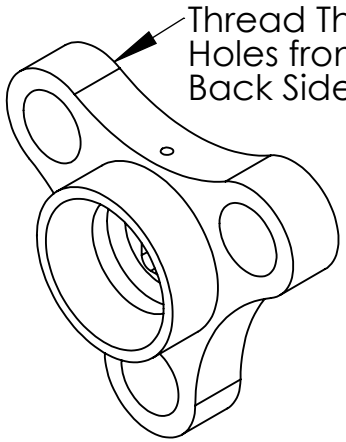

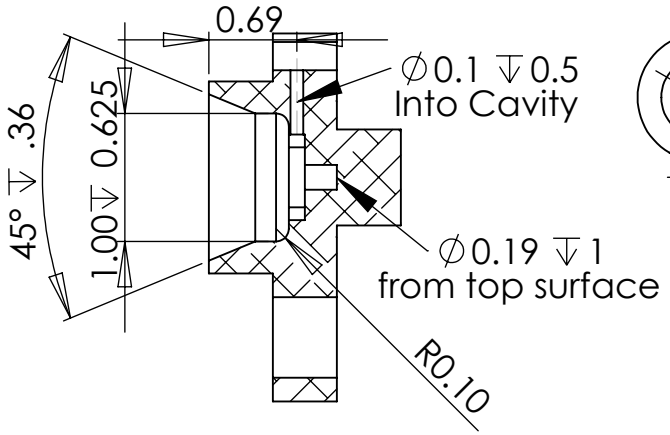

SECTION C-C

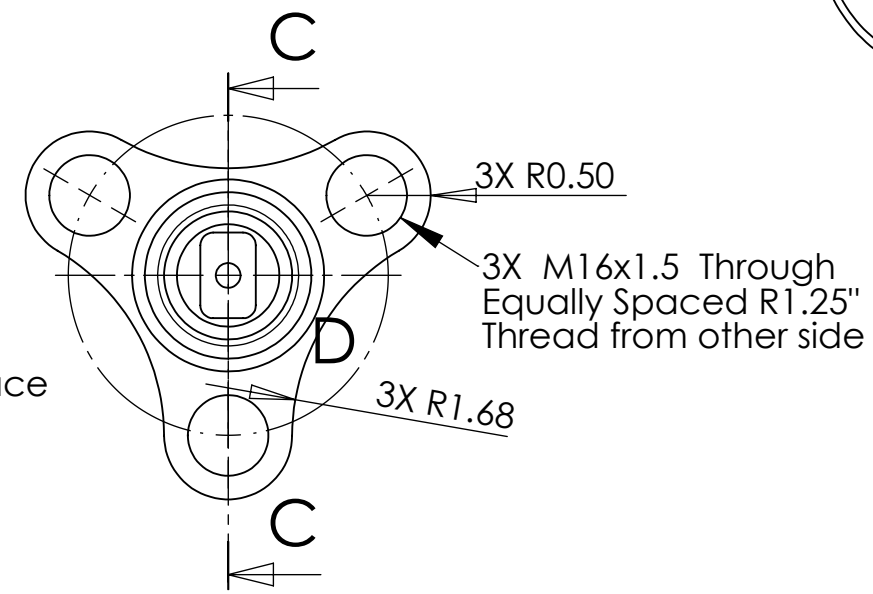

UNLESS OTHERWISE SPECIFIED:		NAME	DATE
DIMENSIONS ARE IN INCHES TOLERANCES: FRACTIONAL ± ANGULAR: MACH ± BEND ± TWO PLACE DECIMAL ± THREE PLACE DECIMAL ±	DRAWN		
	CHECKED		
	ENG APPR.		
	MFG APPR.		
	Q.A.		
INTERPRET GEOMETRIC TOLERANCING PER:	COMMENTS:		
MATERIAL 6061 AL			
FINISH			
DO NOT SCALE DRAWING			

TITLE:
Pronation Coupling
Distal

SIZE	DWG. NO.	REV
A	ArmAsm3-1	

SCALE: 1:1.5 WEIGHT: SHEET 3 OF 13

5 4 3 2 1

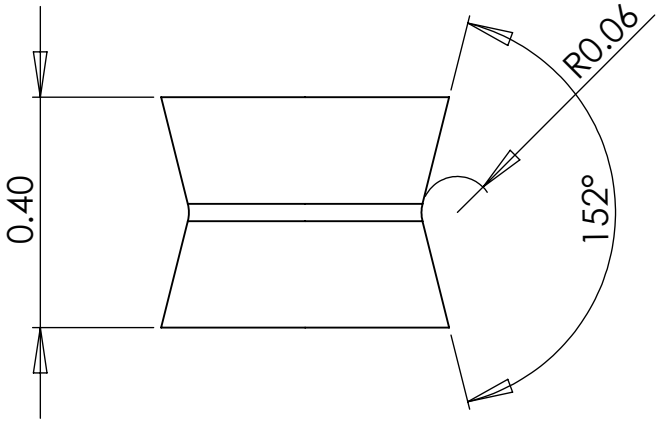

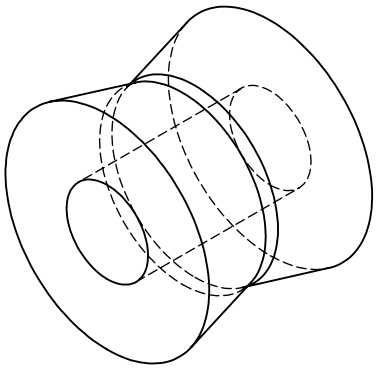

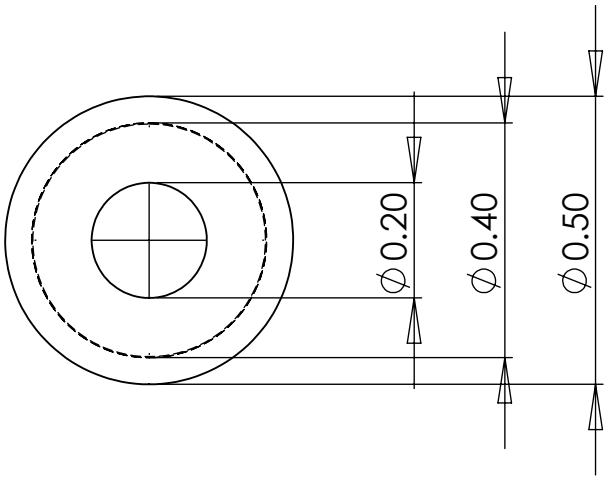

UNLESS OTHERWISE SPECIFIED:		NAME	DATE
DIMENSIONS ARE IN INCHES TOLERANCES: FRACTIONAL ± ANGULAR: MACH ± BEND ± TWO PLACE DECIMAL ± THREE PLACE DECIMAL ±	DRAWN		
	CHECKED		
	ENG APPR.		
	MFG APPR.		
	Q.A.		
INTERPRET GEOMETRIC TOLERANCING PER:	COMMENTS:		
MATERIAL Plastic	Count: 6		
FINISH			
DO NOT SCALE DRAWING			

TITLE: Bolt Roller

SIZE	DWG. NO.	REV
A	ArmAsm3-1	

SCALE: 3:1	WEIGHT:	SHEET 4 OF 13

5 4 3 2 1

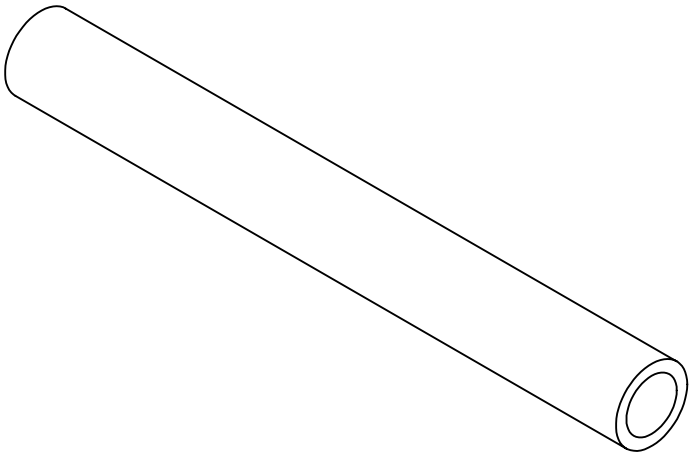

3/4" Pipe
Schedule 80

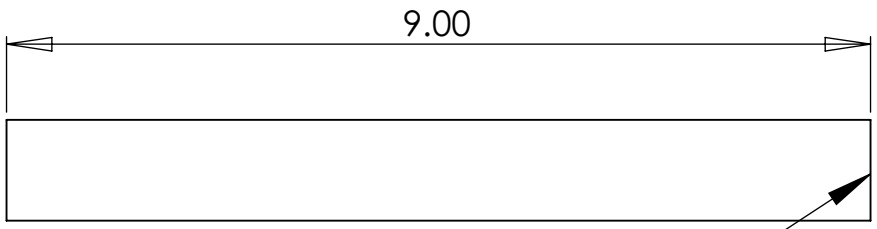

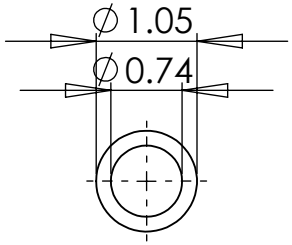

3/4-24 Tap Both Ends
↧0.5

Original parts will be provided

UNLESS OTHERWISE SPECIFIED:		NAME	DATE
DIMENSIONS ARE IN INCHES TOLERANCES: FRACTIONAL ± ANGULAR: MACH ± BEND ± TWO PLACE DECIMAL ± THREE PLACE DECIMAL ±	DRAWN		
	CHECKED		
	ENG APPR.		
	MFG APPR.		
	Q.A.		
INTERPRET GEOMETRIC TOLERANCING PER:	COMMENTS:		
MATERIAL 6061AL			
FINISH			
DO NOT SCALE DRAWING			

TITLE: RadiUlna Skeleton

SIZE	DWG. NO.	REV
A	ArmAsm3-1	

SCALE: 1:2 | WEIGHT: | SHEET 5 OF 13

5 4 3 2 1

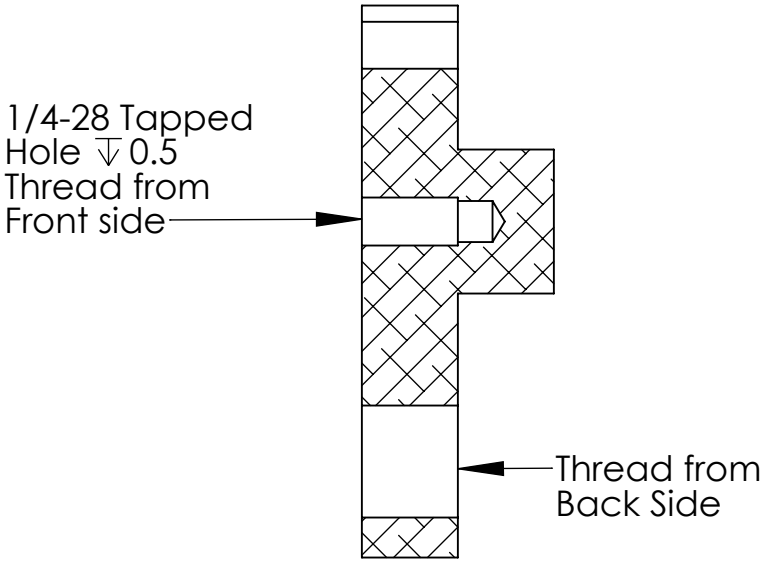

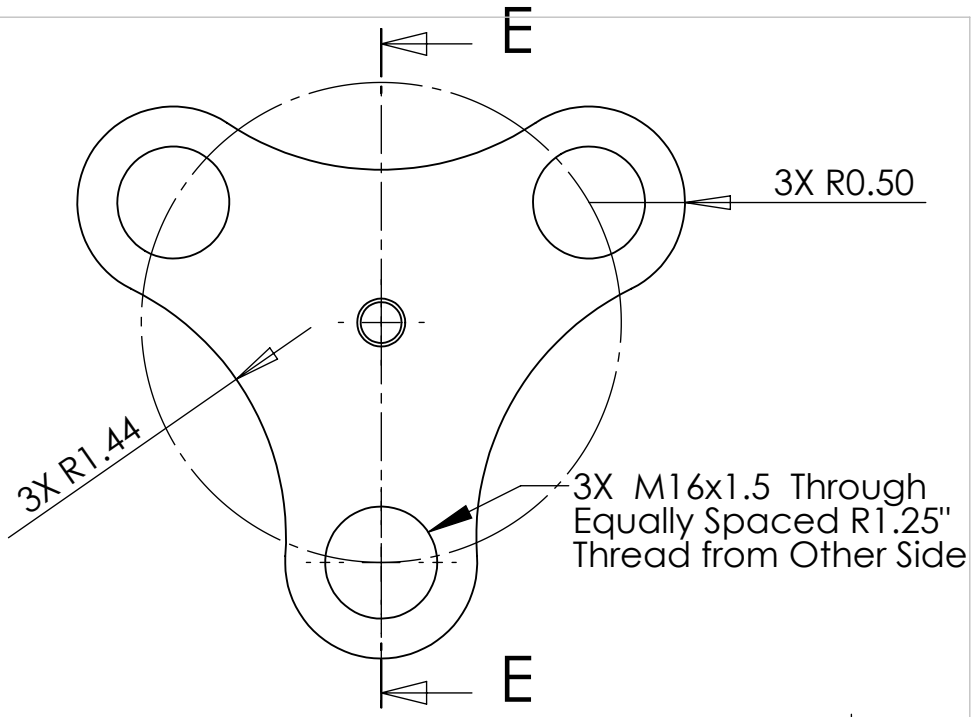

SECTION E-E

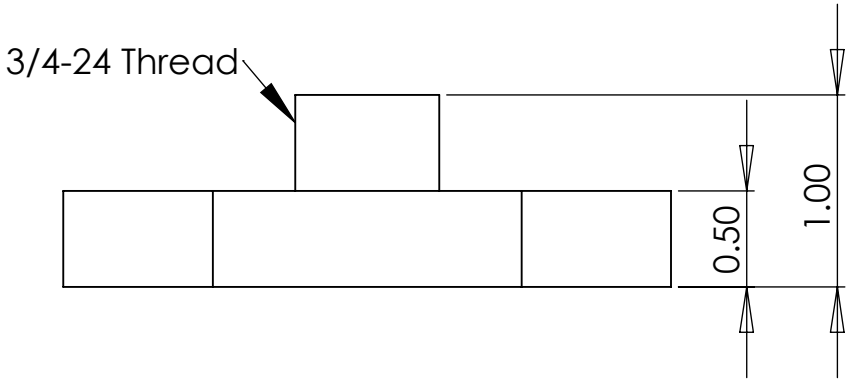

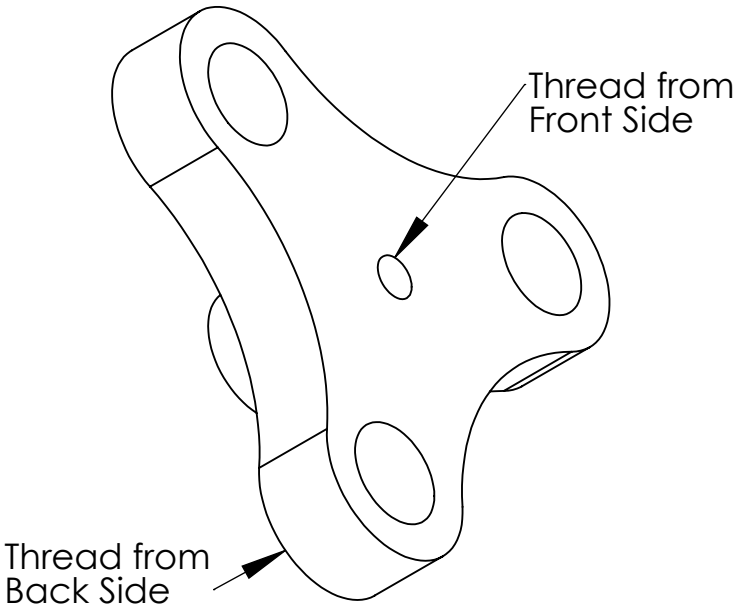

UNLESS OTHERWISE SPECIFIED:		NAME	DATE
DIMENSIONS ARE IN INCHES TOLERANCES: FRACTIONAL ± ANGULAR: MACH ± BEND ± TWO PLACE DECIMAL ± THREE PLACE DECIMAL ±	DRAWN		
	CHECKED		
	ENG APPR.		
	MFG APPR.		
	Q.A.		
INTERPRET GEOMETRIC TOLERANCING PER:	COMMENTS:		
MATERIAL 6061 AL			
FINISH			
DO NOT SCALE DRAWING			

TITLE: Wrist Mount End

SIZE	DWG. NO.	REV
A	ArmAsm3-1	

SCALE: 1:1 | WEIGHT: | SHEET 6 OF 13

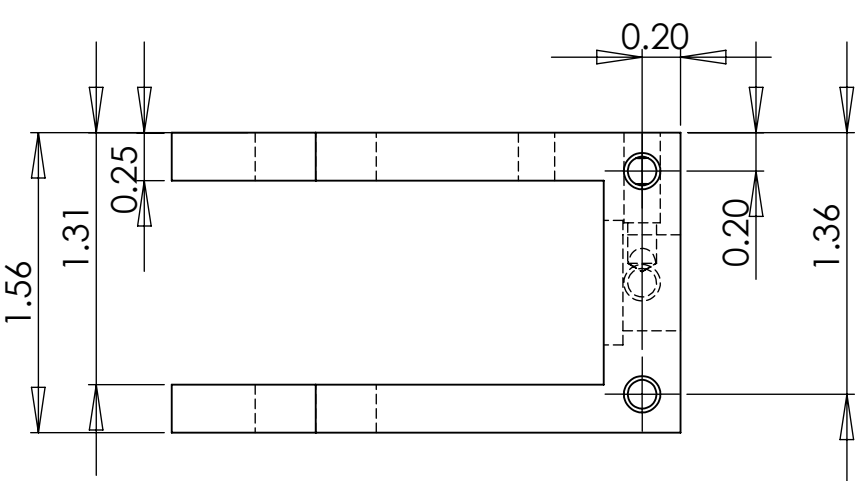

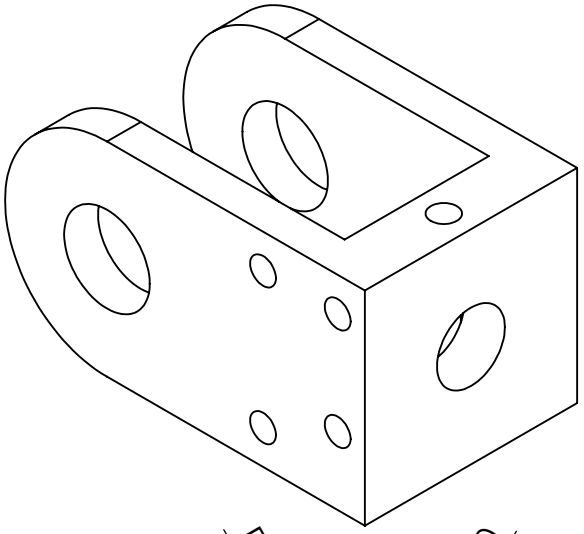

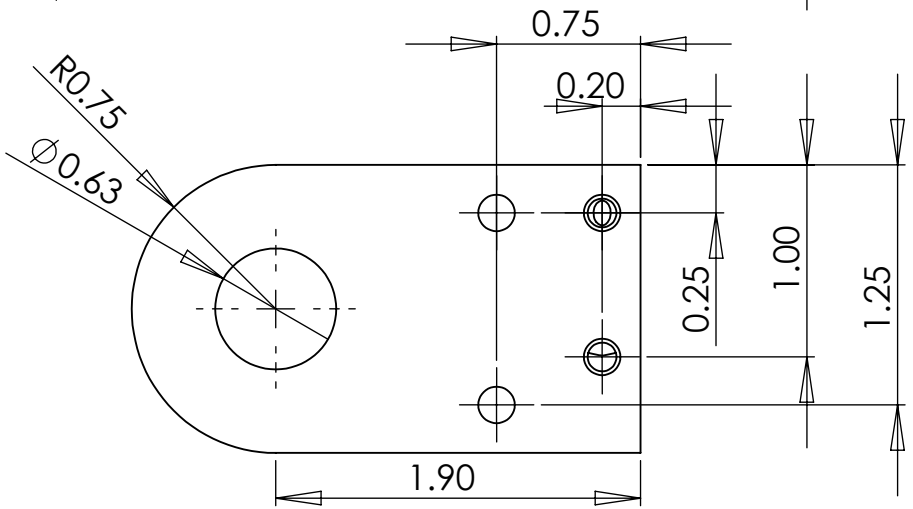

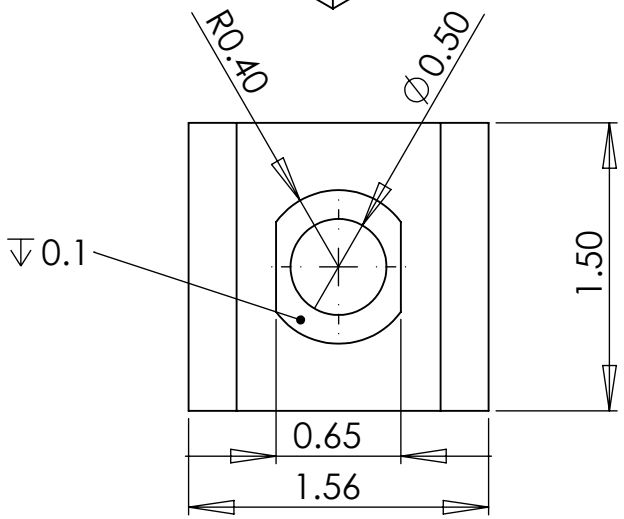

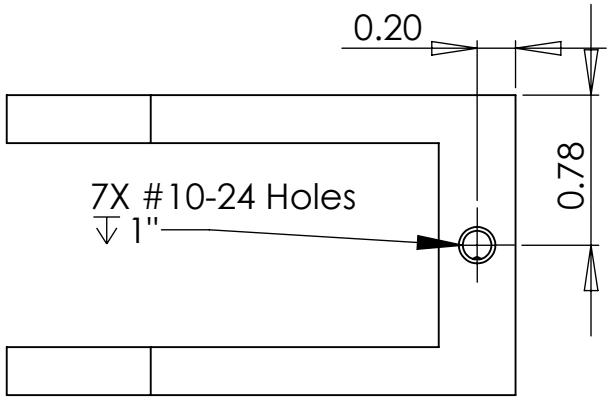

UNLESS OTHERWISE SPECIFIED:		NAME	DATE
DIMENSIONS ARE IN INCHES TOLERANCES: FRACTIONAL ± ANGULAR: MACH ± BEND ± TWO PLACE DECIMAL ± THREE PLACE DECIMAL ±	DRAWN		
	CHECKED		
	ENG APPR.		
	MFG APPR.		
	Q.A.		
INTERPRET GEOMETRIC TOLERANCING PER:	COMMENTS:		
MATERIAL 6061 AL			
FINISH			
DO NOT SCALE DRAWING			

TITLE:

Elbow Bracket

SIZE	DWG. NO.	REV
A	ArmAsm3-1	

SCALE: 1:1	WEIGHT:	SHEET 7 OF 13

5 4 3 2 1

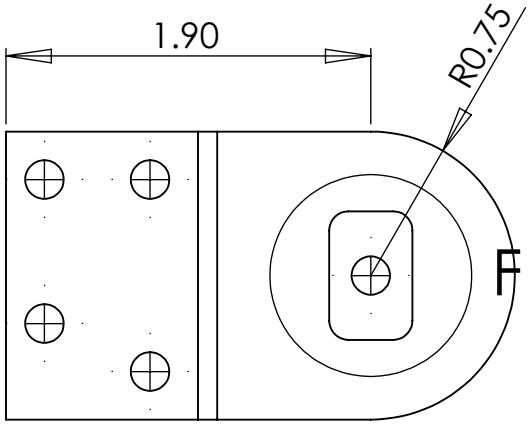

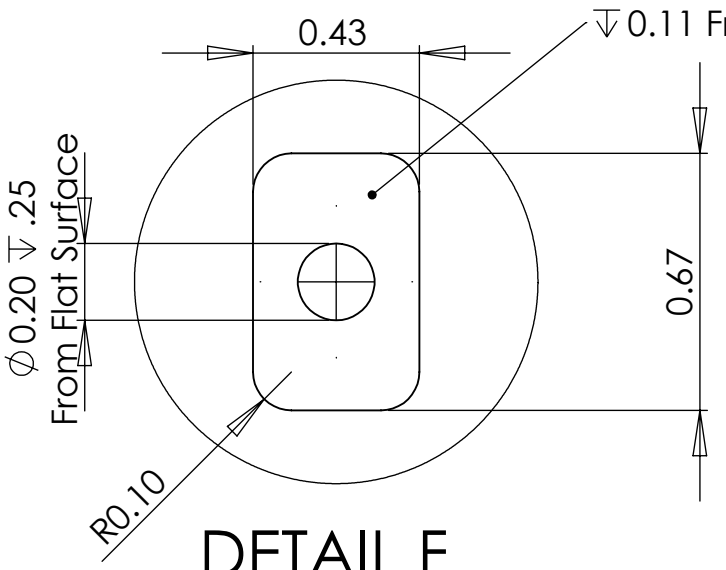

DETAIL F
SCALE 2 : 1

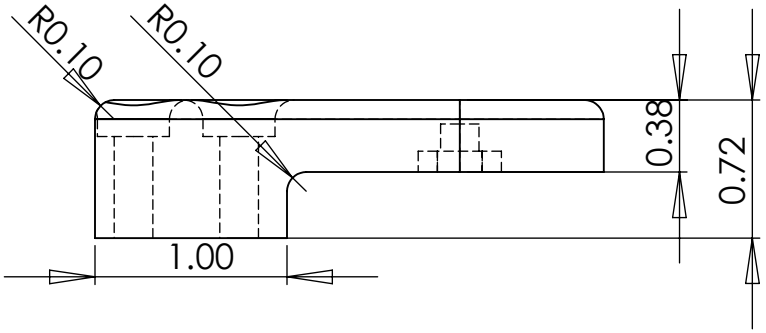

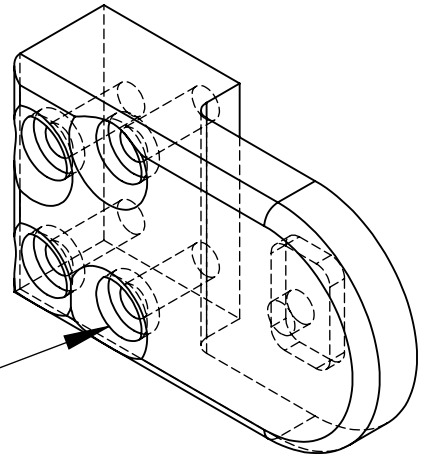

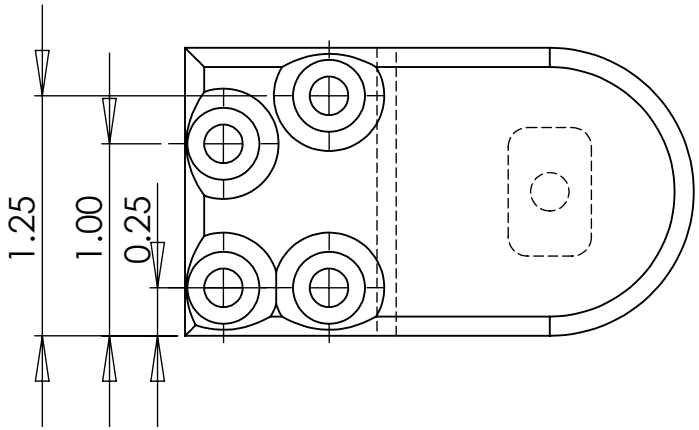

UNLESS OTHERWISE SPECIFIED:		NAME	DATE
DIMENSIONS ARE IN INCHES TOLERANCES: FRACTIONAL ± ANGULAR: MACH ± BEND ± TWO PLACE DECIMAL ± THREE PLACE DECIMAL ±	DRAWN		
	CHECKED		
	ENG APPR.		
	MFG APPR.		
INTERPRET GEOMETRIC TOLERANCING PER:	Q.A.		
MATERIAL Plastic	COMMENTS:		
FINISH			
DO NOT SCALE DRAWING			

TITLE:

Elbow Potentiometer Mount

SIZE	DWG. NO.	REV
A	ArmAsm3-1	

SCALE: 1:1 | WEIGHT: | SHEET 8 OF 13

5 4 3 2 1

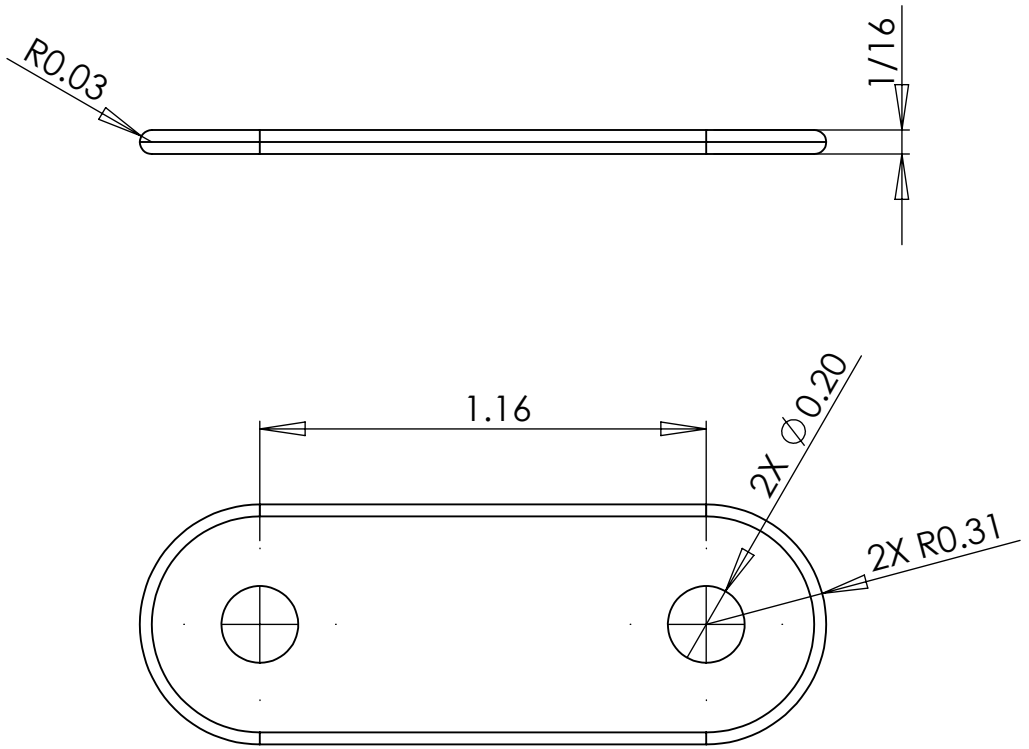

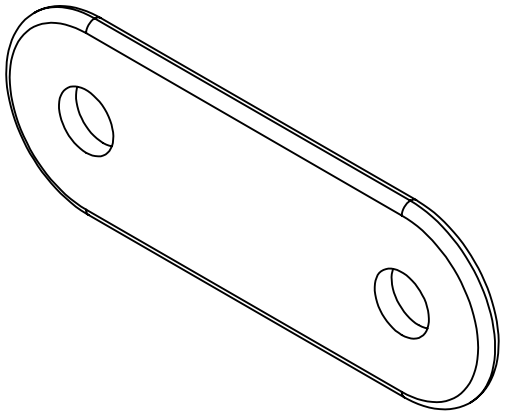

UNLESS OTHERWISE SPECIFIED:		NAME	DATE
DIMENSIONS ARE IN INCHES TOLERANCES: FRACTIONAL ± ANGULAR: MACH ± BEND ± TWO PLACE DECIMAL ± THREE PLACE DECIMAL ±	DRAWN		
	CHECKED		
	ENG APPR.		
	MFG APPR.		
	Q.A.		
INTERPRET GEOMETRIC TOLERANCING PER:	COMMENTS:		
MATERIAL 6061 AL	Count: 2		
FINISH			
DO NOT SCALE DRAWING			

TITLE: Elbow Stop Plate

SIZE	DWG. NO.	REV
A	ArmAsm3-1	

SCALE: 2:1	WEIGHT:	SHEET 9 OF 13

5 4 3 2 1

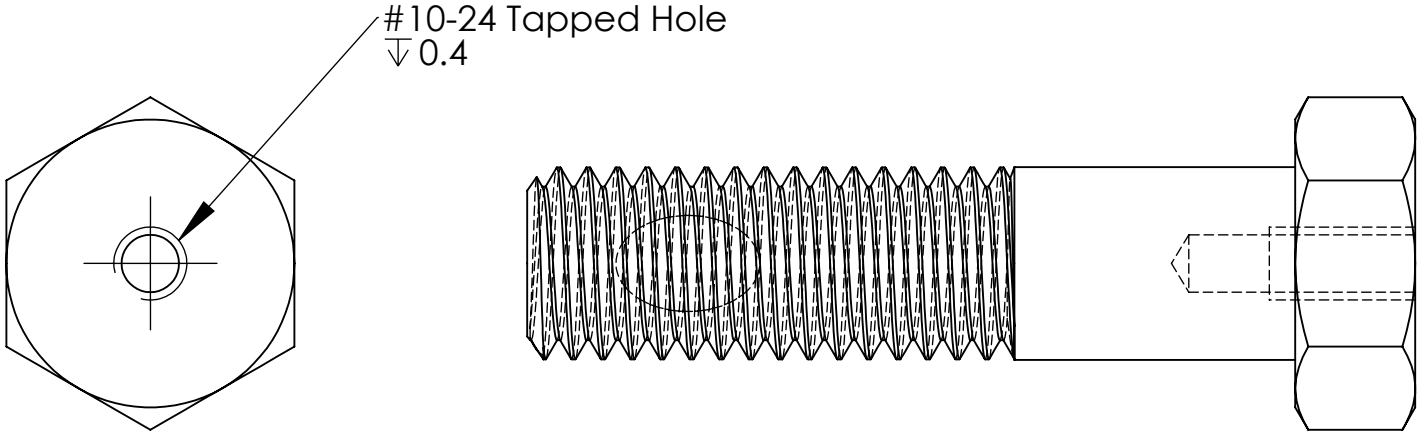

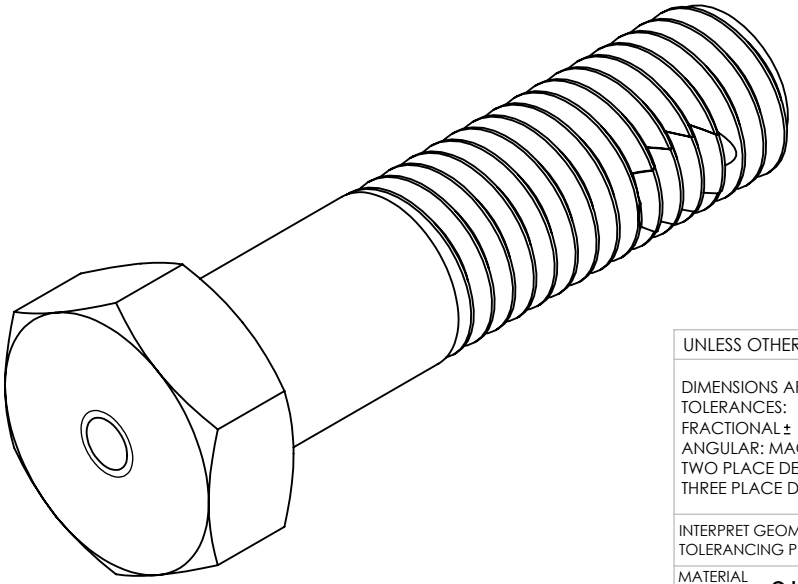

1/2-13 Bolt 2" Long

Original parts will be provided

UNLESS OTHERWISE SPECIFIED:		NAME	DATE
DIMENSIONS ARE IN INCHES TOLERANCES: FRACTIONAL ± ANGULAR: MACH ± BEND ± TWO PLACE DECIMAL ± THREE PLACE DECIMAL ±	DRAWN		
	CHECKED		
	ENG APPR.		
	MFG APPR.		
	Q.A.		
INTERPRET GEOMETRIC TOLERANCING PER:	COMMENTS:		
MATERIAL Steel	Count: 2		
FINISH			
DO NOT SCALE DRAWING			

TITLE: Pronation Pin

SIZE	DWG. NO.	REV
A	ArmAsm3-1	

SCALE: 2:1 | WEIGHT: | SHEET 10 OF 13

5 4 3 2 1

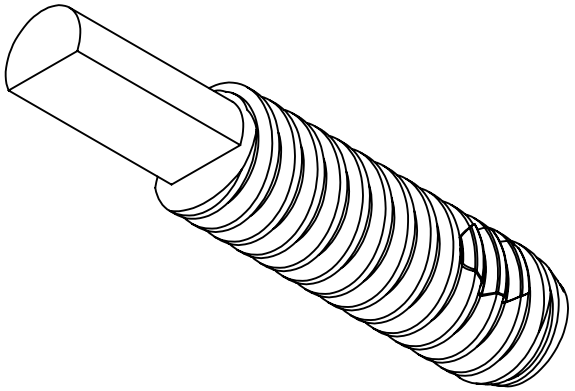

Machine Down #10/24 Bolt

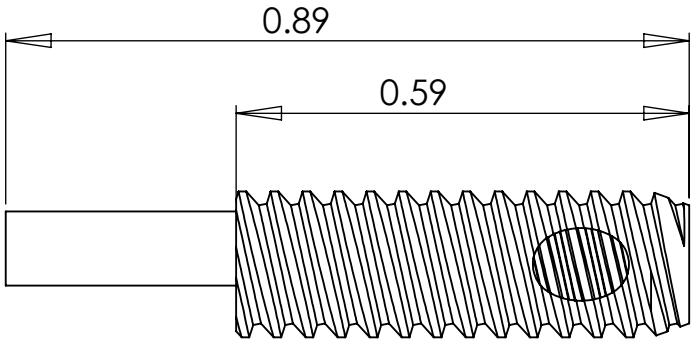

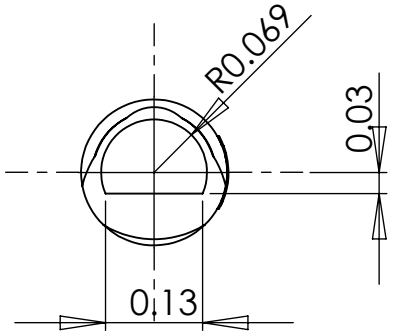

Original parts will be provided

UNLESS OTHERWISE SPECIFIED:		NAME	DATE
DIMENSIONS ARE IN INCHES TOLERANCES: FRACTIONAL ± ANGULAR: MACH ± BEND ± TWO PLACE DECIMAL ± THREE PLACE DECIMAL ±	DRAWN		
	CHECKED		
	ENG APPR.		
	MFG APPR.		
	Q.A.		
INTERPRET GEOMETRIC TOLERANCING PER:	COMMENTS:		
MATERIAL	Count: 4		
FINISH			
DO NOT SCALE DRAWING			

TITLE: Potentiometer Bolt

SIZE	DWG. NO.	REV
A	ArmAsm3-1	

SCALE: 4:1	WEIGHT:	SHEET 11 OF 13

5 4 3 2 1

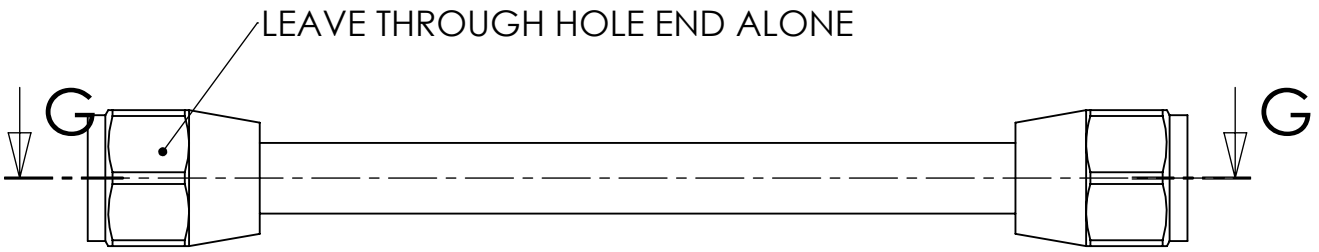

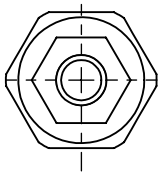

SECTION G-G

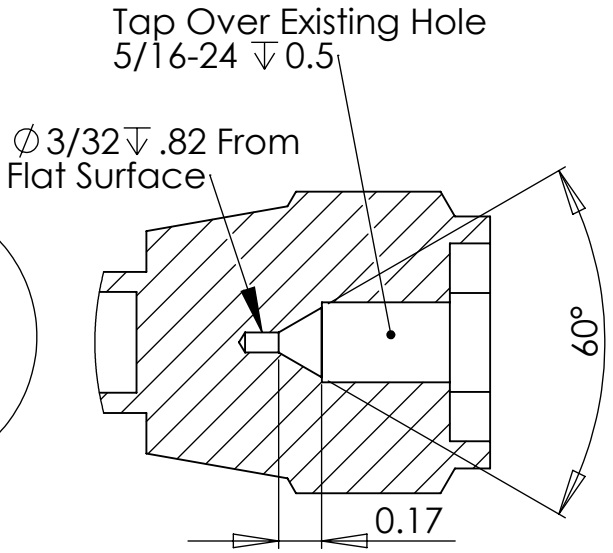

DETAIL H
SCALE 2 : 1.5

Original parts will be provided

UNLESS OTHERWISE SPECIFIED:		NAME	DATE
DIMENSIONS ARE IN INCHES TOLERANCES: FRACTIONAL ± ANGULAR: MACH ± BEND ± TWO PLACE DECIMAL ± THREE PLACE DECIMAL ±	DRAWN		
	CHECKED		
	ENG APPR.		
	MFG APPR.		
	Q.A.		
INTERPRET GEOMETRIC TOLERANCING PER:	COMMENTS:		
MATERIAL			
FINISH			
DO NOT SCALE DRAWING			

Count: 6

TITLE: Festo Muscle 10mm

SIZE	DWG. NO.	REV
A	ArmAsm3-1	

SCALE: 1:1.5 WEIGHT: SHEET 12 OF 13

5 4 3 2 1

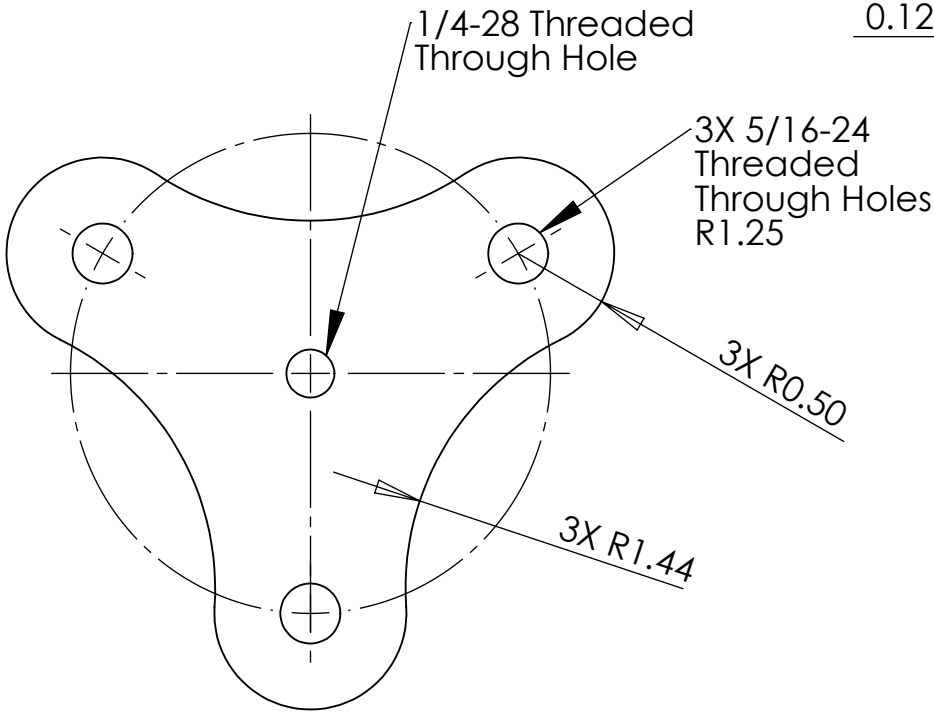

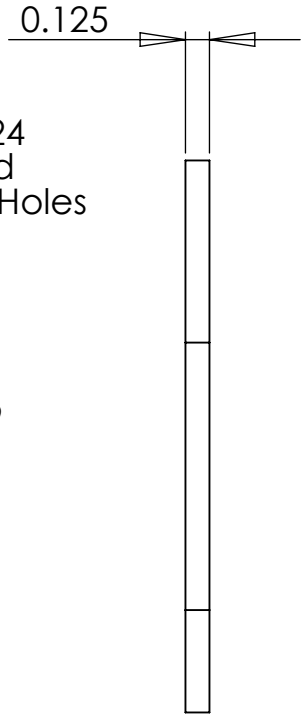

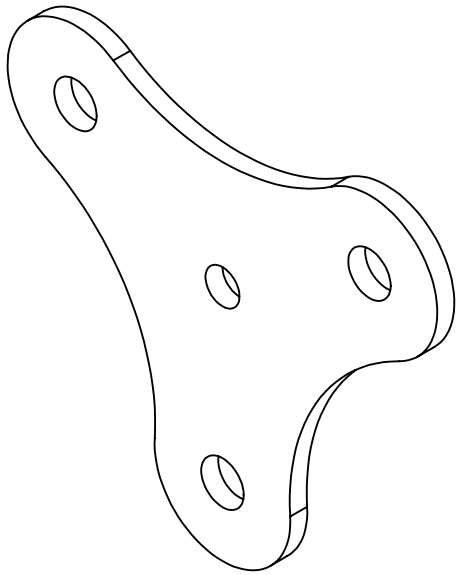

ALL HOLES THREADED
IN SAME DIRECTION

UNLESS OTHERWISE SPECIFIED:		NAME	DATE
DIMENSIONS ARE IN INCHES TOLERANCES: FRACTIONAL ± ANGULAR: MACH ± BEND ± TWO PLACE DECIMAL ± THREE PLACE DECIMAL ±	DRAWN		
	CHECKED		
	ENG APPR.		
	MFG APPR.		
	Q.A.		
INTERPRET GEOMETRIC TOLERANCING PER:	COMMENTS:		
MATERIAL 6061 AL	Count: 2		
FINISH			
DO NOT SCALE DRAWING			

TITLE: Wrist Plate

SIZE	DWG. NO.	REV
A	ArmAsm3-1	

SCALE: 1:1 | WEIGHT: | SHEET 13 OF 13

5 4 3 2 1

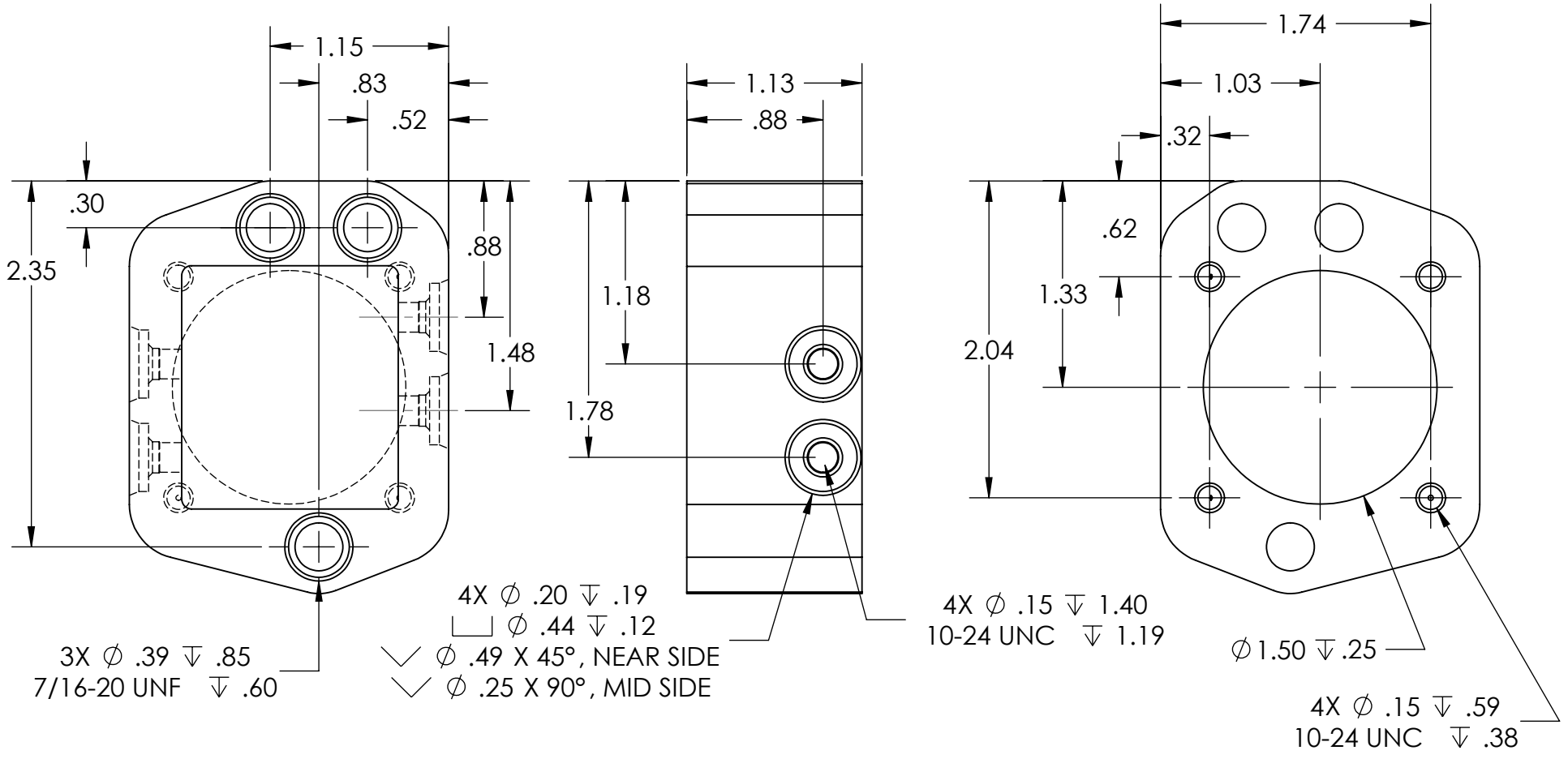

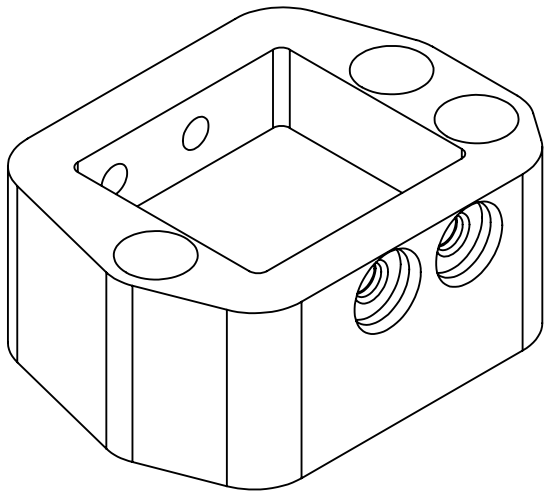

TITLE: Anchor Block For Upper Elbow		
MATERIAL: AL		
SIZE **A**	DWG. NO.	REV
	SCALE: 1:1	SHEET 1 OF 2

5 4 3 2 1

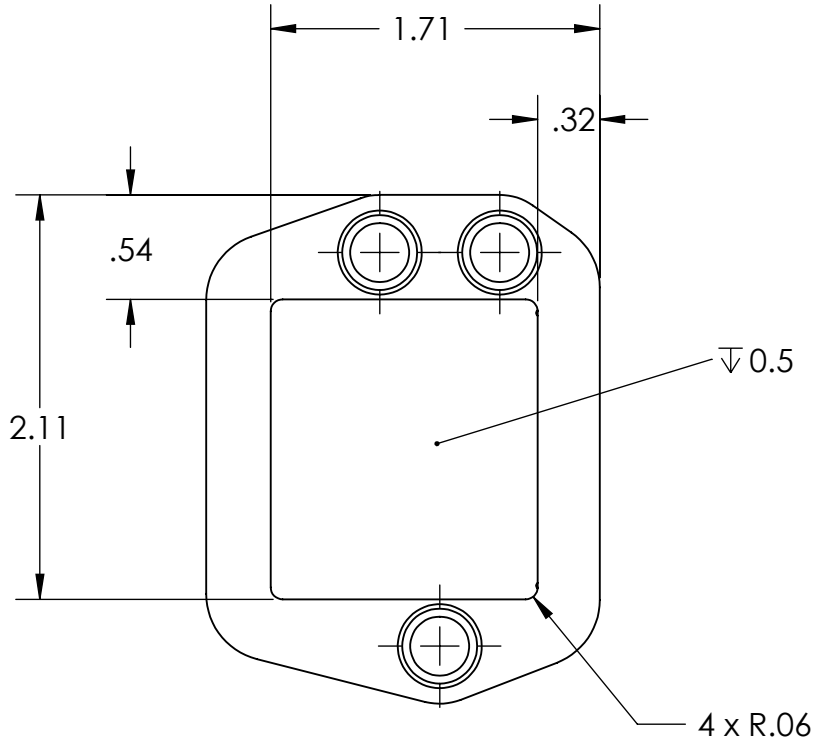

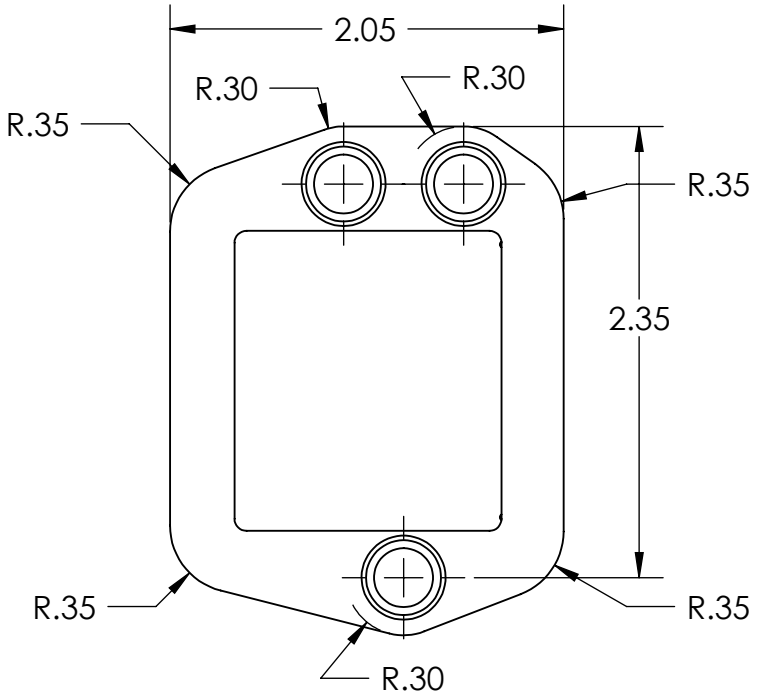

TITLE:		
MATERIAL:		
SIZE **A**	DWG. NO.	REV
	SCALE: 1:1	SHEET 2 OF 2

5 4 3 2 1

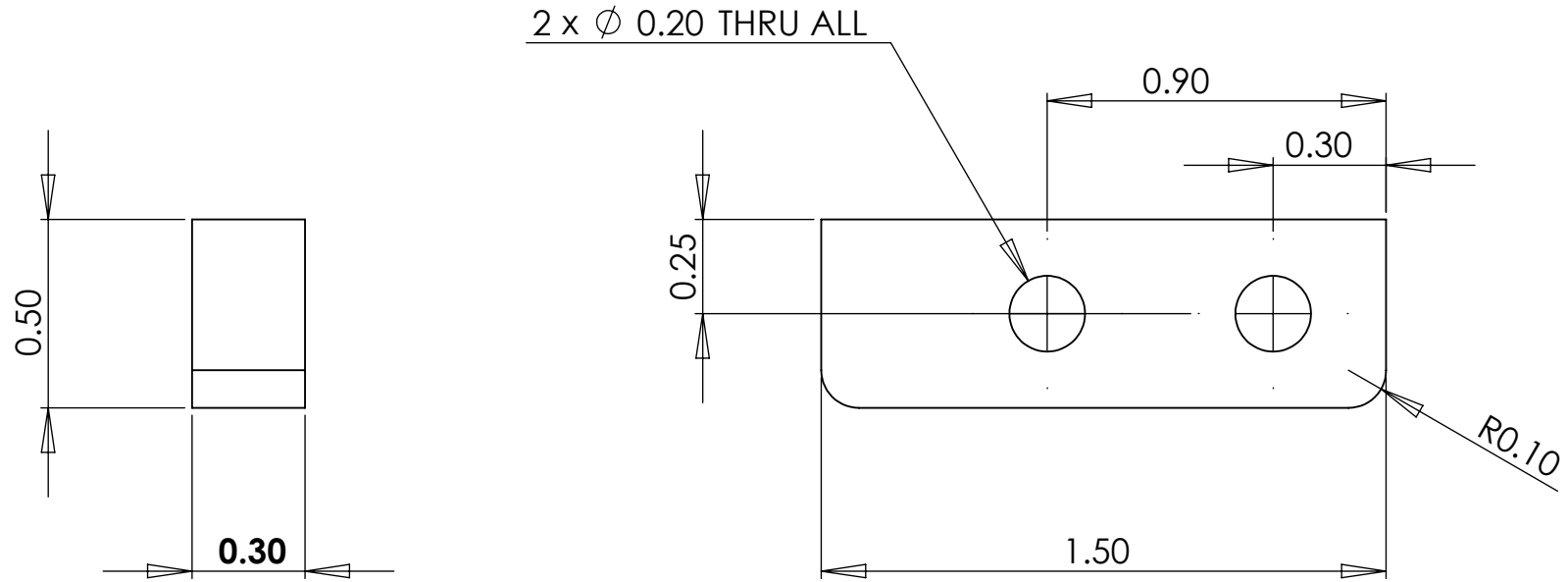

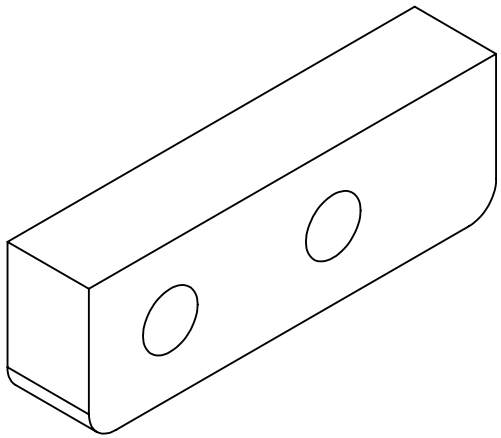

TITLE: Anchor Block Spacer Left		
MATERIAL: AL		
SIZE A	DWG. NO.	REV
	SCALE: 2:1	SHEET 1 OF 1

5 4 3 2 1

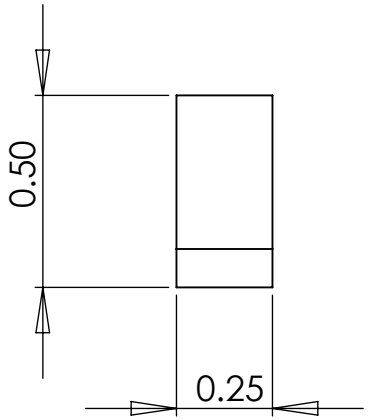

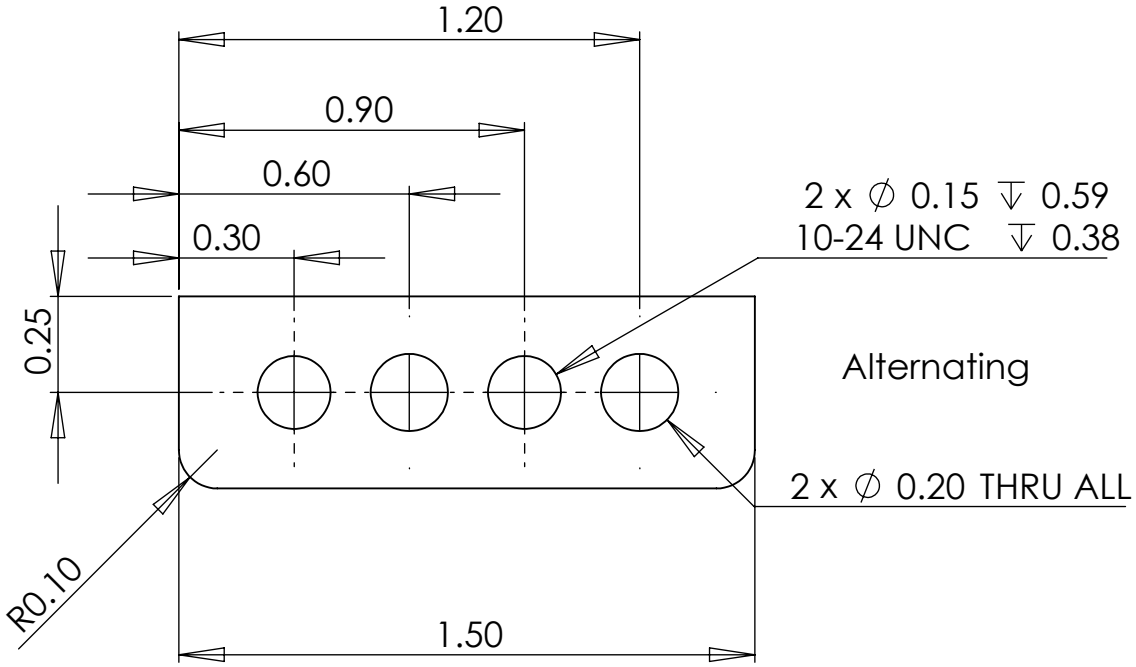

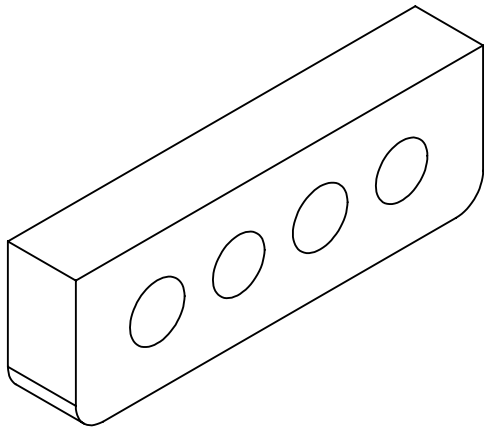

COUNT: 2

TITLE: Anchor Block Spacer Middle		
MATERIAL: AL		
SIZE A	DWG. NO. COUNT: 2	REV
	SCALE: 2:1	SHEET 1 OF 1

5 4 3 2 1

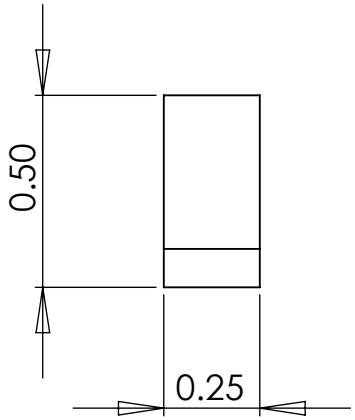

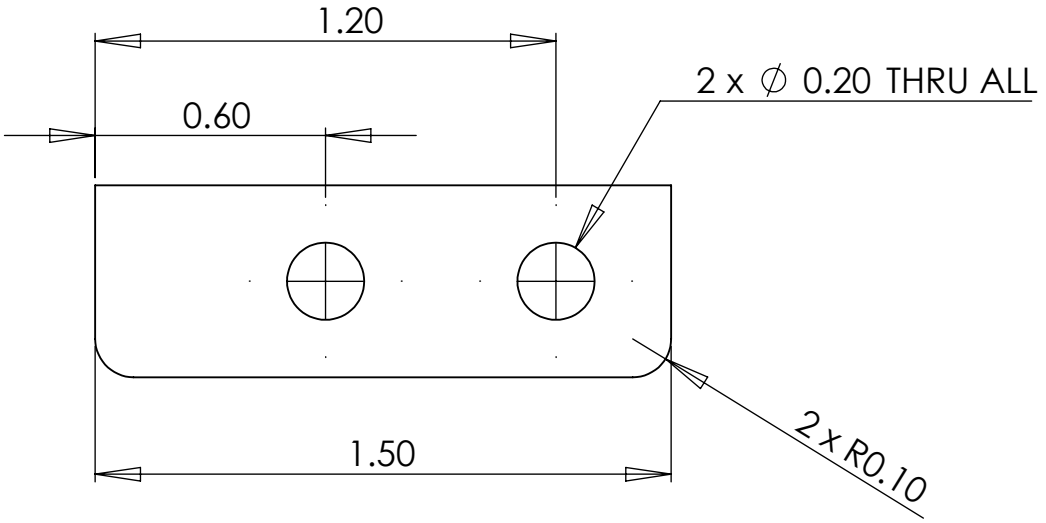

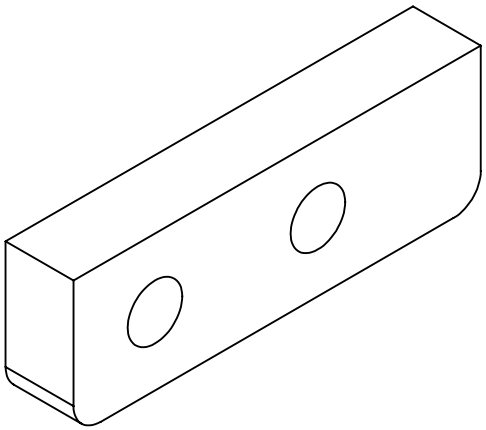

TITLE: Anchor Block Spacer Right		
MATERIAL: AL		
SIZE A	DWG. NO.	REV
	SCALE: 2:1	SHEET 1 OF 1

5 4 3 2 1

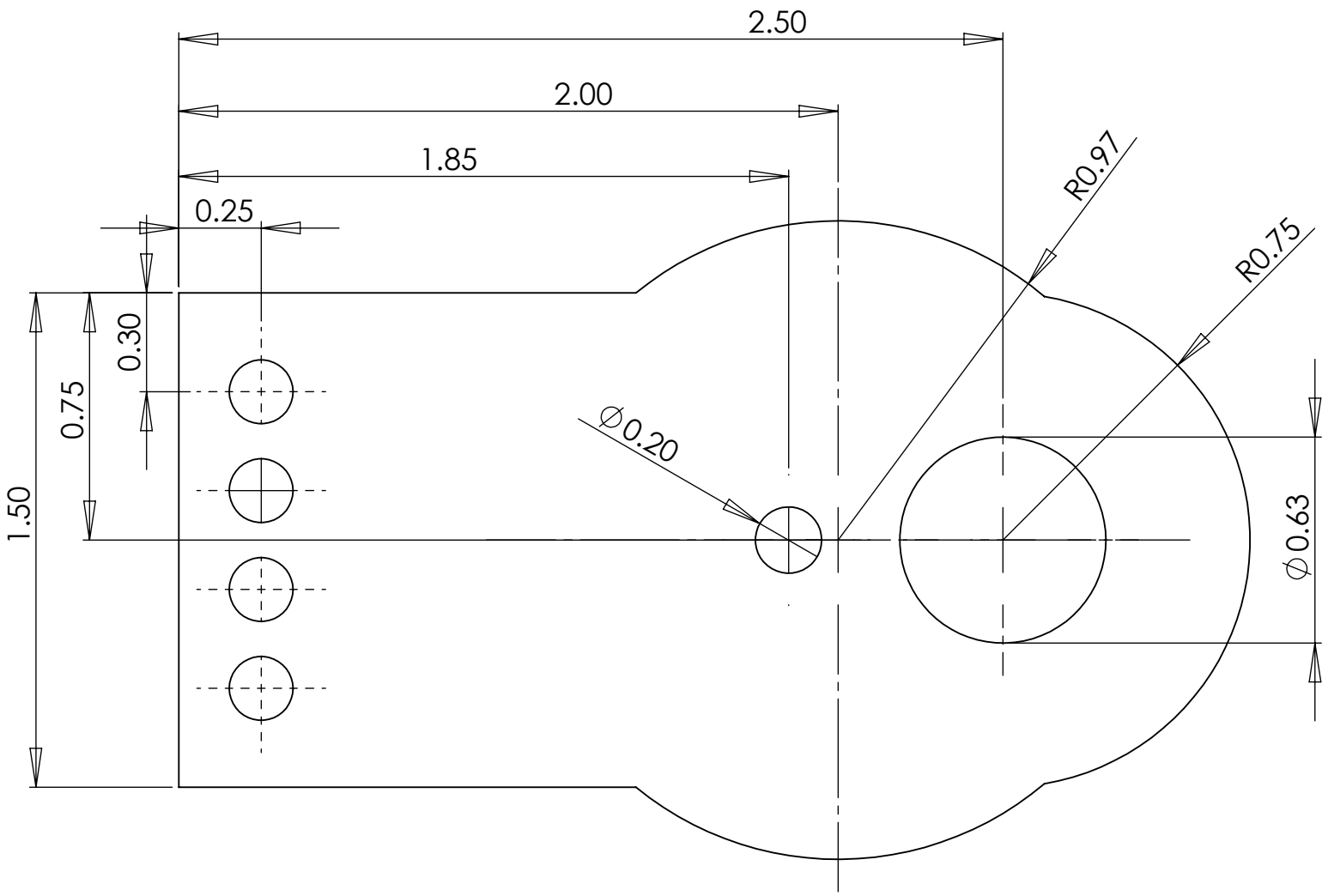

COUNT 3

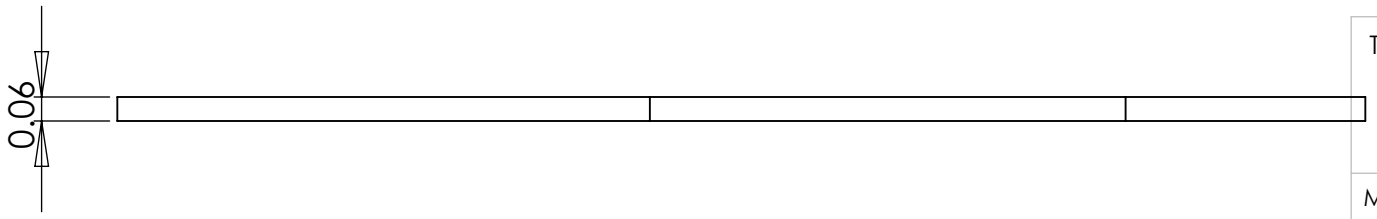

TITLE: Elbow Plate Middle COUNT: 3		
MATERIAL: AL		
SIZE A	DWG. NO.	REV
	SCALE: 2:1	SHEET 1 OF 1

5 4 3 2 1

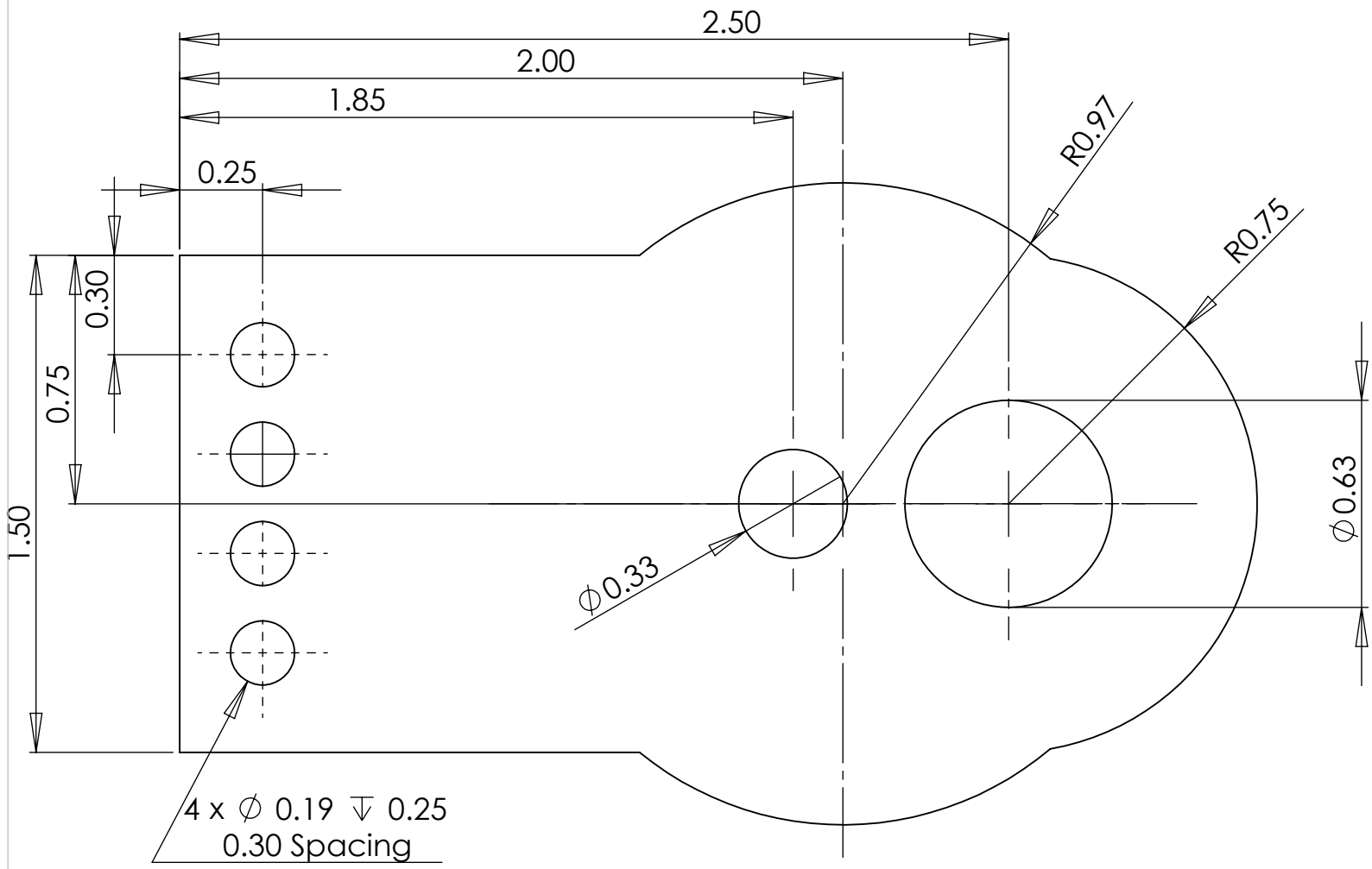

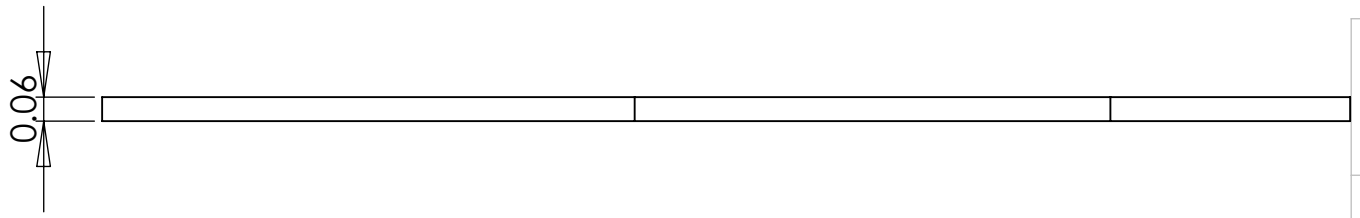

TITLE: Elbow Plate Opposite		
MATERIAL: AL		
SIZE A	DWG. NO.	REV
	SCALE: 2:1	SHEET 1 OF 1

5 4 3 2 1

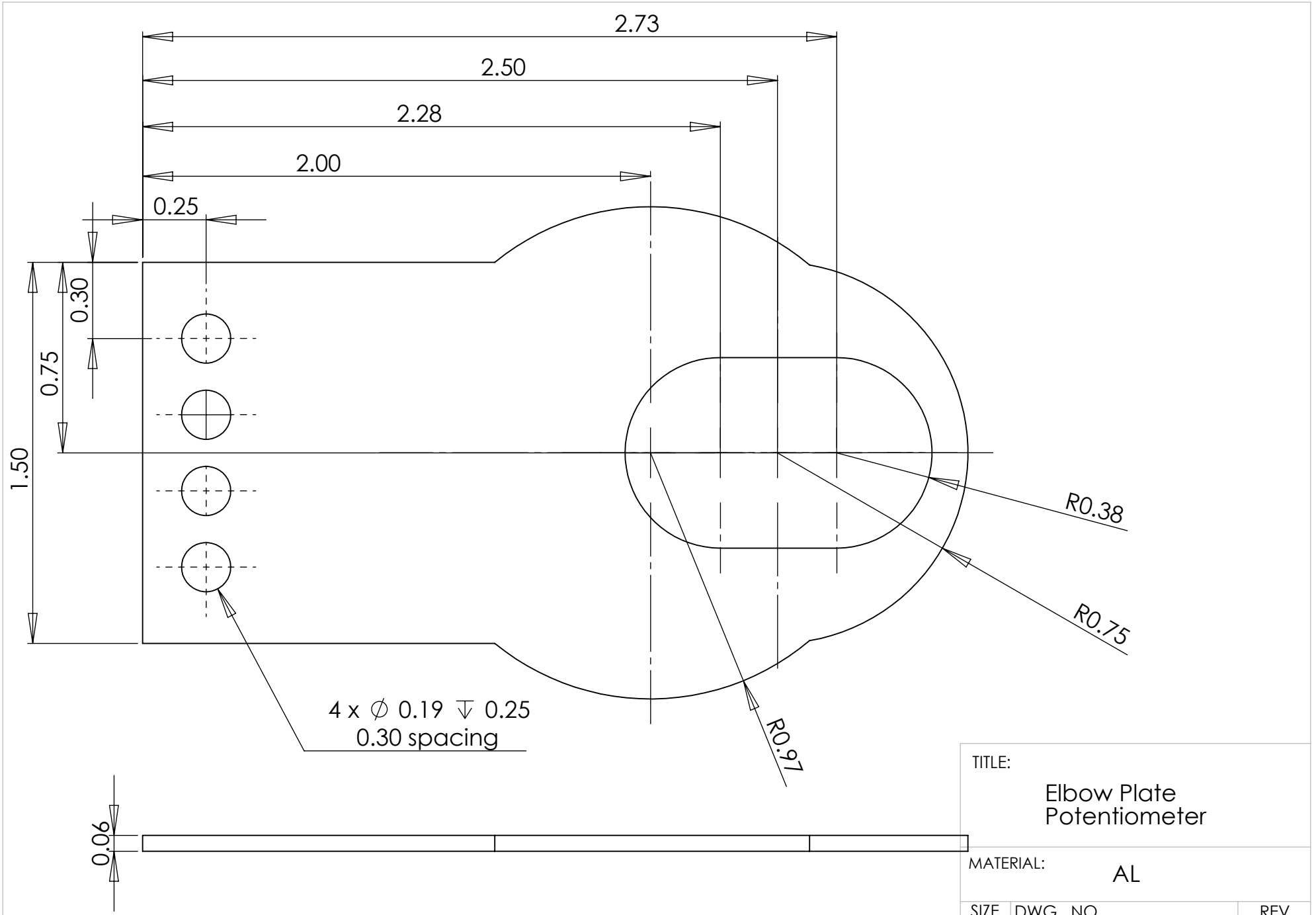

TITLE: Elbow Plate Potentiometer		
MATERIAL: AL		
SIZE A	DWG. NO.	REV
	SCALE: 2:1	SHEET 1 OF 1

5 4 3 2 1

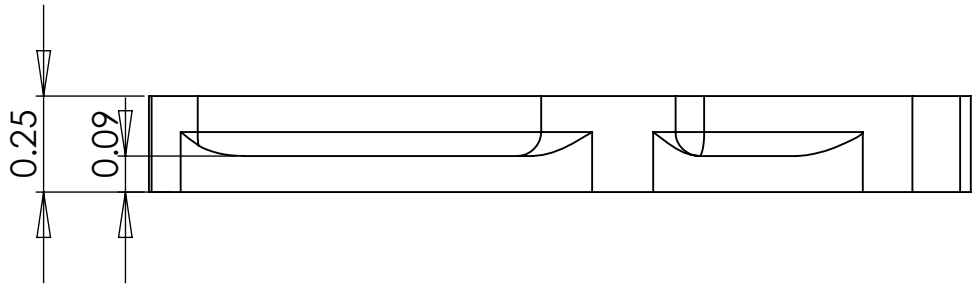

Curved Pulley surface
with Equation:
r=0.6650*x^2+0.7330*x+0.5660
where x=Theta/240
and 0<Theta<202 degrees

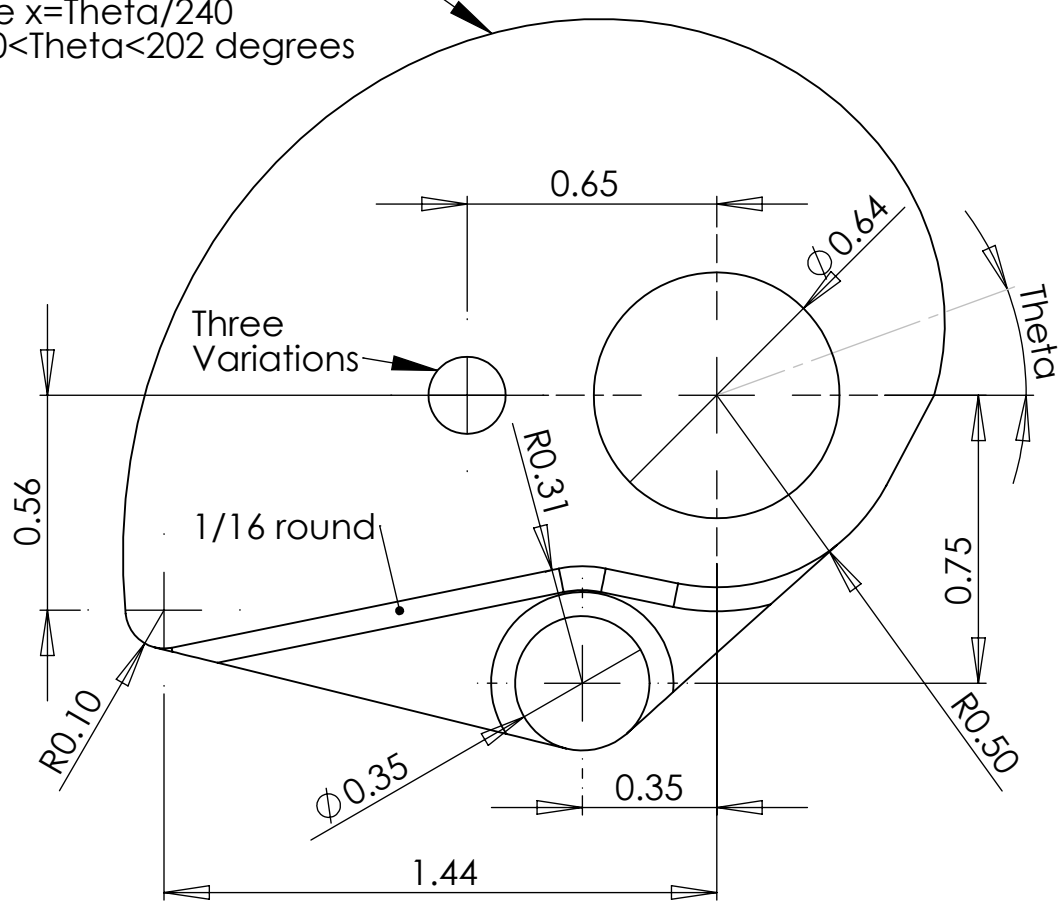

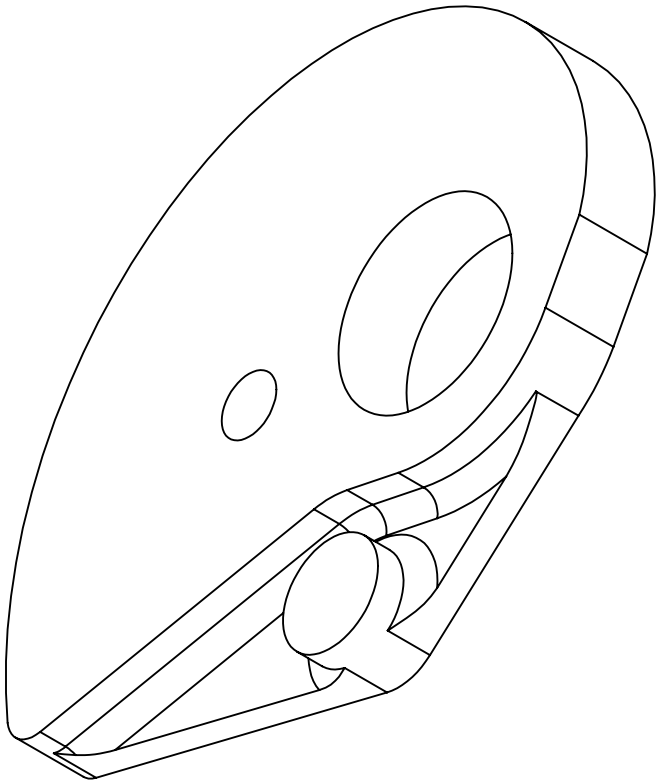

TITLE: Elbow Pulleys Three variations		
MATERIAL: AL		
SIZE A	DWG. NO.	REV
	SCALE: 2:1	SHEET 1 OF 2

5 4 3 2 1

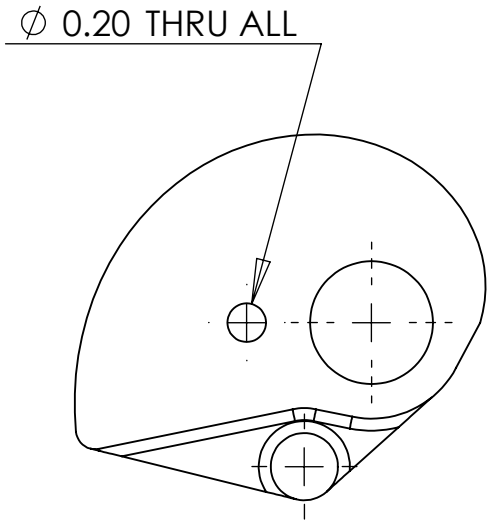

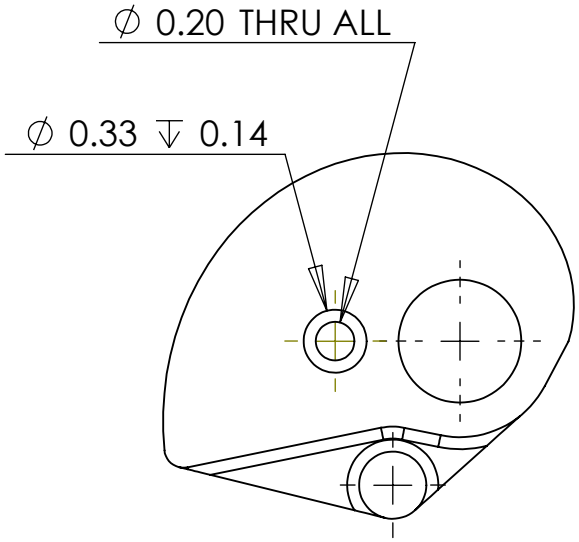

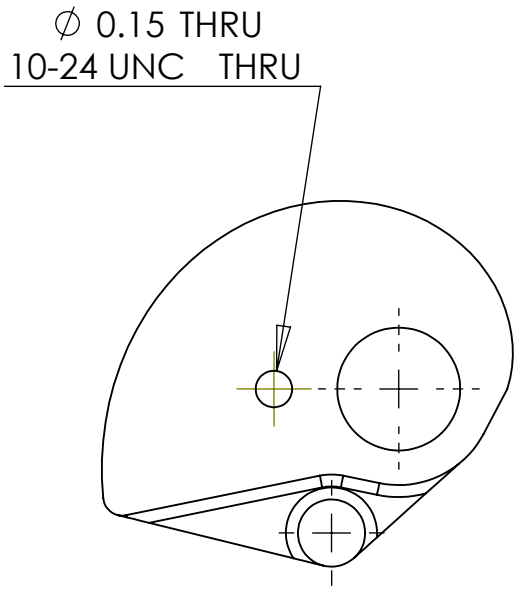

Count: 1 of Each Variation

TITLE:		
MATERIAL:		
SIZE **A**	DWG. NO.	REV
	SCALE: 1:1	SHEET 2 OF 2

5 4 3 2 1

PULLEY SURFACE POINTS

0.5660	0
0.5815	0.0611
0.5911	0.1256
0.5941	0.1930
0.5901	0.2627
0.5785	0.3340
0.5590	0.4061
0.5311	0.4782
0.4946	0.5493
0.4494	0.6186
0.3954	0.6849
0.3327	0.7472
0.2614	0.8044
0.1818	0.8554
0.0945	0.8991
0	0.9344
-0.1009	0.9603
-0.2074	0.9758
-0.3184	0.9801
-0.4329	0.9722
-0.5494	0.9515
-0.6666	0.9175
-0.7831	0.8697
-0.8972	0.8079
-1.0074	0.7319
-1.1119	0.6419
-1.2090	0.5383
-1.2970	0.4214
-1.3742	0.2921
-1.4390	0.1512
-1.4898	0
-1.5251	-0.1603
-1.5435	-0.3281
-1.5439	-0.5016
-1.5252	-0.6791

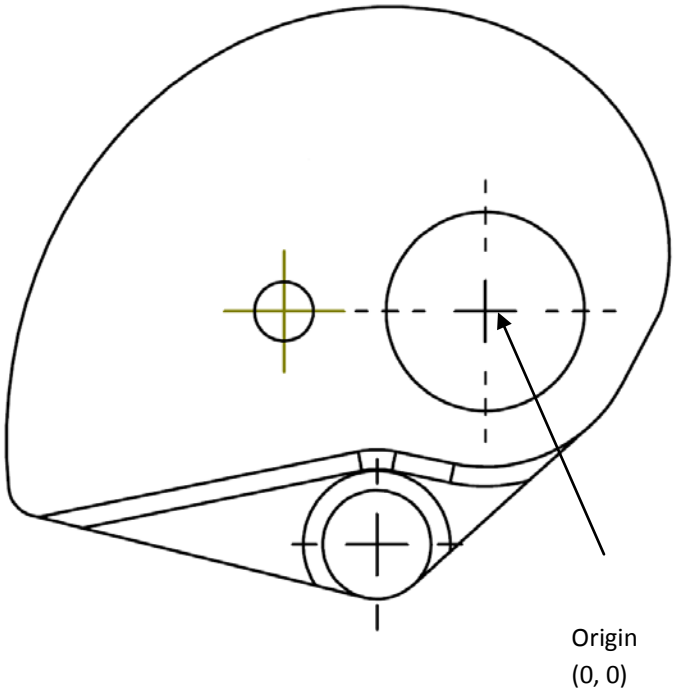

APPENDIX B

MATLAB CODE USED IN LOCAL AND GLOBAL VARIABLE RADIUS PULLEY OPTOMIZATION

```
function [e,r]=secondorderpulleyerrorhires(z)
% y=Ax^2+Bx+C
A=z(1);
B=z(2);
C=z(3);
Lnom=6; %nominal muscle length, in
Tdes=zeros(1,121);
for x= 1:121
    Tdes(x)=-0.01.*((x-1)-60).^2+310;
    %desired torque,inlbs (45 Nm=398.28 inlb)
end%+486.7867;

disp(z)

%presize vectors
r=zeros(1,121);
X=zeros(2410,121);
Y=zeros(2410,121);
xt=zeros(1,121);
yt=zeros(1,121);
reff=zeros(1,121);
TO2=zeros(1,121);
s=zeros(1,121);
S=zeros(1,121);
h=zeros(1,121);
x=zeros(1,2410);
m=zeros(1,121);
mindex=zeros(1,121);
ThetaMX=zeros(1,121);
Alpha=zeros(1,121);
mt=ones(1,2410);
F=zeros(1,121);
Tact=zeros(1,121);
error=zeros(1,121);


xoff=1.7;%in
yoff=1;%in
hoff=sqrt(xoff^2+yoff^2);%in
ThetaHX=atand(yoff/xoff);%degrees
%--ThetaHY=atand(xoff/yoff);%degrees

%Shape Pulley
for i=1:2410
    x(i)=(i-1)/2400;
    r(i)=A*x(i)^2+B*x(i)+C;
end


%Check Pulley Size for relevance
if max(abs(r(1:600)))>.8 %in
    e=1000000;
    disp('Required pulley radius too large in first 60 deg of flexion')
    return
end
```

```
if max(abs(r(600:1200)))>1.25 %in
    e=1000000;
    disp('Required pulley radius too large in last 60 deg of flexion')
    return
end


%Find x&y coords for pulley surface at each angle of elbow rotation(phi)
for phi=1:121 %Elbow Angle +1
    for theta=1:2410 %Pulley Position in polar +1
        if theta/10==phi
            X(theta,phi)=r(theta);
            Y(theta,phi)=0;
        elseif theta/10>phi
            X(theta,phi)=r(theta)*cosd(theta/10-phi);
            Y(theta,phi)=r(theta)*sind(theta/10-phi);
        elseif theta/10<phi
            X(theta,phi)=r(theta)*cosd(phi-theta/10);
            Y(theta,phi)=-r(theta)*sind(phi-theta/10);
        end
    end
end

%find effective point of pulley & tangent line at effective point
for phi=1:121
    for theta=(phi+ceil(ThetaHX))*10:2410
        mt(theta)=(Y(theta,phi)-yoff)/(X(theta,phi)-xoff);
    end
    [m(phi),mindex(phi)]=min(mt);
    xt(phi)=X(ceil(mindex(phi)),phi);
    yt(phi)=Y(ceil(mindex(phi)),phi);
%determine effective radius given tangent line
    ThetaMX(phi)=-atand(m(phi));
    Alpha(phi)=ThetaMX(phi)+ThetaHX;
    reff(phi)=hoff*sind(Alpha(phi));
%calculate total tendon length and get %h of muscle
    TO2(phi)=sqrt((xt(phi)-xoff)^2+(yt(phi)-yoff)^2);
    for i=mindex:240
        s(i)=sqrt((X(i+1,phi)-X(i,phi))^2+((Y(i+1,phi)-Y(i,phi))^2));
    end
    S(phi)=sum(s)+TO2(phi);
    h(phi)=abs(S(phi)-S(1))/Lnom*100;% percent contraction
    %Check h is in physical range
    if h(phi)>25
        disp('Required muscle contraction too high')
        e=20000000;
        return
    end
end

%Check that S is in desired range
if S(1)-S(121)>1.5
    e=3000000;
    disp('Required tendon length too long')
    return
end
```

```
%compute force and torque for each degree of rotation, find error
for i=1:121
    F(i)=0.6058*h(i)^2 - 39.598*h(i) + 630; %N
        %F(i)=F(i)*2.381;% 20mm muscles
    F(i)=F(i)*2;%2 muscles for flexion, with possible wrist rotation
    F(i)=F(i)*0.225;%lbf

    Tact(i)=F(i)*reff(i);
    error(i)=Tact(i)-Tdes(i);
    if error(i)<0
        error(i)=abs(error(i)*1.50);
    end
end

e=sum(error);
disp(e)

%return

phi=1:121;
plot(phi,Tact,phi,Tdes)

pause

for phi=1:121
    plot(X(:,phi),Y(:,phi),0,0)
    line([xoff;xt(phi)],[yoff,yt(phi)])
    axis([min(min(X))-1,max(max(X))+1,min(min(Y))-1,max(max(Y))+1])
    Mov(phi)= getframe;
    clf
end
Mov=[Mov,Mov(121:-1:1)];
movie(Mov,1,30)
```

Optomized input variables:

[0.6650   0.7331   0.5662]

Function Output:

e =

  168.5361